

**Behaviour of the Cross-Laminated Timber diaphragm subjected to in-
plane loading**

by

Mahboobeh Fakhzarei

A thesis submitted in partial fulfillment of the requirements for the degree of

Master of Science

in

Civil (Cross-Disciplinary)

Department of Civil and Environmental Engineering

University of Alberta

Abstract

Residential and commercial uses of cross-laminated timber (CLT) are both on the rise in the North American building industry. The lateral resistance of CLT to wind and seismic stresses is exceptional. This current study examined the in-plane performance of CLT diaphragms subjected to lateral loads.

This study aimed to develop a predictive analytical model for assessing diaphragm deflection and shear forces at panel joints when subjected to loads perpendicular to the panel joints, which was disregarded in prior studies. The model's accuracy was verified against finite element simulations, as well as a partial validation from experimental data. The model considered both bending and shear deflections for each panel, in addition to accounting for slip between panels. A sensitivity analysis was undertaken on the connection stiffness and aspect ratio of the panels in order to minimize the number of model parameters to those that have a substantial influence on the deflection of CLT floors. The findings showed that when loads are applied perpendicular to the panels joints, the primary factor contributing to overall diaphragm deflection is the shear deflection.

Furthermore, the FE modelling approach employed in this project stands as a reliable method for anticipating the in-plane behaviour of CLT diaphragms. This assertion gained substantial support from the successful comparison of model predictions with empirical data gathered from full-scale experiments. The parametric analysis examined the impact of variables like connection stiffness, boundary conditions, and panel layout. Notably, when loads are applied parallel to the CLT panel joints, the stiffness of CLT panel connections significantly affects diaphragm deflection, whereas this impact is moderate when the load is applied perpendicular to the CLT panel joints. Insights gained from varying boundary conditions opened avenues for intentional deformation control,

emphasizing the adaptability of CLT diaphragms in diverse scenarios. Additionally, staggered panel layouts exhibited enhanced load distribution and capacity compared to non-staggered layouts under perpendicular loads.

The results given in this thesis will add to the body of scientific knowledge and will also provide practitioners with a valuable tool for the effective seismic design of CLT platform structures in accordance with the current code requirements.

Preface

This thesis is an original work conducted by Mahboobeh Fakhrzarei, under the supervision of Dr. Ying-Hei Chui, and Dr. Hossein Daneshvar.

Chapter 2 has been accepted and published in the ASCE Journal of Structural Engineering as Fakhrzarei M, Daneshvar H, Chui YH. Analytical Model Development for CLT Diaphragms Loaded Perpendicular to the Length of Panels. journal of structural engineering in March 2023.

An excerpt from Chapter 2 and Chapter 3 has been accepted as “Fakhrzarei, M., Daneshvar, H., and Chui, YH., (2022).” In-plane deflection of cross-laminated timber diaphragms” to the World Conference on Timber Engineering (WCTE), which was held in June 2023 in Oslo.

Chapter 3, under the title “Numerical Parametric Study of Cross-laminated Timber Diaphragms under In-plane Loading”, has been submitted to the journal of construction and building material in August 2023.

Mahboobeh Fakhrzarei was responsible for developing the methodology, performing computation, analyzing the results, original draft preparation, and validation. Ying Hei Chui supervised the findings of this work, provided critical feedback, and reviewed the manuscripts. Hossein Daneshvar also supervised the project by overseeing the results analysis, validation, and manuscript modifications and reviews.

Dedication

To all strong Iranian women fighting for their Freedom

“Women, Life, Freedom.”

Acknowledgments

I wish to thank a few of the many people whose assistance was a milestone in the completion of this project. First, I would like to express my sincere gratitude to my supervisors, Dr. Ying Hei Chui, and Dr. Hossein Daneshvar. It has been a great pleasure to be a member of their research group as they allowed me the freedom to pursue my research in a manner that suited my passion. I am grateful for their continuous support, patience, guidance, and encouragement throughout my research years at the University of Alberta.

Special thanks to Dr. Ali Imanpour, Dr. Lijun Deng, and Dr. Thomas Tannert for allocating their precious time to review my thesis.

I sincerely appreciate the ARTS Group at the University of Alberta for providing professional development opportunities and my colleagues at the ARTS for their collaboration and suggestions to perform the project work.

I would also like to acknowledge Canada's Natural Sciences and Engineering Research Council (NSERC) funding.

Words fall short of expressing my gratitude to my wonderful parents, lovely sisters, and brother for their unconditional love, support, and patience throughout every single challenge in my life.

Finally, yet importantly, I would like to deeply appreciate my beloved husband, Isaac, for his continued support, encouragement, and never-ending patience during the past decade; without his love, this work would have never been possible.

Table of Contents

Chapter 1: Introduction.....	1
1.1 Background.....	1
1.2 Cross-Laminated Timber (CLT).....	2
1.3 In-plane mechanical properties of CLT panels.....	4
1.4 In-plane behaviour of CLT diaphragms.....	9
1.5 Connections in CLT diaphragms	10
1.6 Problem statement.....	16
1.7 Objectives	18
1.8 Research methodology.....	18
1.9 Organization of thesis	19
Chapter 2: Analytical model development for CLT diaphragms loaded perpendicular to panel joints.....	21
2.1 Abstract.....	21
2.2 Introduction and background	22
2.3 Analytical model development	30
2.3.1 Diaphragm responses in X direction (slip among panels)	31
2.3.2 Diaphragm deflection in Y direction	39
2.4 Numerical verification	42
2.5 Verification of analytical model for deflection due to bending and shear.....	43

2.6	Sensitivity analysis.....	45
2.7	Parametric study.....	48
2.8	Conclusion	50
Chapter 3: Numerical parametric study of cross-laminated timber diaphragms under in-plane loading.....		
		52
3.1	Abstract	52
3.2	Introduction.....	53
3.3	Finite element (FE) model development.....	57
3.3.1	Finite element (FE) modelling approach	58
3.3.2	Connections.....	58
3.3.3	Constraints and boundary conditions.....	59
3.4	Model validation	60
3.4.1	Selected experimental study	60
3.4.2	FE model inputs	61
3.4.3	Tension strap modeling.....	64
3.4.4	Comparison of test results and FE model predictions	65
3.5	Parametric study.....	69
3.5.1	Stiffness of panel-to-panel (PPC) and panel-to-beam connections (PBC).....	70
3.5.2	Effect of boundary conditions.....	74
3.5.3	Panel installation pattern (joint staggering versus regular).....	81

3.5.3.1	Diaphragm loaded parallel to panel joints	83
3.5.3.2	Diaphragm loaded perpendicular to panel joints	84
3.6	Conclusions.....	87
Chapter 4:	Summary, conclusion, recommendations, and future work.....	89
4.1	Summary.....	89
4.2	Conclusions.....	89
4.3	Recommendation for future research.....	91
Bibliography	93
Appendix A:	CLT diaphragm design example subjected to lateral load.....	101
A.1.	Introduction.....	101
A.2.	Design example.....	101
A.2.1.	Geometry.....	102
A.2.2.	Material properties	102
A.2.3.	Fastener properties	103
A.2.4.	Loading	103
A.2.5.	Design factors	103
A.2.6.	CLT panel shear capacity.....	104
A.2.7.	Lateral resistance of panel-to-panel nail connections.....	104
A.2.8.	Factored lateral resistance of connection	105
A.2.9.	Force in panel-to-panel connection.....	105

A.2.10. Diaphragm deflection.....	107
A.3. Design summary	107

List of Tables

Table 1-1: Composition factors (k_i) for CLT panels, data from (Blass and Fellmoser 2004)	4
Table 1-2: Effective strength and stiffness for CLT panels (Blass and Fellmoser 2004).....	5
Table 2-1: Stiffness of the connection between the adjacent panels	46
Table 3-1: Elastic mechanical properties of CLT panels and glulam beams used as input for the FE models (Line et al. 2022a)	62
Table 3-2: Summary of connection stiffness characteristics in archetype diaphragms loaded perpendicular to the panel joints	71
Table 3-3: Comparative analysis of diaphragm archetypes under varied boundary conditions in diaphragms loaded perpendicular to the panel joints.....	75
Table 3-4: Summary of diaphragm characteristics with different configurations (staggering pattern), loaded parallel and perpendicular to the panel joints in FE models.....	82

List of Figures

Figure 1.1: CLT panel layout illustration	3
Figure 1.2: Build-up and terms of solid wood panel with cross layers ($m=5$)	5
Figure 1.3: (a) CLT panel without intended spacing ($u=0$) (b) with intended spacing ($u>0$) (Moosbrugger et al. 2006).....	7
Figure 1.4: Conventional CLT panel-to-panel connections: a) internal spline, b) single surface spline, c) double surface spline and d) half-lapped joints, f) inclined butt joint.....	12
Figure 2.1: (a) Diaphragms loaded parallel to panel joints and its deflection components due to (b) bending moment (c) shear force.	25
Figure 2.2: Steps for designing CLT diaphragms (data from Spickler et al. 2015).....	27
Figure 2.3: a CLT diaphragm loaded perpendicular to the panels joints.....	28
Figure 2.4: (a) CLT diaphragm loaded perpendicular to the panel joints (b) infinitesimal segment of finite length dx and the internal force and strain.	31
Figure 2.5: The FE model	42
Figure 2.6: The panel to panel connection modelling.....	43
Figure 2.7: (a) test setup for deep CLT panel under in-plane loading perpendicular to the panel joints (Daneshvar et al. 2021). (b) FE model used to mimic the test results.	44
Figure 2.8: Load-displacement curves for the analytical model, FE model and the experimental data.....	45
Figure 2.9: The diaphragm deflection versus stiffness of the connection.	47
Figure 2.10: Diaphragm deflection against the aspect ratio of the diaphragm.	48
Figure 2.11: Shear, bending and Slip deflection contribution [%] against floor depth	49

Figure 3.1: Diaphragm assemblies when the load direction is applied (a) parallel to the panel joints or (b) perpendicular to the panel joints	58
Figure 3.2: Details of connections in the developed FE models.....	59
Figure 3.3: Test specimen loaded (a) parallel to the panel joints (CLT_01); (b) perpendicular to the panel joints (CLT_02) (figures from (Line et al. 2022a), used with permission).....	60
Figure 3.4: Load-displacement curves for panel-to-beam connections [28]	63
Figure 3.5: Load-displacement curve for panel-to-panel connections [27].....	64
Figure 3.6: Shell elements used to model tension strap.....	65
Figure 3.7: Mid-span load-displacement curve for diaphragm under in-plane loading; numerical versus experimental.	66
Figure 3.8: Load-displacement diagrams for: (a) panel-to-panel connection (PPC), (b) panel-to-beam connection (PBC)	68
Figure 3.9: Variation of diaphragm displacement with the variation of PPC and PBC stiffnesses.	73
Figure 3.10: Deformation patterns of diaphragms with varied beam restraints (Archetypes 1-3)	77
Figure 3.11: Deformation patterns of diaphragms with varied beam restraints (Archetypes 4-7)	78
Figure 3.12: PPC force for diaphragm loading perpendicular to the panel joints	80
Figure 3.13: Mid-span Load-displacement curve for the diaphragm under in-plane loading when the load is parallel to the panel joints.....	83
Figure 3.14: Connections force for diaphragm loading parallel to the panel joints	84
Figure 3.15: Mid-span Load-displacement curve for the diaphragm under in-plane loading when the load is perpendicular to the panel joints.....	85
Figure 3.16: Connections force for diaphragm loading perpendicular to the panel joints	86

Figure 3.17: Stress distribution for the diaphragm under in-plane loading when the load is perpendicular to the panel joints 87

Figure A. 1: A CLT diaphragm loaded perpendicular to panel joints.....102

List of Symbols

A	Cross-sectional area of panel
a	Board width
b	Thickness of the panel
E	Modulus of elasticity of material
E_0	modulus of elasticity parallel to panel joints
E_{90}	modulus of elasticity perpendicular to the panel joints
G	In-plane shear module of panel
G_{eq}	Equivalent shear modulus
G_{eff}	effective shear modulus
G_{\perp}	Shear modulus perpendicular to the grain
G_{\parallel}	shear modulus parallel to the grain
G_Q	shear modulus in the transverse direction for the non-standard configuration
u	is the board spacing
I	Second moment of area
I_s	Moment of inertia of the equivalent solid diaphragm
K_1	Variation for stiffness at the panel joints
K_s	Shear stiffness of the connector
L	Length of the panel
$M_n(x)$	Bending moment in each panel
$M_T(x)$	Total applied moment
N_n	Longitudinal force for each panel

n	Number of the panels
n^*	Number of the connector per row
q	Uniformly distributed load
s	Spacing between the connectors
t	Depth of the panel
U_n^N	Longitudinal displacement function due to longitudinal forces
V_T	Total shear force of the panels
V_n^N	Transverse (vertical) displacement induced by longitudinal forces
u_n	Longitudinal displacement at the base of panel n
u_{n+1}	longitudinal displacement at the base of panel $n+1$
u_n^N	longitudinal displacement induced by the longitudinal forces at the interface between the upper panel and the connection
u_{n+1}^N	longitudinal displacement induced by the longitudinal forces at the interface between the lower panel and the connection
w	Vertical displacement
y	local coordinate with the origin at the top surface of top panel
y'	local coordinate with the origin at the top surface of middle panel
y''	local coordinate with the origin at the top surface of lowest panel
ε_n	Strain at the base of panel n
ε_{n+1}	Strain at the base of panel $n+1$
$\varepsilon_n^M(x)$	Strain-induced by the bending moment at panel n
$\varepsilon_n^N(x)$	Strains induced by the longitudinal forces at the panel n
$\sigma_{xy}(n)$	Shear stress in each panel

$\gamma_{xy} (n)$ Shear strain in each panel
 $\tau(x)$ Shear stress at the interface
 θ Rotation angle of the cross-section

List of Abbreviations

ANSI	American National Standards Institute
AWC	American Wood Council
CLT	cross-laminated- timber
CSA O86	Canadian wood design standard
EWP	Engineered Wood Product
FT	Fully Threaded fastener
GLT	glued laminated timber
LLRS	Lateral Load Resisting System
LVL	Laminated Veneer Lumber
NBCC	National Building Code of Canada
NDS	National Design Specification
OSL	oriented strand lumber
PBC	Panel-to-Beam Connections
PPC	Panel-to-Panel Connections
Pa_NS	Diaphragm loaded parallel to the panel joints with non-staggered CLT panels
Pa_S	Diaphragm loaded parallel to the panel joints with staggered CLT panels
Per_NS	Diaphragm loaded perpendicular to the panel joints with non-staggered CLT panels
Per_S	Diaphragm loaded perpendicular to the panel joints with staggered CLT panels
PSL	parallel strand lumber
PT	Partially Threaded fastener
RVS	Representative Volume Element

RVSE	Representative Volume Sub-Elements
SCL	Structural Composite Lumber
STS	Self Tapping Screws
2D	Two-dimensional
3D	Three-dimensional

Chapter 1: Introduction

1.1 Background

As a result of a rise in pollution, climate change, and the depletion of fossil fuel reserves, the worldwide need for sustainable buildings is growing. Structural materials with a low carbon footprint throughout their whole life cycle, such as wood, have become more popular in recent years. Historically, traditional timber structures have mainly been used as lightweight framework systems with solid wood elements of limited span. In the early twentieth century, steel and concrete became more readily available and cost-effective; thus, timber was primarily replaced with reinforced concrete.

The interest in timber structures re-emerged after introducing a novel category of wood-based products called engineered wood products (EWP). Products such as glued laminated timber (GLT) enabled the construction of more complex and highly robust structures with larger spans. The development of massive timber products with high strength and stiffness, such as cross-laminated-timber (CLT), parallel strand lumber (PSL), oriented strand lumber (OSL), and laminated veneer lumber (LVL) has led to the consideration of timber high-rise structures. One of the emerging building materials is CLT, which was first developed in Europe. With the commencement of CLT production in North America, this product emerges as a credible wood-based structural alternative, facilitating the transition towards sustainable urban and suburban densification. The Tallwood House, located at the University of British Columbia campus, is an excellent example of a mass wood high-rise showcase project, which comprises 16 floors of CLT floor panels (Lau 2016).

In North America, a large body of CLT-related research has been directed toward addressing fire and code issues restricting the height of timber buildings and developing designs for tall timber structures. In particular, emphasis has been placed on applying the CLT to the floor and shear walls that form the primary lateral load resisting system (LLRS) in mid- to high-rise buildings. Floor diaphragms play a crucial role in a building's structural systems by carrying vertical and lateral loads. When subjected to lateral loads, the diaphragms distribute the in-plane loads to the LLRS, which then transfers the loads to the foundation.

While accurate quantification of the in-plane stiffness of CLT floor panels is required to design a CLT structure subjected to lateral loads, no universally accepted guideline is currently available. Limited literature is available on the in-plane behaviour of CLT panels, and even fewer studies exist on the in-plane behaviour of entire CLT floor assemblies. This research aims to investigate how CLT floor diaphragms behave under lateral loading and to improve the comprehension of their in-plane behaviour for designers.

1.2 Cross-Laminated Timber (CLT)

To recognize the behaviour of the CLT diaphragm, it is necessary first to identify the structure of CLT panels. Austria and Germany adopted the use of CLT in building construction in the early 1990s (Gagnon et al. 2013). Since then, CLT has been extensively embraced for residential and commercial usage throughout Europe. As CLT manufacturing has started up in North America, this product is employed as a practical wood-based structural solution for the move toward sustainable densification of urban and suburban centres in North America. CLT panels consist of many layers of boards stacked and bonded together. Typically, three to nine layers of lumber boards are orthogonally bonded to one another (90°) to create a solid panel (see Figure 1.1). The

cross-lamination process enhances the product's dimensional stability. It enables the prefabrication of long floor slabs and single-story walls, making CLT an attractive option for use in floor panels and walls. Assembly of CLT panels needs no specialized tools, and the panels themselves are straightforward to manipulate. The structural system is comprised of prefabricated floor panels and walls that are assembled on-site using a variety of screws and steel connectors (Gagnon et al. 2013). The massiveness of the wood parts provides additional advantages, such as excellent thermal insulation and decent fire performance.

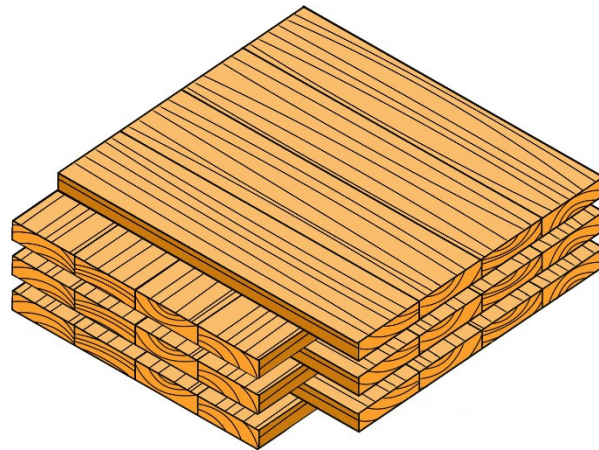
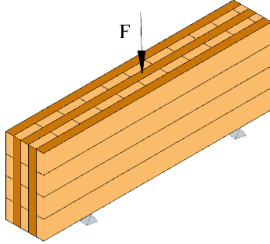
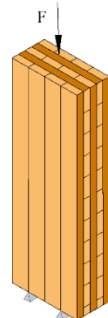


Figure 1.1: CLT panel layout illustration

The American National Standards Institute (ANSI/APA PRG 320) (APA 2019) issued the first CLT standard in 2012. The ANSI outlines performance-rated CLT production, certification, and quality assurance standards. The production requirements of CLT are discussed in depth, including the lamination process, timber species and grades, moisture content, adhesives, and joints in laminations. The standard comprises seven stress classes for key North American wood species and offers standards for CLT certification tests that fulfill the structural performance limits established by the codes. CLT must be evaluated by an authorized organization and meet fundamental structural performance standards.

1.3 In-plane mechanical properties of CLT panels

To construct the CLT diaphragm, it is necessary to comprehend the mechanical characteristics of CLT panels. Several studies aimed to predict the properties of CLT panels loaded in-plane. Based on the composite theory, Blass and Fellmoser (2004) established a technique for designing CLT panels under in-plane bending loads. To accurately assess the strength and stiffness of CLT panels in various directions, a set of factors known as the composition factors (k-factors) were introduced. The specific values for the composition factors, denoted as k_1 and k_2 , pertaining to different loading scenarios related to bending and compression, can be found in Table 1-1.

Table 1-1: Composition factors (k_i) for CLT panels, data from (Blass and Fellmoser 2004)	
Load direction based on the panel length	Composition factors, k_i
	$k_1 = 1 - \left(1 - \frac{E_{90}}{E_0}\right) \frac{a_{m-2} + a_{m-4} + \dots \pm a_1}{a_m}$
	$k_2 = \frac{E_{90}}{E_0} + \left(1 - \frac{E_{90}}{E_0}\right) \frac{a_{m-2} + a_{m-4} + \dots \pm a_1}{a_m}$

Where E_0 and E_{90} are the modulus of elasticity in parallel and perpendicular to the panel joints.

Figure 1.2 shows the build-up and terms of a solid wood panel with five layers. The a_m is the

thickness of the panel, a_{m-2} is the thickness of the panel excluding the outermost longitudinal layers, and a_{m-4} is the thickness of one laminate.

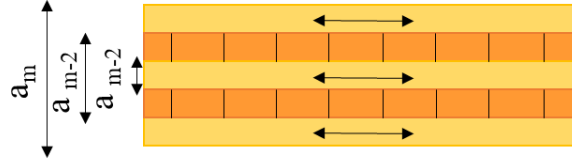


Figure 1.2: Build-up and terms of solid wood panel with cross layers ($m=5$)

These factors were devised to consider the individual layer properties and determine the ratio between the strength or stiffness of a given CLT cross-section and that of a hypothetical homogeneous cross-section. The hypothetical cross-section assumes that all layers within the CLT panel have their grain directions aligned parallel to the direction of stress. Table 1-2 offers formulas for calculating the effective strength and stiffness of CLT panels. Effective strength and stiffness data were used to evaluate the stress distribution and panel deformation of solid wood panels with varying cross sections.

Table 1-2: Effective strength and stiffness for CLT panels (Blass and Fellmoser 2004)

Loading Direction	To the grain of outer skins	Effective strength value	Effective stiffness value
In-plane loading			
Bending	Parallel	$f_{m,0,ef} = f_{m,0} \cdot k_1$	$E_{m,0,ef} = E_0 \cdot k_1$
	Perpendicular	$f_{m,90,ef} = f_{m,0} \cdot k_2$	$E_{m,90,ef} = E_0 \cdot k_2$
Tension	Parallel	$f_{t,0,ef} = f_{t,0} \cdot k_1$	$E_{t,0,ef} = E_0 \cdot k_1$
	Perpendicular	$f_{t,90,ef} = f_{t,0} \cdot k_2$	$E_{t,90,ef} = E_0 \cdot k_2$
Compression	Parallel	$f_{c,0,ef} = f_{c,0} \cdot k_1$	$E_{c,0,ef} = E_0 \cdot k_3$
	Perpendicular	$f_{c,90,ef} = f_{c,0} \cdot k_2$	$E_{c,90,ef} = E_0 \cdot k_4$

Moosbrugger et al. (2006) introduced an innovative model that embraced the regular periodic internal geometry of CLT wall elements while considering uniform shear loading along the boundaries. To capture the intricate internal structure of CLT elements, they devised a Representative Volume Element (RVE) as a fundamental building block. This RVE encompassed the entire plate thickness and was ingeniously subdivided into Representative Volume Sub-Elements (RVSEs), each with its own distinct characteristics. The RVSEs, resembling miniaturized CLT units, featured two perpendicular boards extending half the board thickness. By assuming an infinite periodic arrangement of boards in the thickness direction, the model skillfully bypassed any boundary effects. The model decomposed the complete state of shear loading into two fundamental mechanisms: pure shear occurring within a single board (mechanism I) and torsional-like behaviour observed at the glue interface between two boards (mechanism II). Two equations were developed for estimating the in-plane shear modulus using simplified analytical models for panels. The estimation depends on whether there is spacing between the individual boards. Eq.(1-1) is applicable when there is no intentional spacing ($u = 0$), representing the standard configuration where the narrow faces of the CLT plate elements are not glued together, see Figure 1.3(a). However, CLT panels can also be utilized in non-standard configurations, introducing intentional spacing between the narrow faces of neighbouring boards ($u > 0$), as shown in Figure 1.3(b). In such cases, Eq.(1-2) is employed to calculate the equivalent shear modulus, taking into account the presence of spacing.

$$\frac{G_{eq}}{G} = \frac{1}{1 + 3 \left(\frac{G}{G_{eff}} \right) \left(\frac{t_i}{a} \right)^2} \quad (1-1)$$

$$\frac{G_{eq}}{G} = \left(1 + \left(\frac{u}{a} \right) \left(1 + 2 \left(\frac{G}{G_Q} \right) \right) + 2 \left(\frac{G}{E} \right) \left(\frac{u}{a} \right)^3 + 3 \left(\frac{G}{G_{eff}} \right) \left(1 + \left(\frac{u}{a} \right) \right)^2 \left(\frac{t_i}{a} \right)^2 \right)^{-1} \quad (1-2)$$

Where G_{eff} is the effective shear modulus and is equal to $G_{eff} = (G_I + G_L)/2$, G_L is the shear moduli perpendicular to the grain, and $G_{||}$ or G is the shear moduli parallel to the grain G_{eq} is the equivalent shear modulus, G_Q is shear modulus in the transverse direction for the non standard configuration (CLT panels with intended spacing), E is the modulus of elasticity parallel to the grain t_i is the board thickness, u is the board spacing and a is the board width. The equations rely on the geometric aspect ratio of the panels (i.e., t_i/a , u/a) and the shear moduli. The analytical models were verified by Moosbrugger et al. (2006) using Finite Element (FE) analysis, and a range of thickness-to-width ratios for CLT panels was suggested.

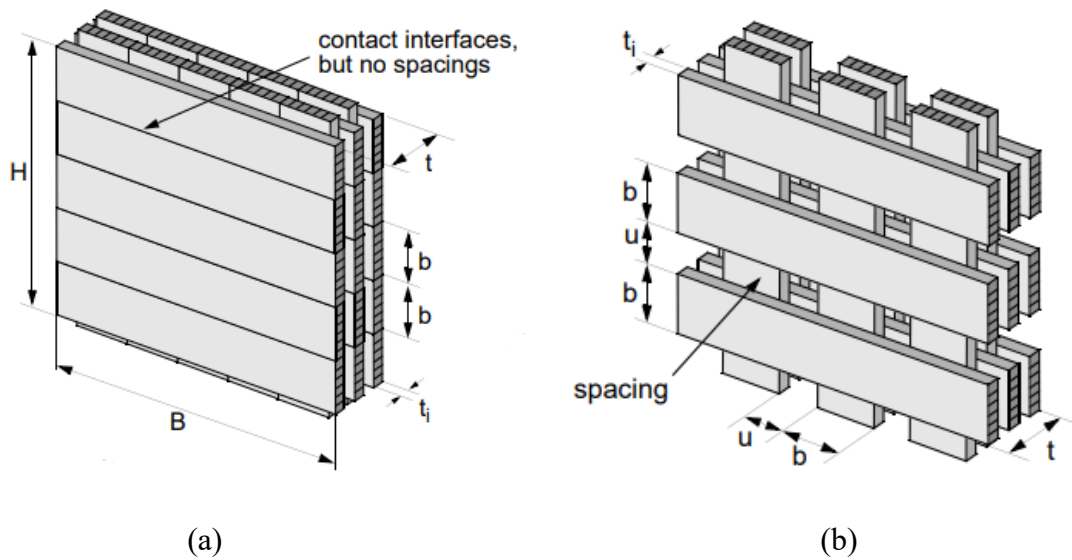


Figure 1.3: (a) CLT panel without intended spacing ($u=0$) (b) with intended spacing ($u>0$) (Moosbrugger et al. 2006)

(Bogensperger et al. 2007) examined the in-plane behaviour of CLT panels and conducted 3-point bending and shear tests in accordance with CEN (2004). FE analysis was used to verify the findings using the identical boundary conditions as in the experiment. In addition, a difference was detected between the stresses and strains of an ideal CLT structure and the test configuration under shear

force. Therefore, it was suggested that a calibration factor of 0.9 be used to compute shear stiffness. Brandner et al. (2013) examined the effect of the test setup and other factors on the in-plane shear strength of CLT panels and discovered three failure mechanisms of CLT elements: Mode I: "net shear," that is, shear perpendicular to the grain; Mode II: "torsion"; and Mode III: "gross shear," that is, shear parallel to the grain. However, their research was limited to the shear resistance of CLT components parallel to the grain (Mode I). They recommended a novel test configuration that would allow for the development of a single shear failure plane as opposed to two shear failure planes in the prior test configuration. In addition, the research revealed that the thickness of the core layer, the orientation of the growth rings, and the gluing interfaces (side face bonding) had a considerable impact on the shear strength of CLT. Brandner et al. (2017) assessed the net-and gross-shear modulus, strength, and shear failures of CLT diaphragms using a unique test design. They employed a test configuration involving column-shaped rectangular specimens obtained by rotating the main orientation of CLT elements by 45 degrees. The study encompassed 23 series, each exploring various parameters such as the number of layers, the ratio between the sum of layer thicknesses in the weak plane direction and that in the strong plane direction, edge gluing, board thickness, and board width. Three- to seven-layer CLT panels ranging in thickness from 60 to 210 mm were used as samples. The in-plane shear modulus and strength were mostly determined by the CLT layer thickness and the absence of edge gluing.

Flaig and Blaß (2013) presented a pioneering shear design approach for in-plane loaded CLT beams. The researchers established mathematical equations for shear stress and stiffness, which they subsequently validated through a comprehensive experimental program. Notably, the test findings revealed three distinct modes of failure for CLT beams under in-plane loading. These were Mode I, characterized by shear failure parallel to the grain in the gross cross-section of the

beam; Mode II, denoting shear failure perpendicular to the grain in the net cross-section of the beam; and Mode III, denoting shear failure in the crossing areas between orthogonally bonded lamellae. Furthermore, Flaig and Blass developed an analytical approach to evaluate the shear stresses occurring in the laminates and crossing areas of CLT beams. The shear strength properties derived from their analytical models were verified based on the results of their experimental program, as well as findings from the existing literature (Flaig and Blaß 2013).

1.4 In-plane behaviour of CLT diaphragms

In the previous ten years, there has been a significant increase in the number of experimental and analytical studies examining and verifying the suitability of CLT as the primary Lateral Force-Resisting System (LFRS) for mid- to high-rise buildings. The reliable design of CLT structures under lateral loads requires an understanding of the in-plane behaviour of CLT diaphragm systems. Brignola et al. (2009) emphasize the significant influence of connection stiffness on the overall stiffness of the diaphragm response in their study. The stiffness properties of connections that link adjacent panels and connect the panels to the framing play a crucial role in determining the behaviour of the diaphragm. Diaphragm response is commonly classified as either flexible or rigid, with flexible diaphragms transferring loads through in-plane bending and rigid diaphragms transferring loads based on support stiffness. The assumption of flexible response is typically applied to light-framed timber diaphragms, while reinforced concrete slabs are considered rigid. Ashtari (2012) investigated the stiffness of CLT floor diaphragms and highlighted the importance of accurately characterizing the diaphragm response to appropriately categorize them as either rigid or flexible. The study embarked on a comprehensive analysis of the in-plane stiffness of CLT floor diaphragms, exploring various configurations, including those with and without openings,

using FE analysis. To capture the behaviour of panel-to-panel connections, a smeared connection model was developed and calibrated using experimental data from Yawalata and Lam (2011). Expanding beyond the calibration, the FE analysis was extended to a parametric study to identify the key parameters influencing the in-plane behaviour of CLT floor diaphragms. Notable observations from the study revealed that the behaviour of CLT panel-to-panel connections, the in-plane shear modulus of CLT panels, the stiffness of shear walls, and the configuration of the floor diaphragm were significant factors influencing the in-plane behaviour of CLT floor diaphragms. Barbosa et al. (2018) performed a numerical investigation involving shake table experiments on a two-story CLT building at full scale by Pei et al. (2018) and observed that the CLT panels did not experience any significant damage during thirty-four earthquake excitations. However, both studies revealed that most of the earthquake damage occurred at the connections. Therefore, the behaviour of the connections will dictate whether a structure can dissipate energy during an earthquake or remain intact through several load cycles (Joyce 2014). CLT diaphragms rely on a wide range of fasteners to establish the necessary connections between panel-to-panel and panel-to-wall interfaces. The in-plane strength and stiffness of CLT connections and diaphragm systems have been the subject of relatively few studies. However, the following section will discuss some of the more noteworthy investigations and their corresponding discoveries.

1.5 Connections in CLT diaphragms

The CLT diaphragm system under lateral loading can be designed for shear, bending or a combination of both. The panel-to-panel connections are designed to resist the shear force between the panels and the panel-to-wall or beam connections are designed for both bending and shear between the diaphragm and the wall underneath. CLT manufacturers typically recommend the use

of proprietary self-tapping screws (STS) for connecting CLT panels, as noted by Gagnon et al. (2013). In practice, the utilization of traditional dowel-type fasteners, including wood screws, nails, lag screws, rivets, bolts, and dowels, for connecting CLT panels is generally restricted and not commonly employed.

Breneman et al. (2016) emphasized the importance of validating the in-plane behaviour of CLT panel-to-panel connections to effectively model and design CLT diaphragms. When establishing a panel-to-panel connection within floor assemblies, the design should focus on transferring in-plane diaphragm forces while ensuring the integrity of both the diaphragms and the overall lateral load-resisting system. Traditionally, there are four primary types of panel-to-panel connections that can be utilized in CLT construction, employing STS as the connecting elements: internal spline, single surface spline, double surface spline, half-lapped joints, and butt joint connections (shown in Figure 1.4).

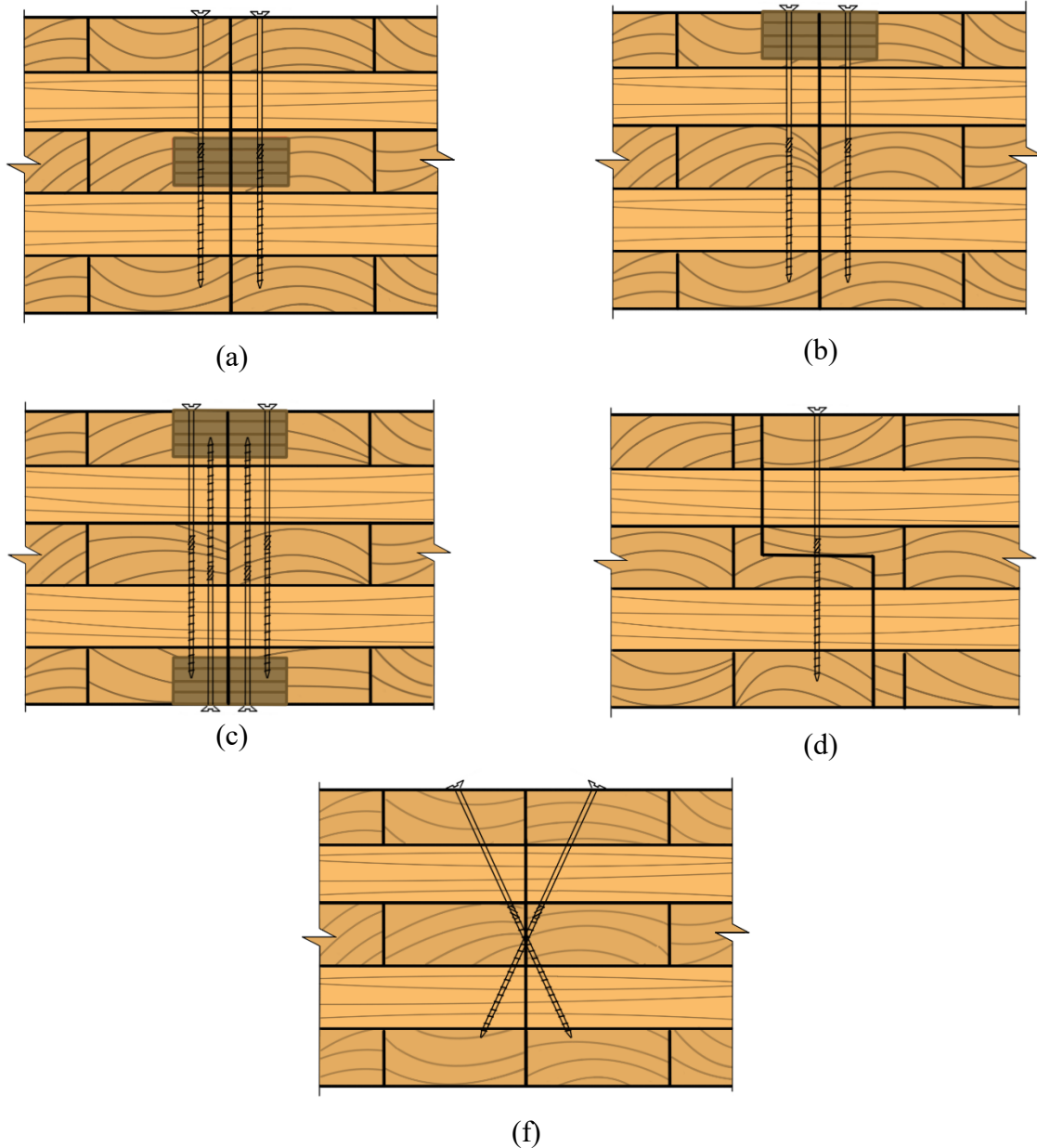


Figure 1.4: Conventional CLT panel-to-panel connections: a) internal spline, b) single surface spline, c) double surface spline and d) half-lapped joints, f) inclined butt joint

The internal spline connection method involves profiling the panels in the middle at the manufacturing plant before their use on-site. This technique utilizes a single wooden spline or strip, which can be made of lumber, plywood, SCL (Structural Composite Lumber), or LVL (Laminated Veneer Lumber), to connect two pieces together using STS, wood screws, or nails, shown in Figure 1.4(a). This connection type offers double shear strength, providing increased

load-bearing capacity. However, it is crucial to ensure accurate profiling of the panels to achieve a proper fit on-site.

The single surface spline connection method involves profiling the edges of the panels to accommodate a single wooden spline or strip made of lumber or SCL (such as LVL). This connection is established using STS, wood screws, or nails, as depicted in Figure 1.4(b). One advantage of this method is its ease of construction on-site, offering convenience during installation.

The double-surface spline connection method is designed to enhance the stiffness and strength of the connection. It involves using two splines, one on the top edge and one on the bottom edge of the panels. Additionally, two sets of screws are used to secure the splines in place. This configuration offers improved resistance and load-bearing capacity compared to the single surface spline connection, shown in Figure 1.4(c). Implementing the double surface spline connection requires additional time, machining, and equipment compared to the simpler connection methods. The process involves carefully profiling the edges of the panels to accommodate the two splines and ensuring accurate alignment during installation.

The half-lapped joint connection method involves milling the panels at the plant to create a half-lapped joint. This joint configuration allows the panels to interlock securely when assembled on-site. To establish the connection, metal fasteners, typically long STSs, are inserted from the top of the joint as shown in Figure 1.4(d).

The butt joint connection is where the ends of two panels are simply placed next to each other and fastened together. This type of connection does not involve any overlap or interlocking of the panels but rather relies on mechanical fasteners, shown in Figure 1.4(f). Partially threaded (PT) or

fully threaded (FT) STS are commonly used as fasteners. In this setup, the screws experience combined shear-compression or shear-tension stress. The connection can be likened to a truss system, with the screws acting as the truss diagonals, effectively distributing and resisting loads. This arrangement enhances the connection's load-bearing capacity and stability.

Richardson et al. (2015) conducted tests on three small-scale CLT connection configurations using non-proprietary fasteners. The study examined the performance of three different connections: the LVL surface spline with lag screws, the half-lap joint with lag screws, and the butt joint with a steel plate fastened with nails. Both monotonic and cyclic tests were performed on these connections. The results indicated that the surface spline and half-lap connections often failed catastrophically. The failures were primarily attributed to the splitting of the spline and the failure of the fasteners. The experimental capacities of these connections were generally 14% lower than what was predicted by the yield models. On the other hand, the half-lap connection exhibited better performance than anticipated, with experimental capacities that were 21% higher than predicted. However, it is important to note that the accuracy of the predicted capacities varied depending on the specific connection type.

Joyce (2014) conducted tests on double spline joints using self-tapping screws (STS) and achieved high ductility when the screws were loaded in shear. They also observed high stiffness when the screws were subjected to withdrawal forces. Sadeghi and Smith (2014) investigated the performance of half-lapped and single-spline joints in edge-to-edge connections of CLT-STC plates. These connections were designed to serve as diaphragms or shear wall elements. The results showed that the half-lapped joints exhibited approximately 50% greater strength and stiffness compared to the single-spline joints when serving as in-plane shear connections in CLT slabs.

In a study by (Gavric et al. 2015), a series of monotonic and cyclic tests were performed on shear connectors to evaluate their effectiveness in panel-to-panel connections in floor assemblies. The tests were conducted using two different configurations: a half-lap joint with a 50 mm overlap and a spline joint made of 28 mm thick and 180 mm wide LVL. For the fastener, STS of 8×140 mm was utilized and the results of the tests revealed that both configurations displayed ductile behaviour, as long as the end/edge distances in the connections were met. The half-lap joints exhibited better performance than the spline joints in terms of stiffness, strength, and ductility. To adhere to seismic design provisions, Gavric et al. (2015) recommended an additional strength factor of 1.6 for screw connections.

In an effort to assess the effectiveness of STS's shear resistance in CLT panels, Hossain et al. (2019) performed both monotonic and cyclic tests on double-angled butt joints. These joints were assembled at a 45° angle between two panels, with the screws installed at an inclination of 32.5° to the face of the panels, resulting in a complex angle of 53.4° between the screw axis and the direction of the wood fibres. To categorize the ductility of the joints, the classification system introduced by Smith et al. (2006) was employed. This system utilizes an average ductility ratio (μ) and defines four categories: brittle ($\mu \leq 2$), low-ductility ($2 < \mu \leq 4$), moderate-ductility ($4 < \mu \leq 6$), and high-ductility ($\mu > 6$). The study revealed that the double-angled butt joints exhibited moderate to high ductility, with average ductility ratios of 4.1 and 7.7 for monotonic and cyclic tests, respectively. Such high ductility ratios indicate that these connectors could be effectively employed in lateral load-resisting systems, particularly in high seismic zones. However, the practicality of accurately assembling these complex-angled connectors in actual construction projects remains unclear.

Sullivan (2017) discovered that surface spline connections display ductile behaviour compared to half-lap joints. The study entailed performing monotonic and cyclic in-plane shear tests on half-lap and surface spline connections with differing spacings of fully and partially threaded STS. The findings confirmed the improved ductility of surface spline connections and concluded that partially threaded (PT) STS have a higher anticipated ductility than fully threaded (FT) STS. This is because FT screws primarily fail in withdrawal due to the increased bearing surface on the connected member. However, there is a lack of consensus on the presence of a group effect for these connections, highlighting the need for additional research into the effect of screw spacing on the in-plane strength and stiffness of surface spline connections.

1.6 Problem statement

One of the most critical structural components in a building system is the floor diaphragm, which supports both vertical and lateral loads. When buildings are exposed to lateral loads, diaphragms are engineered to distribute the in-plane loads to the LLRS, which then transfers these loads to the foundation. In determining the lateral load distribution to the LLRS, the in-plane stiffness of the floor diaphragm is a crucial factor, especially in complex scenarios. There is no commonly acknowledged guideline for accurately quantifying the in-plane stiffness of CLT floors, which is necessary for designing a CLT structure exposed to lateral loads. Therefore, providing recommendations and possibly a formula to estimate the in-plane deformation of CLT diaphragm panels will be helpful in the design of CLT diaphragms.

One of the most essential characteristics of CLT structures under lateral load is the deformation of the diaphragms. However, the stiffness properties of CLT diaphragms have been reported in certain technical approvals (Flaig and Blass 2013). Currently, there are no established procedures

for determining the in-plane stiffness and resistance of CLT diaphragms within the North American wood design standards (CSA O86 (2019) in Canada, (AWC 2018) in the USA. Therefore, an equation to predict the stiffness of CLT diaphragms with varied types and assembly configurations will assist engineers and practitioners in effectively designing CLT structures.

Accurately quantifying the deflection of CLT diaphragms is a crucial parameter in designing CLT buildings for their serviceability and structural functionality. It significantly impacts the overall structural integrity and load distribution within the system. Unfortunately, current standards do not provide guidance on estimating CLT diaphragm deflection. Therefore, it would be beneficial to develop models that consider the actual kinematic behaviour of CLT diaphragms and the influence of loading direction relative to panel joints to estimate total in-plane deflection.

Moreover, the response of CLT diaphragms to in-plane loading depends on various factors, including the elastic modulus of the individual panels, the thickness and aspect ratio of the diaphragm, the geometry and type of connections between the panels, the size and location of openings within the diaphragm, and the orientation of the diaphragm relative to the building's shear walls. Alterations to any of these parameters, even within realistic ranges, can significantly vary the in-plane stiffness and deflection of the CLT floor, resulting in a wide range of possible responses to lateral loading.

This study is driven by the pressing need to comprehend the behaviours and responses of the CLT diaphragms. The primary motivation lies in the creation of a robust analytical model accurately designed to predict the in-plane deformation of the diaphragm. Additionally, conducting a thorough investigation through a comprehensive parametric study aimed at exploring into the influential factors that shape the overall behavior of the system. Ultimately, our motivation stems

from the pursuit of knowledge with the potential to inform and enhance engineering practices, ultimately resulting in the creation of a safe, efficient, and more resilient structures.

1.7 Objectives

This research aims to investigate the in-plane behaviour of the CLT diaphragm, leading to the development of analysis that could be implemented for structural design.

This thesis project has two specific objectives:

- 1) To develop analytical models to calculate the in-plane responses of the CLT diaphragms, including deflection and forces in panel-to-panel connections when the diaphragm is loaded perpendicular to the panel joints.
- 2) To conduct a parametric study using a developed FE model on the behaviour of the CLT diaphragm under in-plane loading applied parallel and perpendicular to the panel joints.

1.8 Research methodology

Three phases were followed to achieve the objectives of this research project. In the first phase, a literature survey was conducted on the in-plane performance of CLT diaphragms. The survey mainly focused on the structure of CLT panels, in-plane mechanical properties of CLT panels, in-plane behaviour of CLT diaphragms, the connections in CLT diaphragms, and numerical modelling efforts. In the second phase, an analytical model was developed to predict the deformation of a diaphragm when it is loaded perpendicular to the panel joints. The model is based on fundamental principles of mechanics and structural behaviour and considers the shear deformation of each panel and slip among the panels. The results of the analytical model were

validated with a numerical model, and sensitivity analyses were conducted by varying the stiffness of the connection and the size of the diaphragm. Additionally, the parametric study was performed to quantify the contribution of each deflection component for each specific case.

In the final phase, a detailed FE model capable of predicting the response of CLT diaphragms under in-plane loading was developed using the commercial FE software, Abaqus (2020). The accuracy of the developed models was evaluated through a comparison with available experimental data. The parametric study was developed to investigate a wide range of CLT diaphragms. Forty-six CLT archetype diaphragms were analyzed by varying the different parameters, such as connection stiffness and boundary conditions (the location and the number of restrained support beams) when the load is perpendicular to the panel joints. Moreover, the panel installation pattern (staggered and non-staggered CLT panels) was analyzed for diaphragm loaded both parallel and perpendicular to the panel joints.

1.9 Organization of thesis

This thesis is organized into four chapters:

Chapter 1 provides a literature review on CLT and its application as a diaphragm as well as the problem statement, research objectives, and research methodology.

Chapter 2 introduces an approach to estimating the in-plane stiffness of CLT panels, which involves both numerical and analytical investigations. The derivation of an analytical model to determine the deflection of the diaphragm under perpendicular loading to the panel joints and force in the panel-to-panel connections is presented. This chapter has been published under the title” Analytical Model Development for CLT Diaphragms Loaded Perpendicular to the Length of Panels” in the ASCE Journal of Structural Engineering. (Fakhrzarei et al. 2023a)

Chapter 3 developed a detailed FE model to accurately simulate the response of CLT diaphragms subjected to in-plane loading. To assess the model's accuracy, it was compared with existing experimental data. Furthermore, a thorough parametric study was conducted to investigate the impact of different factors on the in-plane deflection of CLT diaphragms. These examined factors were connection stiffness, position of beam supports on different CLT diaphragm configurations, panel installation pattern, and panel thickness. This chapter titled "Numerical Parametric Study of Cross-Laminated Timber Diaphragms under In-Plane Loading," has been submitted to the Journal of Construction and Building Materials (Fakhrzarei et al. 2023b)

Chapter 4 provides a summary of the research performed, key findings, conclusions, and finally, recommendations for the topics that needed further investigation in CLT diaphragms.

Chapter 2: Analytical model development for CLT diaphragms loaded perpendicular to panel joints

2.1 Abstract

The main objective of this study was to develop an analytical model for predicting the diaphragm deflection and the induced shear force at the panel joints when the applied load is perpendicular to the panel length. An equivalent finite-element model was developed to capture the elastic behavior of the diaphragm made from the panels and the connections in between. The analytical model's predictions were compared with predictions from finite-element models. The results of an experimental test were used to partially validate the analytical and numerical models in the absence of full-scale diaphragm test data. A sensitivity analysis was carried out with the aim of finding the most influential parameters in the behavior of the CLT diaphragm. The connection's stiffness and diaphragm size were varied. The difference in diaphragm deflection was investigated, and it was found that under realistic material properties and geometry, the diaphragm deflection was not strongly related to the connection's stiffness. However, the floor's geometry was the key influencing parameter. A parametric study was performed, and the contribution of each deflection component was quantified for each specific case. It was observed that the floor's flexibility was dominated mainly by the shear deflection of the cross-laminated timber panels as well as the slip in the panel joints as the length of the diaphragm increased. This study proposes a method that designers may use to estimate the in-plane displacement of the cross-laminated timber diaphragm when it is loaded perpendicular to the panel's joints.

2.2 Introduction and background

In recent years, the use of CLT panels as diaphragm elements in midrise to high-rise buildings has been growing in popularity, mainly due to sustainability reasons (Lenon 2015). The tallest timber buildings in the world, Mjøstårnet in Brumunddal, Norway, and Brock Commons Tall Wood House in Vancouver, Canada, used CLT panels as floors (Tupenaite et al. 2021). The structure of a CLT panel is composed of a crosswise laminate of parallel timber boards, typically connected by complete gluing on a joint's surface. CLTs as diaphragms resist lateral loads caused by either earthquake or wind. They are supported on vertical elements of a LLRS, e.g., shear walls or frames, to eventually transfer the loads to the foundation. The in-plane stiffness of the diaphragm, as well as the stiffness of vertical elements, determine the distribution of the applied lateral load among the different elements of the LLRS. The diaphragm's stiffness strongly depends on the panel material properties, the load-slip behavior of the connection between the adjacent panels, and the load-slip behavior between the panel and the vertical elements (D'Arenzo et al. 2019).

The studies on the CLT diaphragm under lateral loads are limited compared to concrete and steel structures. A survey conducted by Chui et al. (2019) showed that a lack of practical information is one barrier to the versatile usage of CLT as a construction material in Canada. The lack of a recognized design method for CLT diaphragm is one such barrier. Various studies have examined the distribution of lateral loads based on the rigidity or flexibility of the diaphragm. Rigid diaphragms transmitted loads to supports in proportion to the stiffness of the supports, whereas flexible diaphragms transferred loads by in-plane bending (NBCC 2015).

The lateral load distribution between the shear walls supporting a flexible diaphragm relies on the stiffness of the CLT floor diaphragm. This subject was investigated by Ashtari (2012) using a two-

dimensional (2D) Finite Element Analysis (FEA). Analysis was conducted by employing selected CLT floor diaphragm layouts with and without openings. Based on an experimental program conducted by Yawalata and Lam (2011), a smeared panel-to-panel connection model was constructed and calibrated. The results revealed the key parameters that impacted the in-plane behaviour of a CLT floor under lateral loading. They were the panel-to-panel connection stiffness and the shear rigidity of the panels.

Several CLT diaphragm characteristics under in-plane lateral load are still being investigated, such as mechanical properties, type of panel-to-panel connections, diaphragm configuration, and so on. Research has been conducted to quantify the CLT panel's shear strength (Gsell et al. 2007; Flaig and Blaß 2013; Gagnon et al. 2014; Joyce 2014). Brandner et al. (2013) proposed a test configuration for reliably determining the shear strength of CLT elements. They computed the shear resistance perpendicular to the panel joints. The test results indicated that the thickness of the laminates and the gap between the panels had the most significant effect on the panel's shear strength. Moreover, Brandner et al. (2017) conducted an experimental study composed of 23 series of tests with varying test parameters to assess the net and gross shear strength of CLT panels. Their study developed a model based on the beam theory to predict shear strength of CLT panels by considering the contribution of longitudinal and transverse layers.

The connection's behavior is a crucial factor that influences the strength and deflection properties of a diaphragm under lateral loading. The results of investigations into the CLT panel application as shear walls indicates that the CLT panels are typically much stiffer than their connections (Dujic et al. 2004; Dujic et al. 2006; Moosbrugger et al. 2006; (Bogensperger et al. 2010; Popovski and Karacabeyli 2012); Ceccotti et al. 2013; Shahnewaz et al. 2018). These studies revealed that due to the high in-plane stiffness of the CLT panel and the brittle failure of the wood material, the shear

wall ductility comes primarily from the connections. Research on CLT shear walls has provided insight into the behavior of CLT panels under in-plane loading stresses in general. However, the behavior of CLT diaphragms under in-plane loading requires further study that can account for the characteristic use conditions in diaphragm applications.

Experiments on connections in the CLT diaphragms, mainly panel-to-panel connections using self-tapping screws (STS), were done using monotonic tests (Loss et al. 2016), cyclic tests (Gavric et al. 2015) or both (Hossain et al. 2019). In the diaphragms loaded parallel to the panel joints, connectors between panels have been regularly analyzed for the diaphragm's performance because their response dominates the system's behavior (Kode 2018; Barbosa et al. 2021). The stiffness and strength of the panel-to-panel connection using self-tapping screws were also evaluated by Sullivan et al. (2018). Monotonic and cyclic tests were performed on various forms of panel-to-panel connections, including surface spline and half-lap connections employing an array of angles and vertical screws. The results were compared to the design values calculated by the specifications of the US National Design Specification for wood construction (AWC 2018) and Eurocode 5 (CEN 2004). The results showed that the panel-to-panel connections are the main source of in-plane deflection in CLT diaphragms when the load is parallel to the panel joints.

In a technical study based on the specifications of the Eurocode 5, Wallner-Novak et al. (2018) explained the design process of the CLT floor diaphragm. The report investigated diaphragms loaded parallel to the panel joints, as shown in Figure 2.1(a). and determined which connections had a significant influence on the diaphragm's performance. The deflection due to shear force is a result of the slip in the connections between CLT panels, Figure 2.1(b), and in the deflection due to bending occurs as a result of the rotation of the CLT panels as shown in Figure 2.1(c). The study

by Wallner-Novak et al. (2018) did not address the case where the applied load is perpendicular to the panel joints.

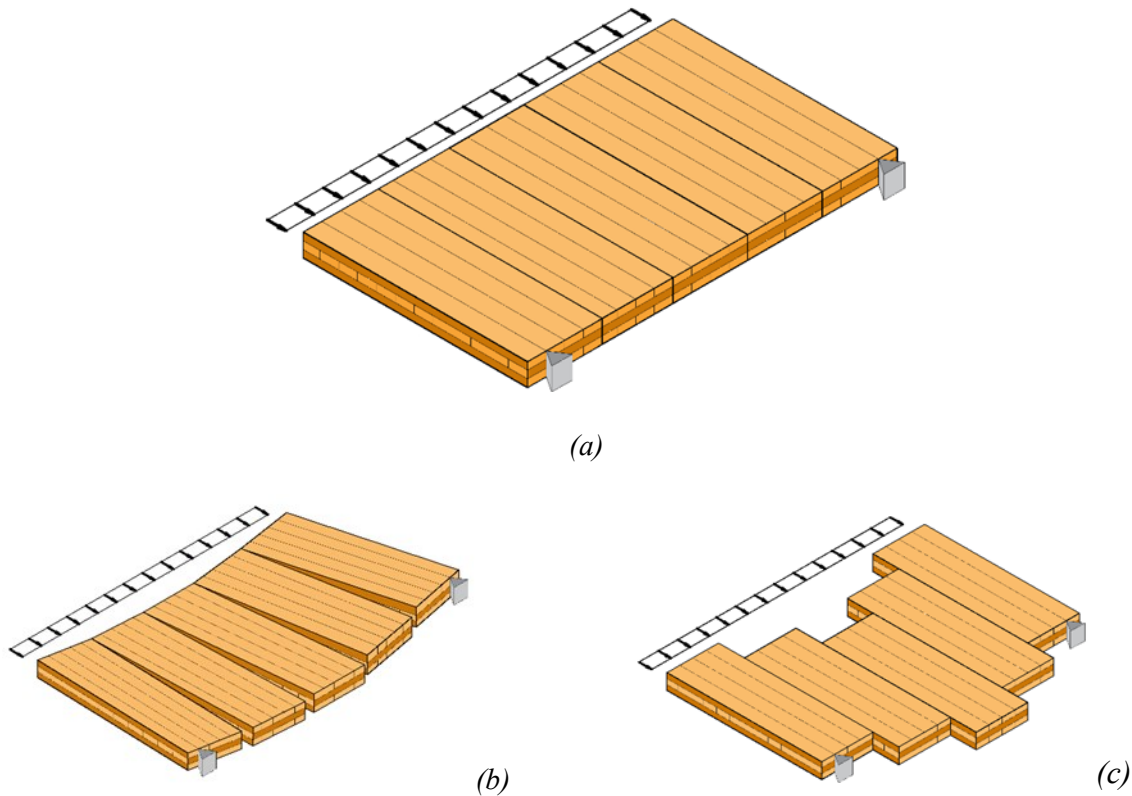


Figure 2.1: (a) Diaphragms loaded parallel to panel joints and its deflection components due to (b) bending moment (c) shear force.

Similar to the research conducted by Wallner-Novak et al. (2018), D’Arenzo et al. (2019) examined the in-plane flexibility of the CLT diaphragm subjected to the load parallel to the panel joints using a two-dimensional (2D) plane model. A sensitivity analysis was performed using experimentally evaluated connection behaviors. An equivalent frame model was presented in order to assist in the depiction of data acquired through sensitivity analysis. The equivalent frame model consisted of springs in parallel or in a series in the spring system and showed shear and bending deflection contributions. The shear deflection equivalent spring was defined so that the three in-series springs accounted for the shear, panel-to-panel connections, and floor-to-wall connections.

In order to model the diaphragm deflection due to bending, a single spring for floor-to-wall connection was schematized in parallel with two in-series springs: one for the bending contribution of the panel; and one for the panel-to-panel connection. The result confirmed that the connection stiffness influenced the strength of the CLT diaphragm loaded parallel to the panel joints.

One option for developing the design methodology for the CLT diaphragm is to adopt the available design procedure for precast concrete due to similarities (Beairsto 2020). In this methodology, CLT panels were assumed to be rigid, similar to precast concrete panels. Moroder (2016) carried out a simple FE analysis in SAP2000 (2005) and confirmed that an equivalent truss method was a valid approach for analyzing mass timber diaphragms. The truss member properties were calibrated by accounting for the panel shear and fastener stiffness.

A number of studies have considered the deflection of the full-scale CLT diaphragms (Beairsto 2020; Barbosa et al. 2021; Kode et al. 2021). However, these studies were limited to loading parallel to the CLT panel joints. Nevertheless, Spickler et al. (2015) have provided a design procedure for a CLT diaphragm under in-plane loads applied perpendicular to the panel joints. The design procedure builds upon the United States timber design standard (NDS 2014) and the Standard for Performance-rated Cross-laminated Timber (ANSI 2012). The proposed design procedure is illustrated in Figure 2.2.

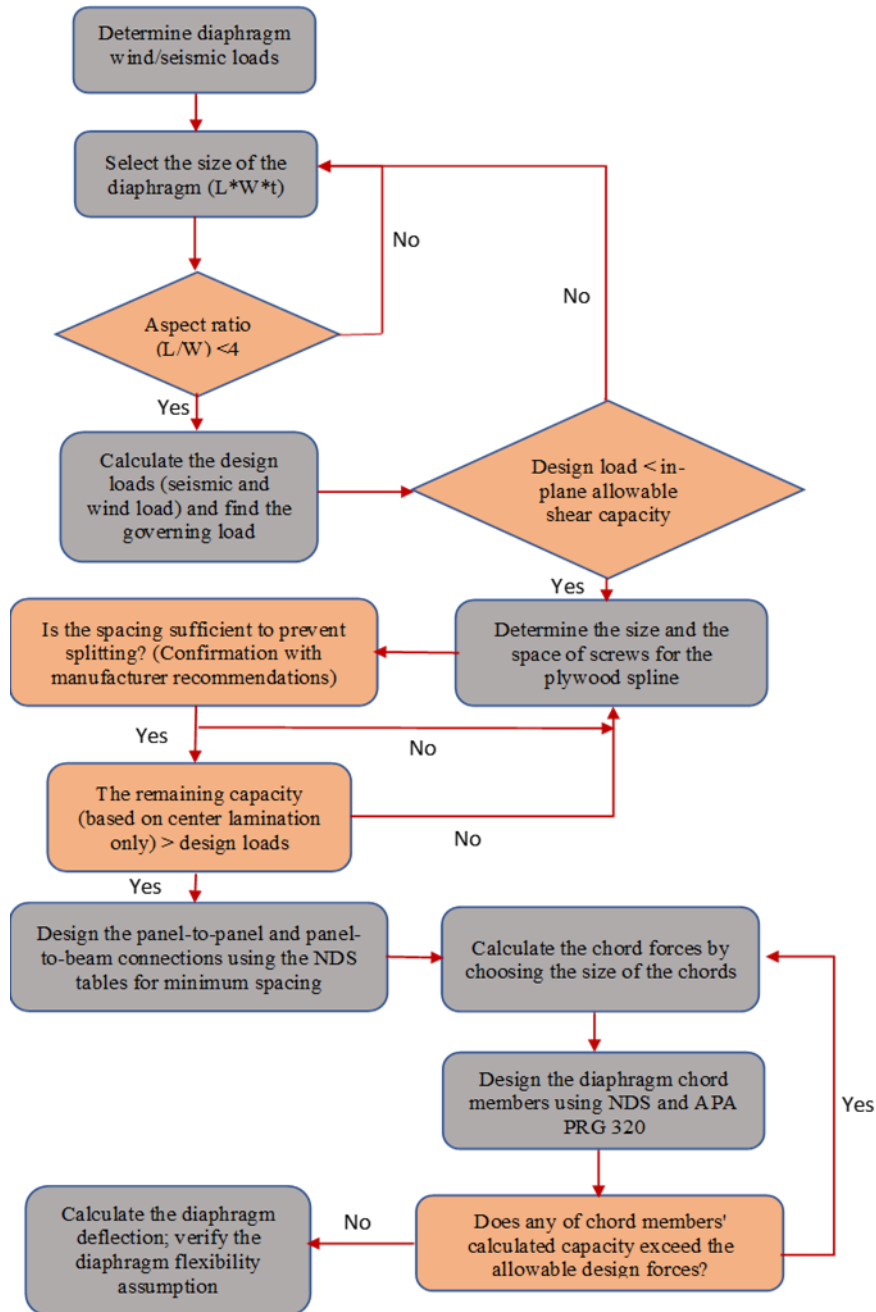


Figure 2.2: Steps for designing CLT diaphragms (data from Spickler et al. 2015).

There are some limitations in Spickler’s design procedure that need to be addressed. For example, the equation used for estimating the diaphragm deflection was based on the light wood frame

diaphragms rather than mass timber. They also used the chord width to determine the diaphragm bending deflection, which might not be a good assumption. To address these shortcomings, Breneman et al. (2016) presented a numerical modelling approach to more realistically capture the response of a CLT timber diaphragm under lateral loading. The model consisted of CLT panels as discrete orthotropic shell elements and panel-to-panel connections as two-point springs. Their numerical model prediction was compared with Spickler's solution, which showed a 14% difference in deflection predictions.

Based on the aforementioned literature review, it is revealed that although there were some attempts to calculate the diaphragm deflection subjected to loads in the direction parallel to the panel joints, there is no such solution for the other direction. The scenario of the applied load being perpendicular to the CLT panel joints in the diaphragm has been ignored in most research to date. This scenario must be considered in CLT diaphragm design because the lateral load due to wind and seismic can be applied in both directions. The current work was motivated by a need to develop an analysis procedure for the CLT diaphragm subjected to loading perpendicular to the panel joints, as shown in Figure 2.3.

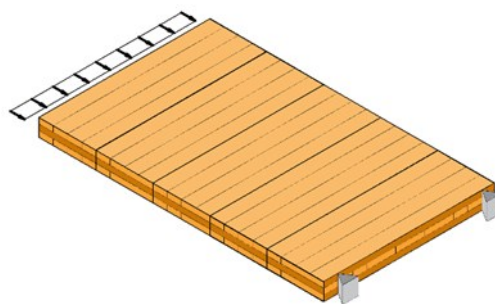


Figure 2.3: a CLT diaphragm loaded perpendicular to the panels joints.

The case of a CLT floor diaphragm loaded perpendicular to the panel joints, similar to the arrangement shown in Figure 2.3, may behave as a series of stacked deep beams, and the slip

movement between the panels can be calculated using the induced shear force between the panels. To the best of the authors' knowledge there are no test results for two or multiple CLT panels in the desired direction of loading for this study. Such a system can be analyzed as a layered beam subjected to loading on the edge. Goodman and Popov (1968) introduced a methodology to analyze this type of system by presenting a closed-form solution for the deflection of simply-supported three-layer beams made of the same material. Chui and Barclay (1998) expanded the work of Goodman and Popov (1968) by accounting for different dimensions and material properties of layers. However, the layered beam theory adopted by these researchers ignores the shear deflection in individual layers, and cannot be directly adopted for deep beam systems, such as a CLT diaphragm. In addition, the K-method suggested in the CLT handbook (Karacabeyli et al. 2019) to determine the displacement of a CLT deep beams is not recommended. The K-method theory, originally developed for plywood panels, is based on a few assumptions when applied to CLT panels. These assumptions include ignoring shear deflections and considering the gross section to be resistant to flexural demand.

Despite these limitations, the above layered beam theory lays the foundation for the development of an analytical model to predict the in-plane performance of CLT diaphragm with semi-rigid panel-to-panel joints and loading applied perpendicular to the joints of the panel. The developed model described below accounts for the influence of shear in the panels and the slip between adjacent CLT panels. Using the model, the shear force transfer between the adjacent CLT panels and the diaphragm deflection can be explicitly calculated. Also, a numerical model was created to validate the results of the analytical model. Using the analytical model a series of sensitivity analysis was performed.

2.3 Analytical model development

The analytical model is based on a three-panel CLT diaphragm with the length L and depth t for each panel is shown in Figure 2.4(a). The deep beam analogy, which is commonly adopted for the analysis and design of diaphragm systems, is implemented. An external in-plane load, q , is applied to the diaphragm centerline, which is transferred through the CLT panels to the shear walls below. The diaphragm is assumed to be supported on simple supports at the two ends. The following assumptions apply in the development of the analytical model:

- The shear stress distribution through the thickness of the panels is linear.
- The curvature at the bottom of the upper panels and the top of the lower panels is the same.
- The in-plane y -axis deflection caused by the induced longitudinal (x -direction) force is zero.
- To align with the beam analogy material properties of the CLT panels are equivalent to the outer layer.

For loading perpendicular to the panel joints, the diaphragm deforms in both the X and Y directions. The deflection in the X direction is primarily due to the slip between the panels, while the Y -direction deflection is caused by shear and bending deflections in the CLT panels and the interlayer slip between the panels. These two deflections are discussed thoroughly in the following two sections.

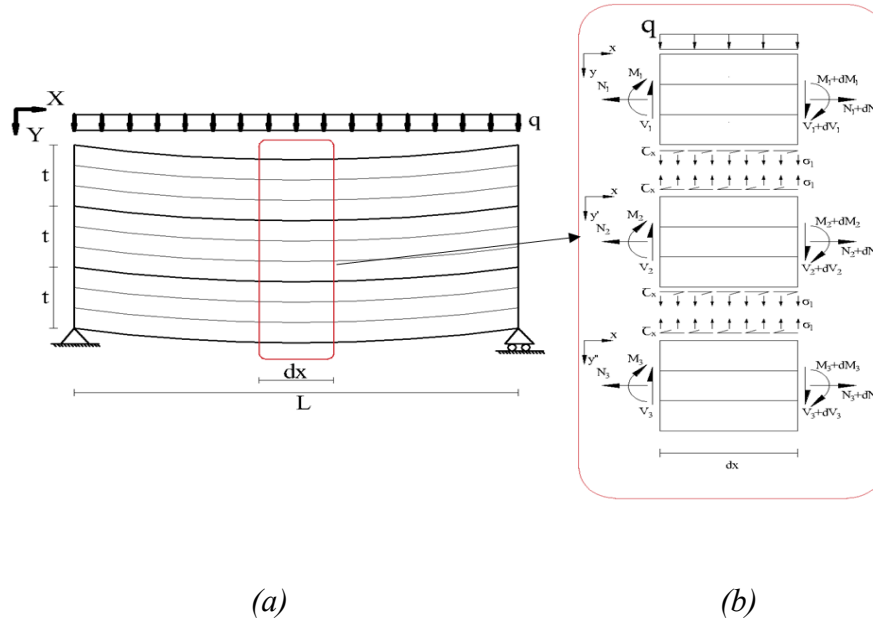


Figure 2.4: (a) CLT diaphragm loaded perpendicular to the panel joints (b) infinitesimal segment of finite length dx and the internal force and strain.

2.3.1 Diaphragm responses in X direction (slip among panels)

Figure 2.4(b) shows an infinitesimal floor segment of finite length dx , the internal forces and moments, as well as the strain distribution in a cross-section of a typical diaphragm system.

The strain in the cross-section of the CLT panel near the interfaces can be expressed as Eq. (2-1):

$$\varepsilon_n(x) = \frac{du_n(x)}{dx} = \varepsilon_n^M(x) + \varepsilon_n^N(x) \quad (2-1)$$

The subscript n denotes the number of the panels, starting with the top panel. The longitudinal displacement at the edge of the CLT panels is $u_n(x)$. The unknown longitudinal strain induced by longitudinal forces at the cross-section is $\varepsilon_n^N(x)$. The strain caused by each panel bending moment is $\varepsilon_n^M(x)$, and it can be calculated using Eq. (2-2):

$$\varepsilon_n^M(x) = \frac{M_n(x) t}{EI} \frac{1}{2} \quad (2-2)$$

$M_n(x)$ is the bending moment in each panel, t is the depth of individual panels, E is the elastic modulus, and I is the second moment of area for each panel. All panels are assumed to have identical properties and exact dimensions in this study:

$$\varepsilon_n^N(x) = \frac{du_n^N(x)}{dx} \quad (2-3)$$

u_n^N represents the displacement caused by longitudinal force at the panel-to-connection interface. Shear deflections between the panels are included in the calculation of longitudinal strains. First, a longitudinal displacement (an in-plane displacement in x-axis direction) in the function is assumed for each panel, and then the displacement at the interface is calculated. It is obvious that the shear stress is not the same throughout the depth of the CLT panel. Hence, a linear assumption for the longitudinal displacement cannot be correct. A parabolic variation is assumed for the longitudinal displacement:

$$U_n^N(x, y) = A_n(x) \cdot y_n^2 + B_n(x) \cdot y_n + C_n(x) \quad (2-4)$$

n signifies the number of the panels and the origin of the local coordinate system, y_n , is the top surface of each panel. A_n , B_n , and C_n are coefficients dictated by the boundary conditions. The distribution of shear stress throughout the depth of the panels is expressed as:

$$\sigma_{xy}(n) = G_{xy} \gamma_{xy} \quad (2-5)$$

where G_{xy} is the shear modulus, $\sigma_{xy}(n)$ shear stress, and γ_{xy} is the shear strain of each panel. As shown in Eq. (2-6), the shear strain is caused by the displacements in x- and y- directions:

$$\gamma_{xy(n)} = \frac{\partial U_n^N}{\partial y} + \frac{\partial V_n^N}{\partial x} = \frac{du(x, y)}{dy} + \frac{dv(x, y)}{dx} \quad (2-6)$$

V_n^N is the displacements in y- directions that are induced by longitudinal forces and can be ignored in the calculations. Therefore, the shear strain can be written as:

$$\gamma_{xy(n)} \approx \frac{\partial U_n^N}{\partial y} \quad (2-7)$$

with the substitution of a derivative of Eq. (2-4) into Eq. (2-5), the shear stress for each panel can be written as:

$$\sigma_{xy(1)} = G_{xy}(2A_1y + B_1) \quad (2-8)$$

$$\sigma_{xy'(2)} = G_{xy}(2A_2y' + B_2) \quad (2-9)$$

$$\sigma_{xy''(3)} = G_{xy}(2A_3y'' + B_3) \quad (2-10)$$

In this study, the analytical model was initially developed for a diaphragm system consisting of three panels, as shown in Figure 2.4. The local coordinates are centered on the upper surface of each panel and are represented as y for the top panel, y' for the middle panel, and y'' for the bottom panel. The compatibility and boundary conditions for the three panels are shown below:

$$\sigma_{xy(1)}(x, t) = \sigma_{xy'(2)}(x, 0) = \sigma_{xy'(2)}(x, t) = \sigma_{xy''(3)}(x, 0) = \tau(x) \quad (2-11)$$

$$\sigma_{xy(1)}(x, 0) = \sigma_{xy''(3)}(x, t) = 0 \quad (2-12)$$

where $\tau(x)$ is the shear stress at the interface.

By applying the boundary condition, the shear stresses in the panels are shown in Eq. (2-13) to Eq. (2-15)

$$\sigma_{xy(1)} = \frac{\tau(x)}{t} y \quad (2-13)$$

$$\sigma_{xy(2)} = \tau(x) \quad (2-14)$$

$$\sigma_{xy''(3)} = \left(1 - \frac{y''}{t}\right) \tau(x) \quad (2-15)$$

In turn, the shear strain in the panels is shown in Eq. (2-16) to Eq. (2-18):

$$\gamma_{xy(1)} = \gamma_1 = \frac{\tau(x)}{G_{xy}t}y \quad (2-16)$$

$$\gamma_{xy(2)} = \gamma_2 = \frac{\tau(x)}{G_{xy}} \quad (2-17)$$

$$\gamma_{xy(3)} = \gamma_3 = \frac{\tau(x)}{G_{xy}} \left(1 - \frac{y''}{t}\right) \quad (2-18)$$

The longitudinal displacement function U_n^N , due to longitudinal forces, is given by:

$$U_1^N = U_1^N(0) + \int_0^y \gamma_1(y)dy + U_1^N(t_1) \quad (2-19)$$

$$U_2^N = U_2^N(0) + \int_0^{y'} \gamma_2(y')dy' + U_2^N(t_2) \quad (2-20)$$

$$U_3^N = U_3^N(0) + \int_0^{y''} \gamma_3(y'')dy'' + U_3^N(t_3) \quad (2-21)$$

$U_n^N(0)$ and $U_n^N(t_n)$ indicate panel displacement at the top and bottom edges of a panel, respectively, and can be calculated by subtracting the panel's displacement at each interface from the connection displacement. It can be shown that:

$$U_1^N(0) = 0, U_1^N(t) = u_1^N - \frac{\tau(x)}{2G}t \quad (2-22)$$

$$U_2^N(0) = u_2^N, U_2^N(t) = u_2^N - \frac{\tau(x)}{G}t \quad (2-23)$$

$$U_3^N(0) = u_3^N, U_3^N(t) = 0 \quad (2-24)$$

Rewriting the set of longitudinal displacement function equations in terms of longitudinal displacement at interfaces leads to the following equations results in the following:

$$U_1^N = u_1^N + \frac{\tau(x)}{2G_{xy}t}y^2 - \frac{\tau(x)t}{2G_{xy}} \quad (2-25)$$

$$U_2^N = 2u_2^N + \frac{\tau(x)}{G_{xy}}(y' - t) \quad (2-26)$$

$$U_3^N = u_3^N + \frac{\tau(x)}{G_{xy}} \left(y'' - \frac{y''^2}{2t} \right) \quad (2-27)$$

The longitudinal force acting on each panel is equal to:

$$N_n = b \int_0^t \sigma_n^N(y) dy \quad (2-28)$$

where b is the thickness of the panel and σ_n^N is the panel longitudinal normal stress. Eq. (2-28) for each panel can be rewritten as follows, by expressing longitudinal force in terms of elastic properties, cross-sectional area, and displacement function:

$$\begin{aligned} N_1 &= Eb \int_0^t \frac{dU_1^N}{dx} dy = Eb \int_0^t \frac{d \left(u_1^N + \frac{\tau(x)}{2G_{xy}t} y^2 - \frac{\tau(x)t}{2G_{xy}} \right)}{dx} dy \\ &= EA \left(\frac{du_1^N}{dx} - \frac{d\tau(x)}{dx} \left(\frac{t}{3G_{xy}} \right) \right) \end{aligned} \quad (2-29)$$

$$\begin{aligned} N_2 &= Eb \int_0^t \frac{dU_2^N}{dx} dy' = Eb \int_0^t \frac{d \left(2u_2^N + \frac{\tau(x)}{G_{xy}} (y' - t) \right)}{dx} dy' \\ &= EA \left(\frac{2du_2^N}{dx} + \frac{d\tau(x)}{dx} \left(\frac{t}{2G_{xy}} \right) \right) \end{aligned} \quad (2-30)$$

$$\begin{aligned} N_3 &= Eb \int_0^t \frac{dU_3^N}{dx} dy'' = Eb \int_0^{t_3} \frac{d \left(u_3^N + \frac{\tau(x)}{G_{xy}} \left(y'' - \frac{y''^2}{2t} \right) \right)}{dx} dy'' \\ &= EA \left(\frac{du_3^N}{dx} + \frac{d\tau(x)}{dx} \left(\frac{t}{3G_{xy}} \right) \right) \end{aligned} \quad (2-31)$$

Now that the two required functions for the longitudinal strain between two adjacent panels are obtained, by substituting Eq. (2-29) to Eq. (2-31) into Eq. (2-3) and then into Eq. (2-1), the strain can be expressed as shown in Eq. (2-32) to Eq. (2-34):

$$\varepsilon_1(x) = \frac{du_1(x)}{dx} = \frac{M_1(x)t}{2EI} + \frac{N_1(x)}{EA} + \frac{d\tau(x)}{dx} \left(\frac{t}{3G_{xy}} \right) \quad (2-32)$$

$$\varepsilon_2(x) = \frac{du_2(x)}{dx} = \frac{-M_2(x)t}{2EI} + \frac{N_2(x)}{2EA} - \frac{d\tau(x)}{dx} \left(\frac{t}{2G_{xy}} \right) \quad (2-33)$$

$$\varepsilon_3(x) = \frac{du_3(x)}{dx} = \frac{-M_3(x)t}{2EI} + \frac{N_3(x)}{EA} - \frac{d\tau(x)}{dx} \left(\frac{t}{3G_{xy}} \right) \quad (2-34)$$

The shear stress between two adjacent panels can be expressed as:

$$\tau(x) = \frac{K_s \cdot n^*}{S} (u_{n+1}(x) - u_n(x)) \quad (2-35)$$

where K_s is the shear stiffness of a fastener (kN/mm), n^* is the number of fasteners per row, and S is the distance between two adjacent fasteners. The longitudinal displacements, $u_{n+1}(x)$ and $u_n(x)$, are at the top of panel $n+1$ and at the bottom of panel n . After substituting Eq. (2-32) – Eq. (2-34) into the derivative of Eq. (2-35), the interlayer shear stress can be expressed as:

$$\begin{aligned} \frac{d\tau(x)}{dx} = \frac{K_s \cdot n^*}{S} \left[\frac{-M_2(x)t}{2EI} + \frac{N_2(x)}{2EA} - \frac{d\tau(x)}{dx} \left(\frac{t}{2G_{xy}} \right) - \frac{M_1(x)t}{2EI} - \frac{N_1(x)}{EA} \right. \\ \left. - \frac{d\tau(x)}{dx} \left(\frac{t}{3G_{xy}} \right) \right] \end{aligned} \quad (2-36)$$

The first derivative of the equation gives:

$$\begin{aligned} \frac{d^2\tau(x)}{dx^2} = \frac{K_s \cdot n^*}{S} \left[\frac{-t}{2EI} \frac{dM_2(x)}{dx} - \frac{d^2\tau(x)}{dx^2} \left(\frac{t}{2G_{xy}} \right) - \frac{t}{2EI} \frac{dM_1(x)}{dx} - \frac{1}{EA} \frac{dN_1(x)}{dx} \right. \\ \left. - \frac{d^2\tau(x)}{dx^2} \left(\frac{t}{3G_{xy}} \right) \right] \end{aligned} \quad (2-37)$$

Satisfying horizontal equilibrium gives:

$$N_1(x) = -N_3(x) = -N(x) = -b \int_0^x \tau(x) \quad (2-38)$$

And consideration of the moment equilibrium gives:

$$M_T(x) = M_1(x) + M_2(x) + M_3(x) + N_1(x).h + N_3(x).h \quad (2-39)$$

where $h = \frac{t}{2} + \frac{t}{2} = t$, knowing that the depth of all individual panels is the same and $M_T(x)$ is the total applied moment. The curvature at the interface is equal for all panels, and all panels are assumed to have the same deflection. Therefore:

$$\frac{M_1(x)}{EI} = \frac{M_2(x)}{EI} = \frac{M_3(x)}{EI} \quad (2-40)$$

Substitution Eq. (2-38) and Eq. (2-40) into the Eq. (2-39) gives:

$$\frac{M_T(x) - b \int \tau(x).2t}{3EI} = \frac{M_1(x)}{EI} = \frac{M_2(x)}{EI} = \frac{M_3(x)}{EI} \quad (2-41)$$

and with the first derivative of the equations:

$$\frac{dM_1(x)}{dxEI} = \frac{dM_2(x)}{dxEI} = \frac{dM_3(x)}{dxEI} = \frac{dM_T(x)}{dx3EI} - \frac{2tb\tau(x)}{3EI} \quad (2-42)$$

The substitution of Eq. (2-42) and the derivative of Eq. (2-38) into Eq. (2-37) yields:

$$\frac{d^2\tau(x)}{dx^2} \left(\frac{S}{n^*K_s} + \left(\frac{t}{2G_{xy}} \right) + \left(\frac{t}{3G_{xy}} \right) \right) = \frac{-dM_T(x)t}{dx3EI} + \frac{2t^2b\tau(x)}{3EI} + \frac{dN(x)}{dxEA} \quad (2-43)$$

The interlayer shear stress governing differential formula can be restated as follows:

$$\frac{d^2\tau(x)}{dx^2} - K_1b \left(\frac{2t^2}{3EI} + \frac{1}{EA} \right) \tau(x) + K_1 \left(\frac{t}{3EI} \right) V_T = 0 \quad (2-44)$$

where V_T is the total shear force of the panels. The coefficient K_1 can be calculated as Eq. (2-45)

and depends mainly on the depth of the panel and the shear modulus:

$$K_1 = \frac{1}{\frac{S}{n^*K_s} + \left(\frac{5t}{6G_{xy}} \right)} \quad (2-45)$$

The general solution to the shear stress equation can be given as:

$$\tau(x) = B_1 \cosh \cosh (\lambda x) + B_2 \sinh \sinh (\lambda x) + mV_T(x) \quad (2-46)$$

Where:

$$\lambda^2 = K_1 b \left(\frac{2t^2}{3EI} + \frac{1}{EA} \right) \quad (2-47)$$

and

$$m = \frac{K_1}{\lambda^2} \left(\frac{t}{3EI} \right) \quad (2-48)$$

The coefficients B_1 and B_2 are obtained by applying the boundary conditions.

For simplicity's sake, the general solution is limited to the uniformly distributed load over the length of the CLT panels. The applied bending moment and axial force of each panel at $x = 0$ are equal to zero. Moreover, because of the symmetry of the applied force, the shear stress at the midspan is required to be zero. Therefore, the interface shear stress can be expressed as:

$$\begin{aligned} \tau(x) = -m \frac{q}{\lambda} \left(\tanh \tanh \left(\frac{\lambda l}{2} \right) \cosh \cosh (\lambda x) - \sinh \sinh (\lambda x) \right) \\ + m q \left(\frac{L}{2} - x \right) \end{aligned} \quad (2-49)$$

In a connection with infinite stiffness, the CLT diaphragm can be considered as a solid section, and Eq. (2-49) can be simplified to:

$$\tau(x) = mV(x) = V \frac{4}{9t} \quad (2-50)$$

Eq. (2-50) is equal to the shear flow for the solid section. Therefore, the interface shear stress formula can be readily verified. The force at the panel joints along the panel interface can be determined after substituting the value of $\tau(x)$ into Eq. (2-38). The maximum amount of axial force can be calculated at the edge of the panels ($x=0$ or L):

$$N(x) = \left(-m \frac{q}{\lambda^2} \left(\tanh \tanh \left(\frac{\lambda l}{2} \right) (\lambda x) - (\lambda x) + 1 \right) + m q \left(\frac{L}{2} x - \frac{x^2}{2} \right) \right) \quad (2-51)$$

2.3.2 Diaphragm deflection in Y direction

The deflection of the diaphragm, as stated earlier, loaded perpendicular to the panel joints, corresponds with the conventional equation for a deep beam (Timoshenko 1983). However, for multi-panel diaphragms, it has an additional term to account for the slip between the panels. The Timoshenko beam theory establishes the following relationship between the bending moment, shear force, the deflection, and rotation of the cross-section:

$$\frac{dw}{dx} = \theta - \frac{EI}{kAG} \left(\frac{d\theta}{dx} \right) \quad (2-52)$$

$$-EI \frac{d\theta}{dx} = M_n \quad (2-53)$$

Where w is the deflection of the panels in the y -direction and θ represents the cross-section angle of rotation. Substituting Eq. (2-41) into Eq. (2-53) leads to:

$$\frac{d\theta}{dx} = - \frac{M_T(x) - b \int \tau(x) \cdot 2t}{3EI} \quad (2-54)$$

By using Eq. (2-44), the above equation can be restated as:

$$\frac{d\theta}{dx} = -M_T \left(\frac{1}{3EI} - \frac{K_1 \left(\frac{t}{3EI} \right)}{K_1 \left(\frac{2t^2}{3EI} + \frac{1}{EA} \right)} * \frac{2t}{3EI} \right) + \frac{2t}{3EI} * \frac{1}{K_1 \left(\frac{2t^2}{3EI} + \frac{1}{EA} \right)} * \frac{d^2N(x)}{dx^2} \quad (2-55)$$

It can easily be shown that the coefficient of M_T in this equation is the reciprocal of the flexural stiffness of an equivalent diaphragm section with three panels. As a result, Eq. (2-55) yields:

$$\frac{d\theta}{dx} = \frac{M_T(x)}{27EI} + \frac{8}{9tK_1} * \frac{d^2N(x)}{dx^2} \quad (2-56)$$

For the diaphragm subjected to a uniformly distributed load (q), the moment function is expressed as follows:

$$M(x) = q \frac{L}{2} x - q \frac{x^2}{2} \quad (2-57)$$

Substitute the above equation into Eq. (2-56), perform the integration and put it back in Eq. (2-52):

$$\frac{dw}{dx} = \frac{-q}{24EI_s} (4x^3 - 6Lx^2 + L^3) + \frac{8}{9tK_1} * \frac{dN(x)}{dx} - \frac{-q}{kAG_{eq}} \left(\frac{L}{2} - x \right) \quad (2-58)$$

The equivalent shear modulus G_{eq} comprises the total thickness, the number of layers, and the panel depth, as defined by Brandner et al. (2017). The second moment of area of the equivalent solid diaphragm is referred to by I_s . After performing the integration of Eq. (2-58) and applying the boundary condition, the deflection of the CLT diaphragm can be calculated as:

$$w(x) = -\frac{q}{24EI_s} (x^4 - 2Lx^3 + L^3x) - \frac{q}{kAG_{eq}} \left(\frac{Lx}{2} - \frac{x^2}{2} \right) + \frac{8}{9tK_1} N(x) \quad (2-59)$$

At mid-span, the deflection is simplified to:

$$w(x = L/2) = \frac{5qL^4}{384EI_s} + \frac{qL^2}{8kAG_{eq}} + \frac{mqL^2}{9tK_1} \quad (2-60)$$

The above equation can be expanded to more than three panels. However, it needs to be separated into two different formulas based on the number of panels. If there are an even number of panels in the diaphragm (n), Eq. (2-56) can be rewritten as:

$$\frac{d\theta}{dx} = \frac{M}{(3n^2 + n)EI} + \frac{3n^2}{(3n^2 + n)tK_1} * \frac{d^2N(x)}{dx^2} \quad (2-61)$$

If there are an odd number of panels (n) in the diaphragm, Eq. (2-56) is expressed as:

$$\frac{d\theta}{dx} = \frac{M}{(3(n-1)(n+1) + n)EI} + \frac{3(n-1)(n+1)}{(3(n-1)(n+1) + n)tK_1} * \frac{d^2N(x)}{dx^2} \quad (2-62)$$

So, for a diaphragm with n number of panels, the midspan deflection is equal to:

$$w(x = L/2) = \frac{5qL^4}{B384EI} + \frac{qL^2}{8kAG_{eq}} + \frac{Cm'qL^2}{8tK_1} \quad (2-63)$$

The m' factor for the slip between the panels can be written as:

$$m' = \frac{K_1}{\lambda^2} \left(\frac{t}{nEI} \right) \quad (2-64)$$

where for an odd number of the panels λ^2 is equal to:

$$\lambda^2 = K_1 b \left(\frac{(n-1)(n+1)t^2}{4nEI} + \frac{1}{EA} \right) \quad (2-65)$$

and for an even number of the panels, it is:

$$\lambda^2 = K_1 b \left(\frac{n^2 t^2}{4nEI} + \frac{1}{EA} \right) \quad (2-66)$$

When n is an odd number, B and C are as follows:

$$B = (3(n-1)(n+1) + n) \quad (2-67)$$

$$C = \frac{3(n-1)(n+1)}{B}$$

When n is an even number, B and C are shown below:

$$B = 3n^2 + n \quad (2-68)$$

$$C = \frac{3n^2}{B}$$

It is essential to acknowledge that diaphragms in structural systems can experience diverse loading and support conditions beyond the specific scenario of a uniform distributed load (UDL) supported by beams at two ends. These alternative conditions might involve point loads, varying load distributions, and different support types. The fundamental principle of diaphragm behavior analysis remains applicable across these varying conditions. By applying the same underlying principles, engineers can derive new equations tailored to each specific loading and support configuration, thus expanding the analytical to address a wide range of practical scenarios in structural engineering design. This adaptability ensures that structural engineers can effectively

assess and design diaphragms for various real-world situations while maintaining the consistency of analytical methods.

2.4 Numerical verification

A three-dimensional (3D) model was developed using an advanced FE software (Abaqus 2020) to validate the proposed analytical model. The maximum in-plane deflection of a diaphragm at the centre line predicted by the FE model was compared to that predicted by the analytical model.

As illustrated in Figure 2.5, the diaphragm under consideration consisted of three panels, each with a length of 10m and a depth of 2.4 m, and was subjected to an in-plane uniform load of 15 kN/m. Each CLT panel was composed of three 35mm thick orthogonal layers, with a total thickness of 105 mm. Each panel elastic modulus was determined in accordance with the composite theory by Blass and Fellmoser (2004) and the used shear modulus was suggested by Brandner et al. (2017).

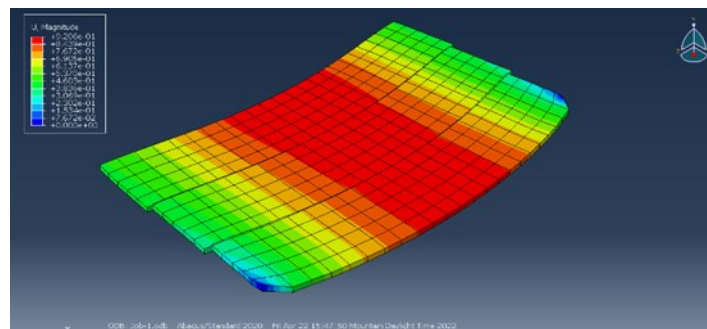


Figure 2.5: The FE model

The connection between two adjacent panels was modelled by 50 pairs of springs that were uniformly placed along the length of the panels. The connection stiffness was obtained from the study by Loss et al. (2016) who tested a connection with inclined self-tapping screws as illustrated in Figure 2.6. The y-direction stiffness of the spring was assigned a large value to ensure that all

three panels deflect by the same amount. The boundary conditions of the diaphragm are the same as the analytical model. The mid-span in-plane displacement of the diaphragm was calculated using the FE and analytical models, and assumed $K_s = 3 \text{ kN/mm}$ based on Loss et al. (2016). The calculated deflection was 3.3mm and 3.36mm based on the FE and analytical model, respectively. This represented a 2% difference between the two models. More detailed results are provided in the sensitivity analysis section.

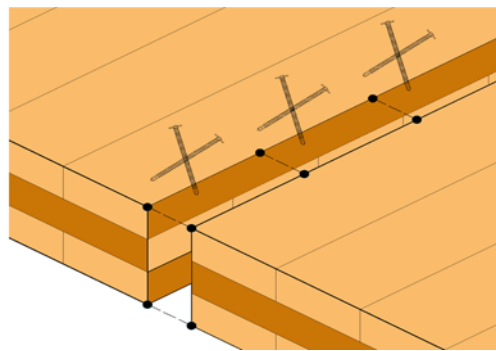


Figure 2.6: The panel to panel connection modelling.

2.5 Verification of analytical model for deflection due to bending and shear

To the authors' best knowledge, there have been no experiments in which the CLT diaphragm was subjected to a load perpendicular to the panel joints with the stated boundary conditions assumed in the analytical model. Therefore, to ensure the accuracy of the proposed analytical and numerical models, a partial verification was performed using a set of experimental result. As can be seen in Eq. (2-63), the proposed equation for diaphragm deflection under lateral loading consisted of three components. The first two terms of the equation represented the deflection induced by panel deflection (due to bending and shear), whereas the third term was related to the slip in the panel-to-panel connection. For experimental verification of the first two terms, the diaphragm was

modelled as one deep CLT panel, and the midspan displacement was compared to the experimental data on the deep CLT beam tested by Daneshvar et al. (2021), Figure 2.7(a). The test specimen was a deep CLT panel with a depth, length, and thickness of 1216mm, 5994mm, and 191mm, respectively, loaded on the edge. The CLT panel was modelled using an orthotropic 8-node solid element with similar boundary conditions to the experimental set-up. The experimental load at the proportional limit (816 kN), where the load-displacement curve started to deviate from a linear relationship, was applied to verify the model behavior in the linear regime. The numerical model under that applied in-plane load is shown in Figure 2.7(b).

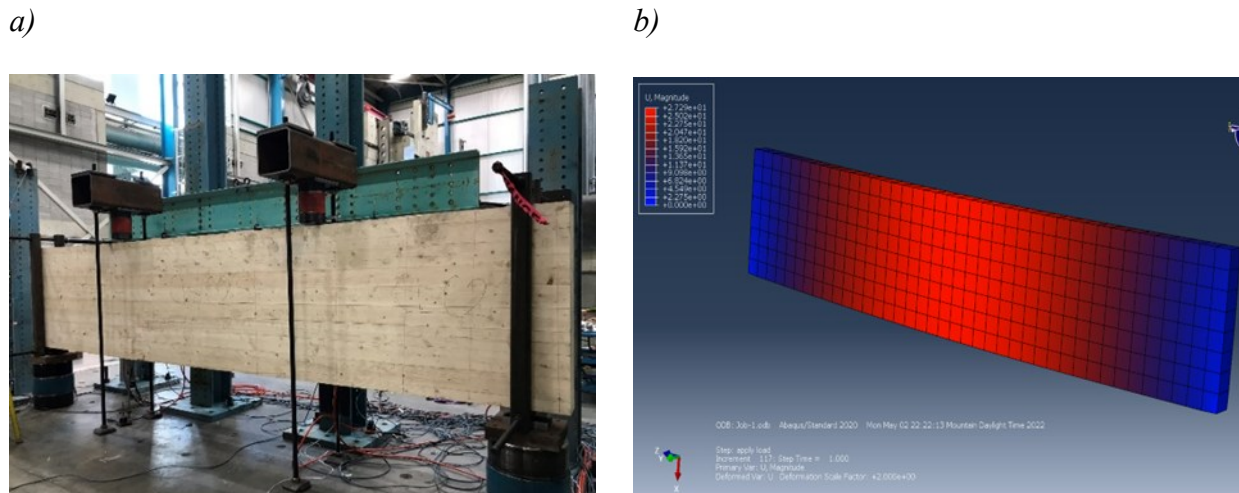


Figure 2.7: (a) test setup for deep CLT panel under in-plane loading perpendicular to the panel joints (Daneshvar et al. 2021). (b) FE model used to mimic the test results.

Figure 2.8 compares load-displacement curves of the two first terms of the analytical model, the FE model, and the experiment. It can be seen that the deflection behavior of the panel as predicted by the analytical and FE models was similar to that obtained in the experiment. The displacements from the three sources at 816 kN were about 22mm. Therefore, the results show that the first two

terms of the proposed deflection equation properly reflected the in-plane deflection of the deep CLT panels.

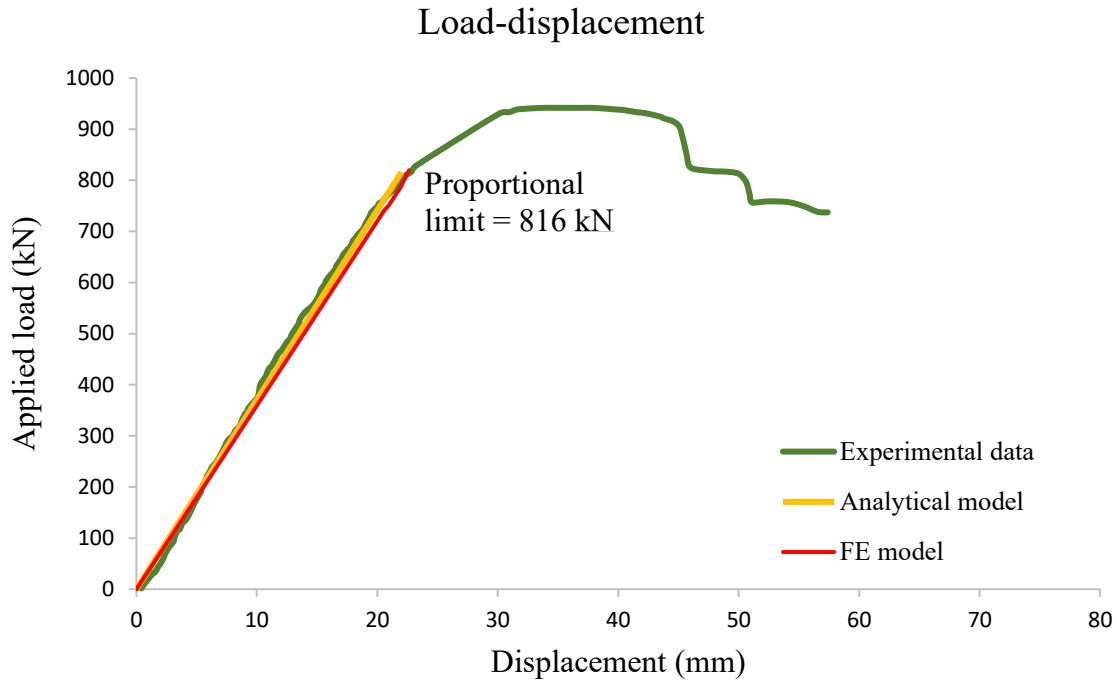


Figure 2.8: Load-displacement curves for the analytical model, FE model and the experimental data.

As indicated earlier, there was no experiment in the desired direction for verifying the third term of Eq. (2-63). However, the stiffness of the spring model adopted herein was able to reproduce the connection stiffness tested and available in the literature, e.g., Loss et al. (2016), and gave the authors confidence regarding its correctness and accuracy.

2.6 Sensitivity analysis

The in-plane deformability of the CLT diaphragm was investigated by comparing the analytical model and the finite element through a sensitivity analysis with the aim of finding the most influential parameter on the stiffness of the CLT diaphragm. The sensitivity analysis was

undertaken by varying the geometry and stiffness of the panel-to-panel connections. It was seen that the deflection of the diaphragm when the load was perpendicular to the panel joints was not strongly related to the stiffness of the connections between the panels. However, the aspect ratio has a significant effect on the deflection of the diaphragm.

Based on the test results established by Joyce (2014), Loss et al. (2016), and Hossain et al. (2019), various values for the panel-to-panel connection stiffness were considered, as shown in Table 2-1.

Table 2-1: Stiffness of the connection between the adjacent panels

Connection Configuration	Stiffness for an 8mm Screw (kN/mm)
Inclined screw, lap joint (Hossain et al. 2019)	1.8
	2.3
	2.8
Inclined screw, butt joint (Loss et al. 2016)	3
	2.6
	3.9
Inclined Screw (Joyce 2014)	0.92
	1.06
	1.4

The initial stiffness properties of the connections were calculated as per CEN (2004). In order to maximize the floor stiffness, Loss et al. (2016) placed the screws with the minimum allowed spacing and reported the joint stiffness per meter assessed with the experimental test. Hossain et al. (2019) derived a function of the slip modulus of the individual connector using a common practice for initializing the connection stiffness of laterally loaded screws provided by CEN (2004). According to Joyce (2014), the initial stiffness was calculated as the slope of the secant passing between points on the load-slip curve corresponding to 10% and 40% of the maximum load. A set of mechanical properties was derived from the plots, including the stiffness.

Different arrangements of panels with regard to the loading direction and embedment length accounted for the variation in stiffness values. In these experiments, every wood element was restrained to avoid deflection in the out-of-plane direction.

A range of screw stiffness between 1 kN/mm and 4 kN/mm was adopted in this study. As can be seen in Figure 2.9, the analytical model was not sensitive to the change of connection stiffness at all, within the stiffness range considered. However, while such connection stiffness alteration in the FE model would lead to an approximate change of 10% in the diaphragm deformation. As a result, as verified by the results of both the Abaqus model as well as the analytical model, it can be observed that the stiffness of the connections had no significant effect on the diaphragm deflection. Equation (1-45) demonstrates that the coefficient K_1 , which is influenced by the connection stiffness in the formula, primarily relies on the panel's depth and the shear modulus.

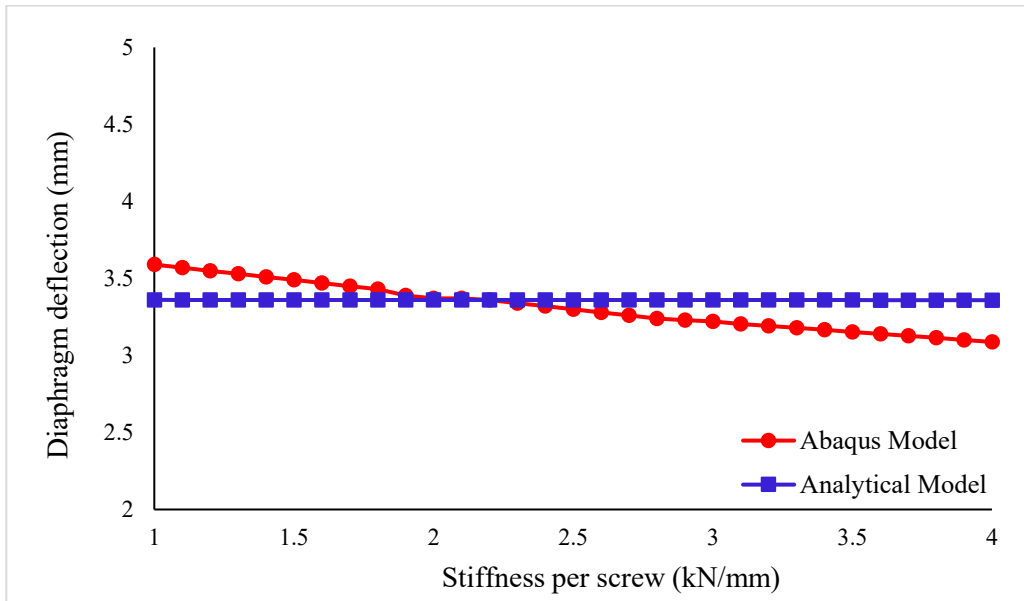


Figure 2.9: The diaphragm deflection versus stiffness of the connection.

A sensitivity analysis of the panel aspect ratio was carried out in order to investigate the impact of panel depth on the shear-induced deflection. The diaphragm length, L , and thickness, b , were

constant, whereas the diaphragm depth ranged from 5 to 12 m. As shown in Figure 2.10, the aspect ratio, defined as the ratio of the diaphragm length to the depth (L/W), significantly impacted the diaphragm deflection that occurred along the Y-direction.

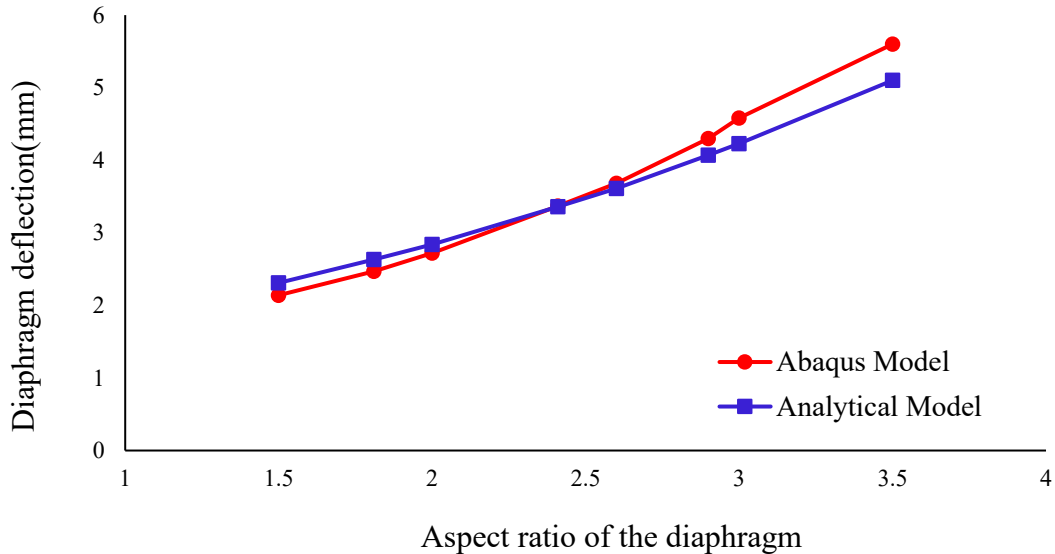


Figure 2.10: Diaphragm deflection against the aspect ratio of the diaphragm.

2.7 Parametric study

When the load was applied perpendicular to the panel joints, the total deflection of the diaphragm was a result of the bending deflection, shear deflection, and slip in the panel-to-panel connection, as evident in Eq. (2-63). A parametric study was carried out based on the analytical model to provide insights into the contribution of each of these components to the overall diaphragm deflection. The diaphragm was subjected to an in-plane uniform horizontal load, $q = 15 \text{ kN/m}$, as seen in Figure 2.4(a). The thickness was 105mm while the length diaphragm $L = [5, 10, 15, 20, 25, 30] \text{ m}$, and the total depth of the diaphragm $B = [7.2, 9.6, 12, 14.4, 16.8] \text{ m}$. Figure 2.11 shows the diaphragm deflection for all the combinations of diaphragm dimensions. The x-axis represents

the diaphragm depth with the constant CLT panel depth of 2.4 m and the y-axis represents the contribution of each deflection component to the overall diaphragm deflection. The composite elastic modulus, E , and the shear modulus, G_{eq} , were assumed to be 11500 MPa and 500 MPa, respectively.

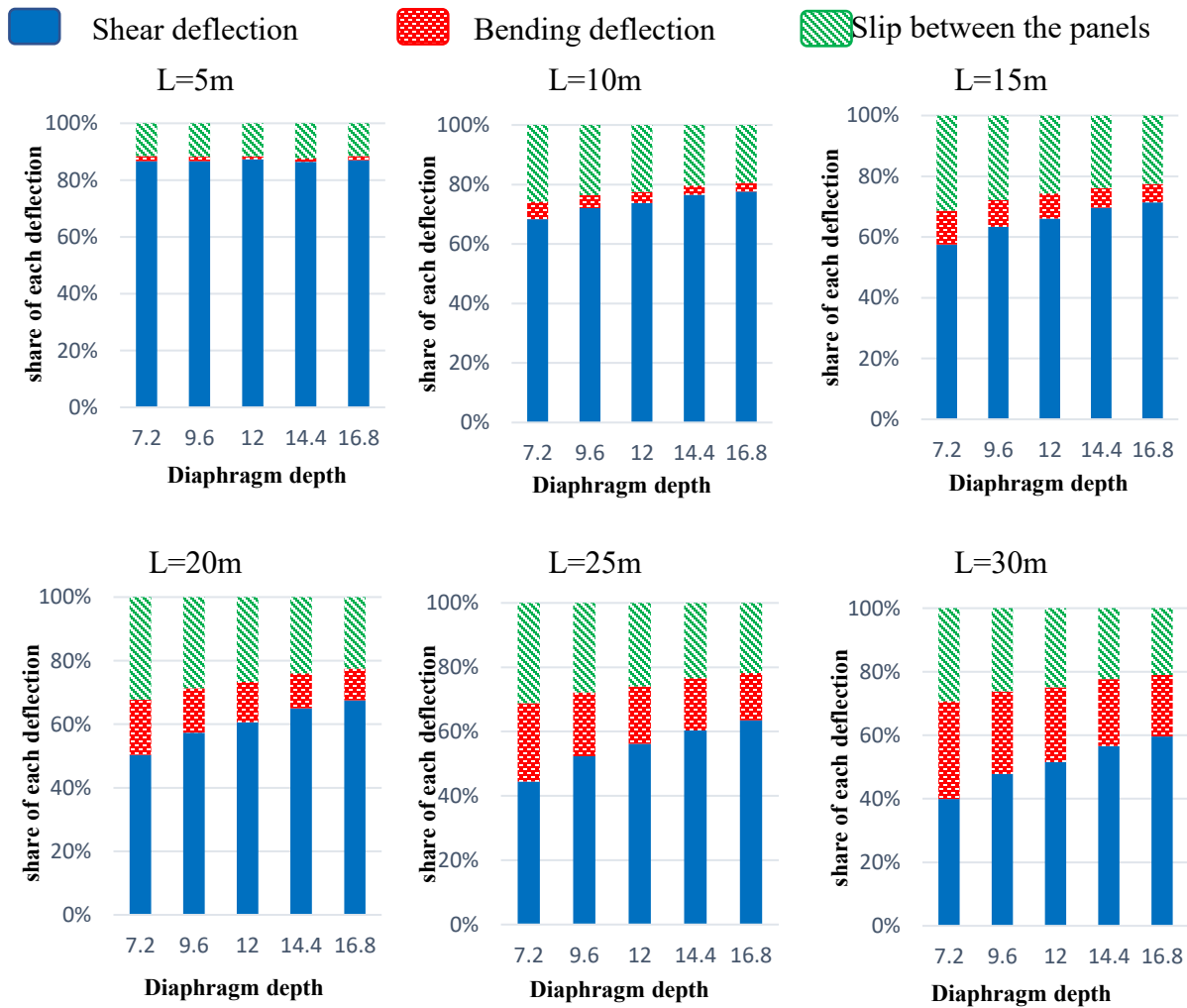


Figure 2.11: Shear, bending and Slip deflection contribution [%] against floor depth

As can be seen in Figure 2.11, the majority of the deflection was due to shear deflection, and the bending made more contributions as the span length increased. It is worth noting that as the diaphragm length increased, the slip between panels increased. This can be assigned to the

increased number of connection joints in the floor, the most flexible part of the system. Nevertheless, for L more than 20 m, the contribution of slip deflection to the total deflection was decreasing, relative to the contribution of bending and shear deflection. The largest contribution of slip was for the case where the depth of the diaphragm was 7.2 m and $L = 20$ m (32.3%). The maximum slip and minimum shear contributions occurred at a minimum diaphragm depth.

For L up to 20m, (larger L are more common situation in practice) the shear contribution was always more than 50% where the slip between the panels accounted for the majority of the remaining contribution. As a result of the high shear contribution of the panels, the depth and the thickness of the panels had a significant effect on the diaphragm's performance.

2.8 Conclusion

The key conclusions that can be drawn from this study are the following.

- Based on the layered deep beam theory, an analytical model was developed for calculating the mid-span deflection of a simply supported diaphragm when loaded perpendicular to the CLT panel's joints. The model accounted for the effect of bending and the shear deflections of each panel and the slip between the panels. The same derivation also led to the development of an analytical model for predicting the force in the connection between adjacent CLT panels. When compared with FE results, it was confirmed that the analytical model predictions are in good agreement with those predicted by a FE model.
- The results from a parametric study to investigate the contributions of bending, shear, and connection slip contributions to total diaphragm deflection have revealed that shear deflection in the CLT panels provided the largest contribution to the total diaphragm

deflection when loaded perpendicular to the panel joints. The proportion of bending deflection increased with the diaphragm's span.

Chapter 3: Numerical parametric study of cross-laminated timber diaphragms under in-plane loading

3.1 Abstract

CLT is a mass timber product that has gained recognition as a viable structural product for tall and large structures. While CLT provides several advantages, such as being eco-friendly, lightweight, and improving thermal insulation compared to other primary structural materials, its application in the horizontal diaphragms, specifically for floors and roofs, has not been thoroughly investigated. This paper presents the development of a detailed finite element FE model capable of simulating the response of CLT diaphragms under in-plane loading. The accuracy of the developed models was evaluated through a comparison with available experimental data. Additionally, a comprehensive parametric study was conducted to examine the influence of various factors, including connection stiffness, boundary condition, panel installation pattern, and panel thickness, on the in-plane deflection of the CLT diaphragm. The research indicates that panel-to-panel connections play a more critical role in determining the stiffness of CLT structures than panel-to-beam connections. Furthermore, it was demonstrated that the deflection of CLT panels was influenced by different parameters depending on the orientation of the applied load. When the load is applied perpendicular to the panel joints, panel thickness influences the diaphragm deformation. Conversely, when the load is applied parallel to the panel joints, the panel-to-panel connection stiffness has a more significant effect on the deformation of the diaphragm. Findings also revealed that staggered CLT panel layouts provided more load distribution and

higher capacity than non-staggered layouts when the loading was applied perpendicular to the panel joints.

3.2 Introduction

CLT has recently garnered attention as a new structural material in buildings. CLT panels consist of several layers of laminations stacked crosswise and glued together, leading to various benefits. These include enhanced dimensional stability and the capacity to prefabricate large floor slabs and walls. Compared to other materials in the construction industry, CLT is eco-friendly, lightweight, and provides better thermal insulation. However, in North America, a lack of knowledge and resources regarding its performance under different loading scenarios is one of the main obstacles to the widespread use of CLT as a primary building material (Chui et al. 2019).

One application of CLT panels not yet thoroughly investigated in research is the horizontal diaphragm as floors and roofs. The design of the CLT diaphragm is required to withstand the applied lateral load and transfer it to the vertical lateral-load resisting systems (LLRS). However, factors affecting the performance of the CLT diaphragm, such as in-plane elastic properties, Panel-to-Panel Connections (PPC), Panel-to-Beam Connections (PBC), and supporting beams, are poorly understood. Consequently, current codes and standards provide inadequate guidance on the methods to analyze and design CLT diaphragms.

A few studies have been conducted to investigate the in-plane shear strength of CLT panels (Brandner et al. 2013; Flaig and Blaß 2013; Gagnon et al. 2014; Gsell et al. 2007; and Joyce 2014) which might be relevant to the topic under investigation. Based on beam theory, Brandner et al. (2017) performed an experimental investigation to determine the net and gross shear strengths of CLT diaphragms. Twenty-three feature series with different parameters, such as the various

number of layers, presence/absence of edge gluing, and different board widths and thicknesses, were tested. These tests indicated that layer thickness and gap execution were the most significant factors in determining the in-plane shear strength.

In terms of the influence of connection behavior, experiments on the CLT PPC comprising self-tapping screws (STS) subjected to monotonic loading (Loss et al. 2016), cyclic loading (Gavric et al. 2015), or both (Afrin 2019) have been conducted. (Sullivan et al. 2018) examined various PPC, such as surface spline and half-lap connections. The results were compared with the design values derived from the US National Design Specification (NDS) for wood construction (AWC 2014) and Eurocode 5 (CEN 2004). The findings indicated that when the load is parallel to the panel joints, the primary cause of in-plane deflection in CLT diaphragms is the PPC.

A few researchers have examined the behavior of CLT diaphragms under in-plane loading in full-scale experiments. Beairsto (2020) tested two CLT diaphragms ($4.57 \text{ m} \times 4.57 \text{ m}$) under monotonic and cyclic loading to evaluate diaphragm ductility. The tests showed that the ductility of the CLT diaphragm is strongly dependent on the performance of PPC, as the panels behaved mostly rigidly. Kode et al. (2021) studied a $5.0 \text{ m} \times 4.7 \text{ m}$ CLT diaphragm in a cantilever configuration under cyclic loading. The experimental design was developed by incorporating engineering mechanics principles and the US National Design Specification (NDS) requirements for wood construction (AWC 2018). These results confirmed the rigid behavior of the panels and showed that most energy dissipation occurred in the connections.

Pei et al. (2018) conducted a series of shake table tests on a two-storey, 6.7 m tall CLT structure. The roof and floor diaphragms in the specimens consisted of 3-ply CLT panels, using a plywood surface spline with screws to connect the panels. The maximum roof displacement was approximately 350 mm, corresponding to a 5.2% overall drift across the building height. The

results demonstrated that CLT diaphragms are significantly more rigid than wood-frame floor diaphragms with wood-based sheathing panels and could withstand seismic forces without exceeding a drift value of 5%. Barbosa et al. (2021) described the behavior of the CLT diaphragm during a shaking table experiment. They confirmed that a comprehensive diaphragm design must account for the sources of overstrength, e.g., panel material properties, and connection characteristics. Barbosa et al. (2018) proposed a Finite Element (FE) modeling approach for CLT diaphragms that utilizes nonlinear springs to represent the connectors and orthotropic four-node shell elements to model the CLT panels. The results of the nonlinear analysis agree well with the shake table test data. They found that it was essential to incorporate friction between the panels in the analysis in order to calibrate the force-deformation curves. Breneman et al. (2016) proposed another two-dimensional FE model to predict the response of a CLT diaphragm under in-plane loading. The connections between the panels were modeled as two-point springs, and the CLTs were modeled using an orthotropic shell element. They compared the FE model predictions with results from design calculations presented by Spickler et al. (2015) to validate the modeling approach. Although the proposed numerical modeling approaches were promising for design purposes, proper validation using test data is required before they can be used with confidence, by designers.

Previous studies on diaphragm behavior revealed that panels behaved mostly rigidly while the connections accommodated inelastic deformation (Popovski and Karacabeyli (2012); Ceccotti et al. 2013; Shahnewaz et al. 2018). Additionally, the results of the previous studies highlighted the need to design tension and compression chords to resist the imposed in-plane bending action of the diaphragm. When the load is applied parallel to the panel joints, PBC are designed to resist the tensile and compressive forces in chords, while panels resist the in-plane bending action when the

load is applied perpendicular to the panel joints, as shown in Figure 3.1. Therefore, to examine the response of the connections, more tests were conducted, studying the case where in-plane loads are applied parallel to the CLT panel joints. However, the case of the load applied perpendicular to the panel joints in the CLT diaphragm has been neglected, even though, in practice, any CLT diaphragm is subjected to loads in both directions.

Fakhrzareei et al. (2023) developed an analytical model for the in-plane behavior of CLT diaphragms subjected to loads applied perpendicular to the panel joints. The model takes into account the effects of bending, shear deflections of CLT panels, and slips in the PPC. This study quantified the contribution of each deflection component and found that the shear deflection in CLT panels contributes the most to the total diaphragm deflection when the load is perpendicular to the panel joints. Furthermore, the research study verified that the PPC played a significant role in causing diaphragm deformation. Recently, Line et al. (2022) conducted experiments on two CLT diaphragms loaded parallel to and perpendicular to the panel joints. The first part of the research objective was to evaluate the current CLT diaphragm design provisions in ANSI/AWC Special Design Provisions for Wind and Seismic (AWC 2021). The CLT panels in their test specimens were connected with plywood surface splines and fastened to glulam beams using STS. In the second part of the research, Line et al. (2022b) conducted a series of correlated diaphragm connection tests to generate input data for evaluating the ANSI/AWC special design provisions (AWC 2021) and to predict the load-displacement response of the CLT diaphragms tested in Line et al. (2022). Their study was motivated by the need to analyze the CLT diaphragm when loaded parallel or perpendicular to the panel joints. Their research was expected to contribute to the next edition of the US timber design standard by providing valuable information on diaphragm response under lateral loading, considering different sizes and configurations of diaphragms.

This study presents the development of several FE models to assess the performance of CLT diaphragms when an in-plane load is parallel and perpendicular to the panel joints. Experimental data from a previous study by Line et al. (2022b) was first used to validate the predictive capabilities of the models. Subsequently, a comprehensive parametric study was conducted to evaluate the impact of various parameters, including connection stiffness, the effect of boundary conditions on the deflection of various CLT diaphragm configurations, CLT panel installation patterns in the diaphragm, and panel thickness. It is worth mentioning that D'Arenzo et al. (2019) conducted a parametric study on the behavior of CLT diaphragms subjected to in-plane loading parallel to the panel joints only and conducted a sensitivity analysis on the stiffness of the connections between panels. The present research focused on the response of CLT diaphragms in both directions, as well as investigating other parameters in addition to connection stiffness. The results of the current study will provide designers with information on the behavior of CLT diaphragms as a part of the LLRS of buildings so that they can use such an environmentally friendly option for floor or roof systems with confidence.

3.3 Finite element (FE) model development

The commercial FE software, Abaqus (2020), was used to develop three-dimensional (3D) models of the CLT diaphragms loaded parallel and perpendicular to the panel joints. To adequately account for the influential factors on diaphragm performance, the model consisted of three primary components: CLT panels, glulam beams underneath, and connections (PPC and PBC). In the following sections, the diaphragm modeling details are discussed.

3.3.1 Finite element (FE) modelling approach

Two diaphragms were simulated, each comprising twelve CLT panels oriented in two orthogonal directions. One diaphragm was subjected to in-plane loading parallel to the panel joints, while the other was exposed to loading that was applied perpendicular to the panel joints. Glulam beams were used and modeled at the boundary of the panels to support the CLT panels. The glulam beams were positioned to resist the weight of the CLT panels and to function as tension and compression chords when the load was applied parallel to the panel joints. The panels and beams were considered orthotropic deformable components, while the PBC and PPC were simulated as nonlinear springs. Figure 3.1(a) and (b) show the diaphragm assemblies when the load is applied parallel and perpendicular to the panel joints, respectively.

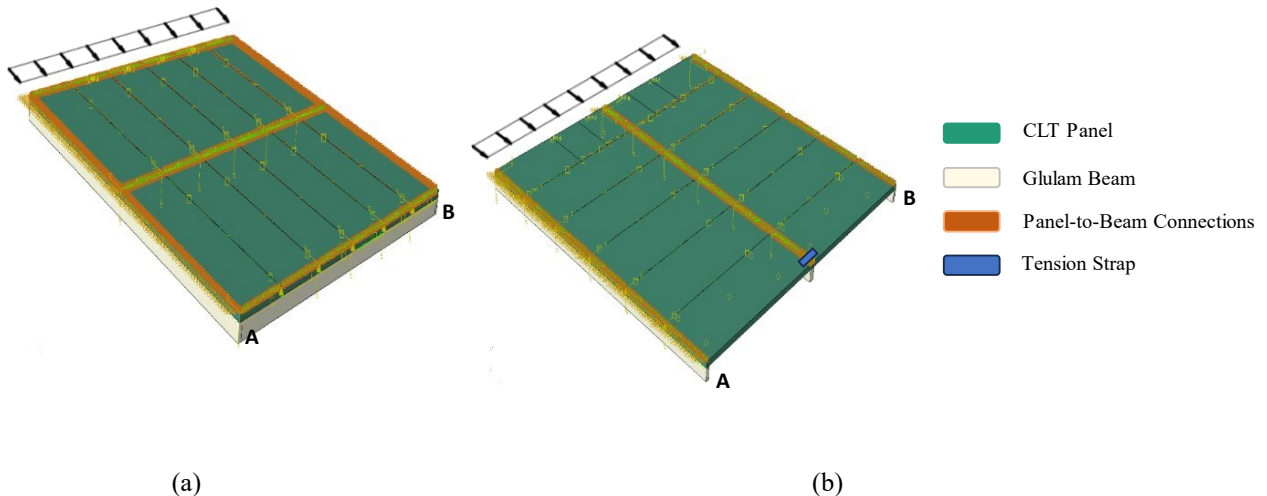


Figure 3.1: Diaphragm assemblies when the load direction is applied (a) parallel to the panel joints or (b) perpendicular to the panel joints.

3.3.2 Connections

Two-point spring elements were employed to model the PPC and PBC. Each fastener point was connected to a CLT panel through a connector element that links the displacement and rotation of

each fastener point to the mean displacement and rotation of the surrounding nodes. Using the connector element to simulate the fasteners requires the definition of the target and source faces for the linked parts. This attachment set gives the FE model a line between points to apply the spring characteristics. The locations of the springs correspond to the locations of the fasteners in the diaphragm. Figure3.2 illustrates the PPC and PBC in the Abaqus model.

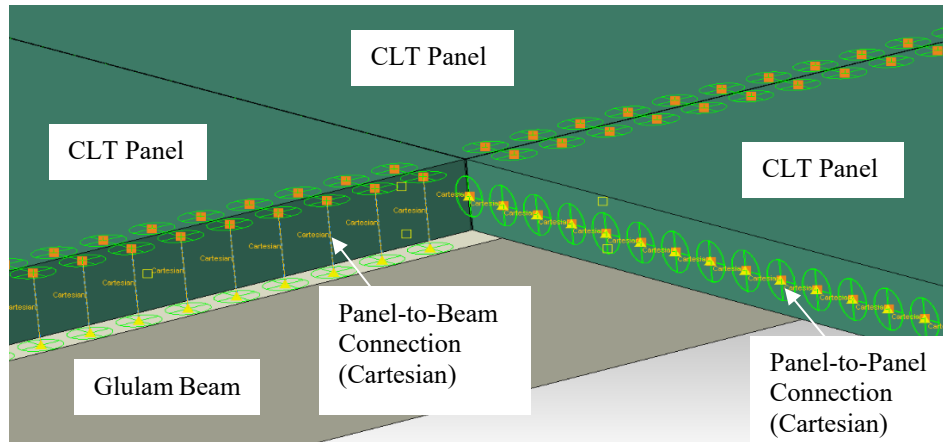


Figure3.2: Details of connections in the developed FE models.

3.3.3 Constraints and boundary conditions

As shown by points A and B in Figure 3.1, the diaphragms are assumed to be pinned at their far corners in the plane of loading. The edges of the perimeter beams were pinned so the assembly could bend inward while its movement was restrained in the direction of loading. A coupling constraint approach known as fully restricted contact behavior was used to ensure stable application of the expected load. The restriction prohibits slave nodes (the location of the applied loads) from detaching or sliding along the master surface (the edge surface of CLT panels). For simulating the physical contact between two individual components, contact was defined as frictionless tangential behavior and normal behavior with hard contact, preventing significant movement or shifting of the components towards each other.

3.4 Model validation

3.4.1 Selected experimental study

FE models were compared with the results from full-scale CLT diaphragm tests reported by Line et al. (2022a) introduced in Section 3.2, to evaluate the validity of the modeling approach. In their experiments, two diaphragms were tested: one loaded parallel to the panel joints and the other perpendicular to the panel joints, as shown in Figure 3.3. Twelve 1.22 m × 3.66 m CLT panels of spruce-pine-fir (SPF) locally sourced E1M5 grade (Structurlam 2021) were used to form the diaphragms, with plywood splines at the joining lines of the panels. The manufacturer formulated this specific configuration of a three-ply layup in accordance with ANSI/APA PRG 320 (APA 2019). Machine stress-rated lumber was employed for the exterior plies, while the central ply was constituted using visually graded lumber.

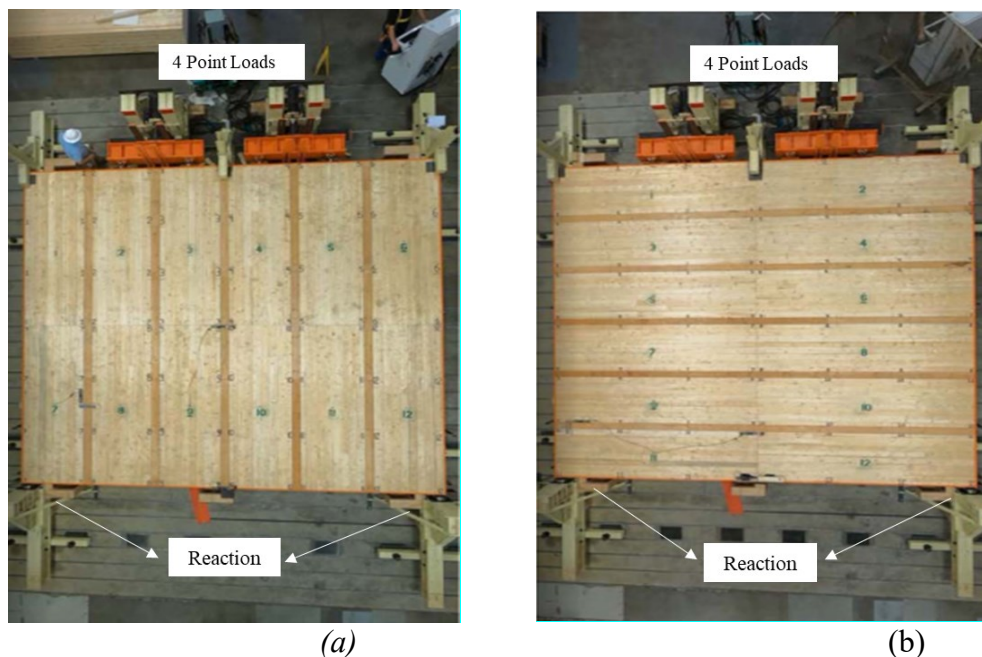


Figure 3.3: Test specimen loaded (a) parallel to the panel joints (CLT_01); (b) perpendicular to the panel joints (CLT_02) (figures from (Line et al. 2022a), used with permission).

The diaphragms were tested using a four-point bending arrangement with simple support conditions. The load was applied monotonically using a constant cylinder crosshead speed of 7.6 mm/min. When the load is perpendicular to the panel joints, a custom metal tension strap was employed to connect the panels at the tension chord. The PPC utilizes 18.3 mm thick plywood and power-driven nails (3.3 mm × 63.5 mm). Self-tapping screws were used without pre-drilling for the PBC (7.9 mm × 200 mm). The deflection of the diaphragm at mid-span was measured using a linear variable differential transformer (LVDT).

3.4.2 FE model inputs

For each diaphragm test, twelve CLT panels measuring 1.22 m × 3.66 m were simulated in the model. The thickness of the panels was set to 105 mm, representing a three-ply CLT panel. For glulam beams, a rectangular cross-section beam was used with the same arrangement as the experimental study (Line et al. 2022b), such that a width dimension of 130 mm was selected for the center bearing point of the beam and 80 mm for the beams around the diaphragm perimeters. The widths accommodate the edge panel end and edge distance requirements of the screws used for panel-to-beam attachment (Line et al. 2022b). The elastic property values employed in the modeling are shown in Table 3-1

Table 3-1: Elastic mechanical properties of CLT panels and glulam beams used as input for the FE models (Line et al. 2022a)

Elastic property	CLT Panels	Glulam beams
Elastic Modulus (MPa)	$E_1 = 11721$ $E_2 = 8274$ $E_3 = 500$	$E_1 = 12411$ $E_2 = 620$ $E_3 = 992$
Shear Modulus (MPa)	$G_{12} = 500$ $G_{13} = 600$ $G_{14} = 600$	$G_{12} = 886$ $G_{13} = 886$ $G_{14} = 89$
Poisson's ratio	$\nu_{12} = 0.4$ $\nu_{13} = 0.4$ $\nu_{23} = 0.4$	$\nu_{12} = 0.3$ $\nu_{13} = 0.3$ $\nu_{23} = 0.3$

The connector definition set for the PPC and PBC was the basic cartesian connector type with no rotation (Abaqus 2020). The behavior of the fasteners was characterized by elastic, elasto-plastic, and damage responses, including damage initiation and propagation. Initiation of damage was defined as when the force in a connection reached its maximum capacity. Upon additional loading, there is a further evolution of damage, leading to irreversible damage and eventual failure [30]. If damage has occurred, the force response in the connector component will change according to the following general form Abaqus (2020), at the damage evolution stage.

$$F = (1 - d_i)F_{effi}, \quad 0 \leq d_i \leq 1$$

Where d_i is a scalar damage variable and F_{effi} is the response in the connector component of relative motion i if damage were not present. Prior to damage initiation, d_i is zero. Once the damage has been initiated, the damage variable will monotonically increase to its maximum value of 1.0. Complete failure occurs when $d = 1.0$ (Abaqus 2020). The connection stiffness values in elastic and plastic regions, as well as maximum deformation, were generated from the load-displacement

graphs of a series of correlated connection tests, performed and reported by Line et al. (2022b). The observations from the results depicted in Figure 3.4 for PBC indicate that when the applied load reaches a value of 60 kN for loading perpendicular to the panel joints and 48 kN for loading parallel to the panel joints, initial damage occurs in the connection (Line et al. 2022b). As the degree of scalar damage increases, the load-carrying capacity of the connection decreases. The progressive evolution of the damage continues until failure occurs in the connection tests.

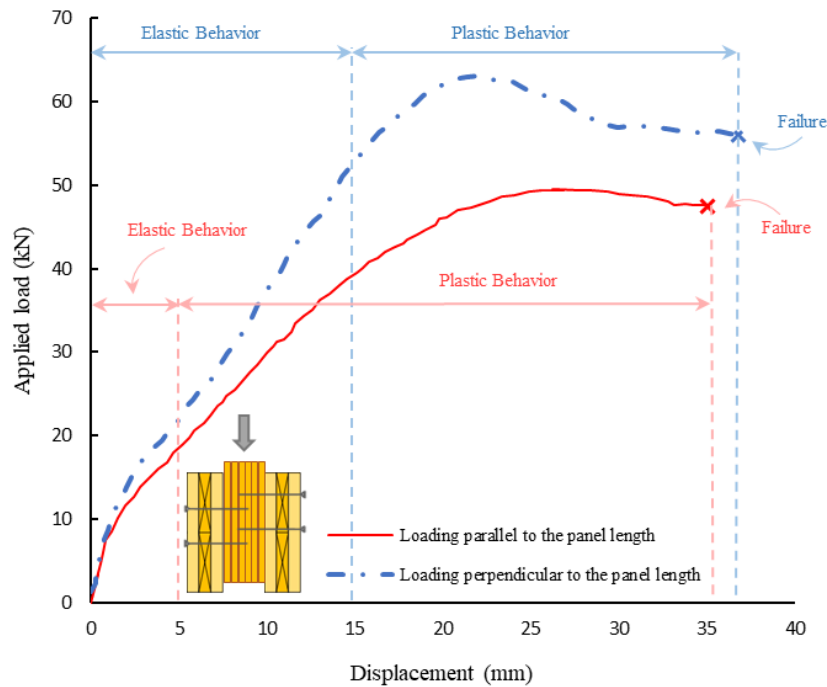


Figure 3.4: Load-displacement curves for panel-to-beam connections [28]

Figure 3.5 shows the PPC load-displacement curve with both CLT and plywood oriented with their face grain parallel to the load. The elastic stiffness of the connections was derived from the linear section of the load-displacement curve, while the plastic properties were obtained from the nonlinear section. The damage values were obtained from the final stages of the test. The load in

the graphs has been reduced by a factor of 4 to account for the fact that each connection specimen contained four nails or screws.

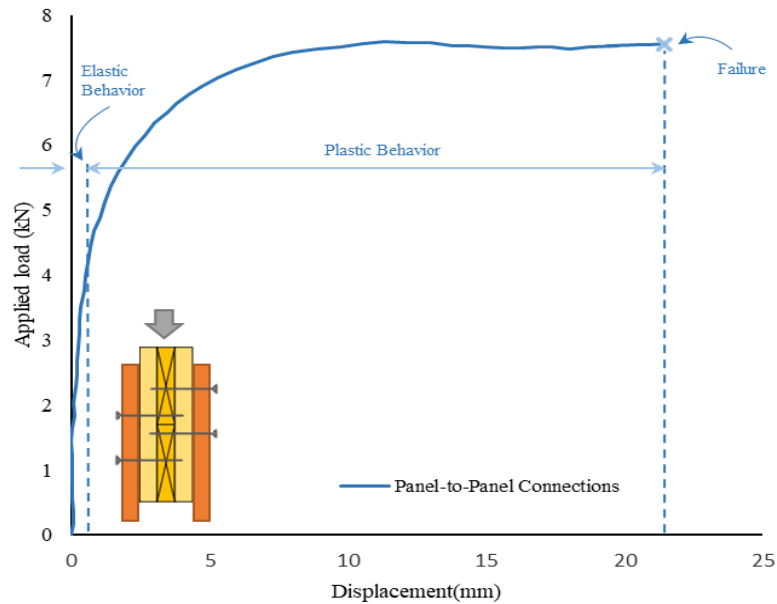


Figure 3.5: Load-displacement curve for panel-to-panel connections [27]

3.4.3 Tension strap modeling

The tension strap was modeled as deformable shell elements of size 22 mm × 140 mm using a 4-node thin shell element with reduced integration (S4R) (Abaqus 2020), as shown in Figure 3.6 (red color element). The yield stress and Poisson's ratio of the steel are assumed to be 690 MPa and 0.2, respectively (Line et al. 2022b).

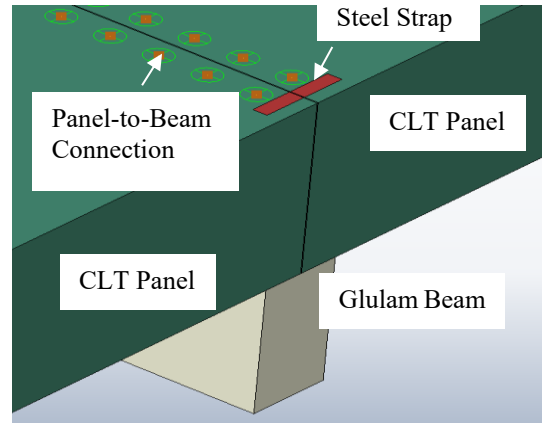


Figure 3.6: Shell elements used to model tension strap.

3.4.4 Comparison of test results and FE model predictions

The experimental and numerical load-displacement curves are compared in Figure 3.7 when the applied load (reaction load) is parallel to the panel joints (CLT_01) and perpendicular to the panel joints (CLT_02). The dashed lines represent the experimental results, and the solid lines represent the FE simulation results. A comparison between the experimental and numerical results shows close agreement between the two.

Results obtained from the experimental investigation of PBC reveal that all the examined screw configurations successfully attained the nominal capacity targets, irrespective of their type, penetration, or load orientation (Line et al. 2022b). These outcomes offer insights into the stress levels observed and the absence of failures in PBC in full-scale diaphragm testing (Line et al. 2022a). At the peak reaction loads in diaphragms CLT_01 and CLT_02, the PBC loads were 6.43 kN and 7.61 kN per screw, respectively, with the associated panel-to-beam slip of approximately 10.9 mm and 10.2 mm (Line et al. 2022b). In contrast, the FE simulation predicted screw loads of 7.2 kN and 8.4 kN (only 10% difference) per screw along the reaction beams for specimens CLT_01 and CLT_02 at the same peak reaction loads, respectively. In addition, the corresponding panel-to-beam slips were predicted to be 12.1 mm and 15 mm (Line et al. 2022b). The

experimental and numerical results revealed the yielding of the PBC in both specimens, CLT_01 and CLT_02. However, they remained below their maximum load capacity.

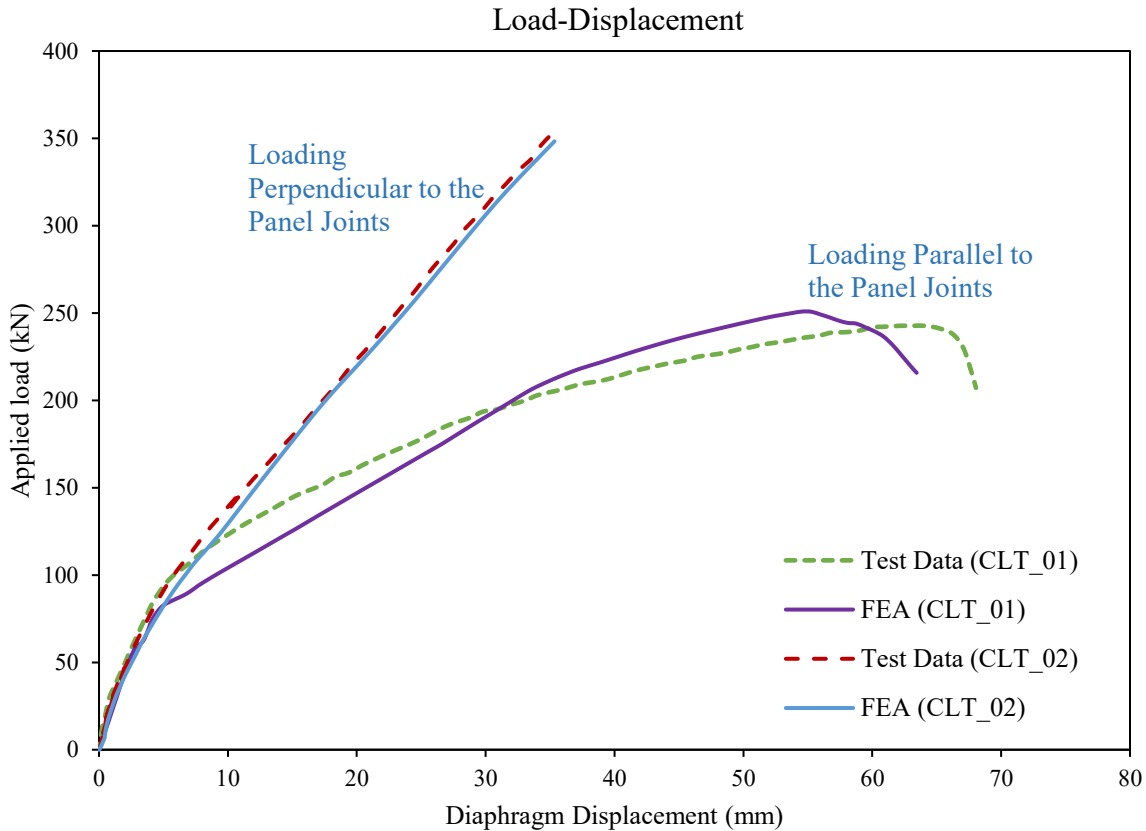
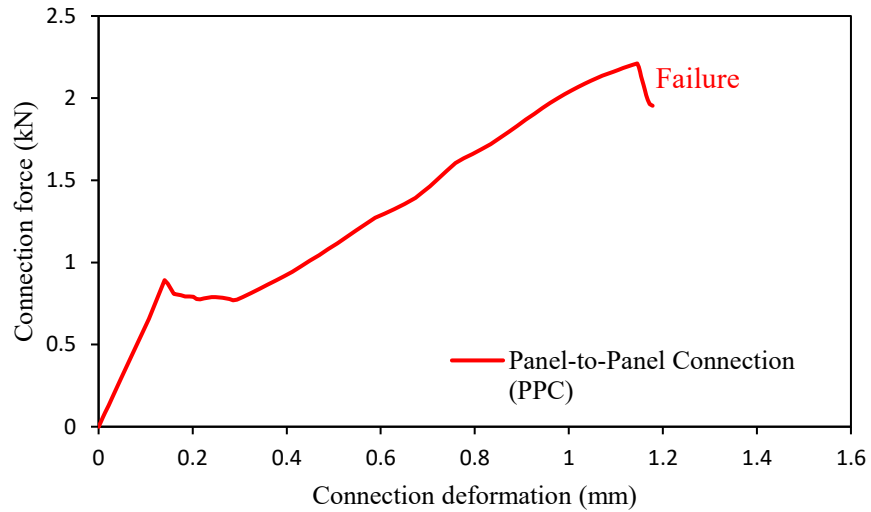


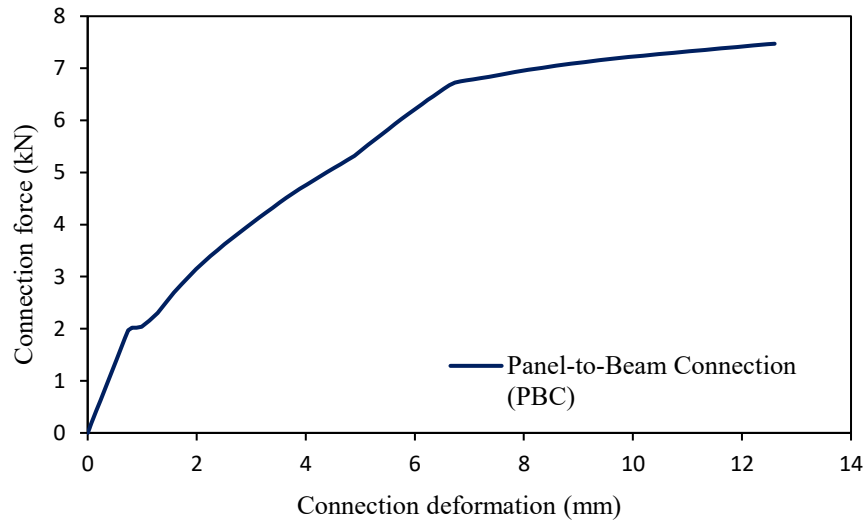
Figure 3.7: Mid-span load-displacement curve for diaphragm under in-plane loading; numerical versus experimental.

In the full-scale diaphragm experiment, when the diaphragm was loaded parallel to panel joints, failure was seen at PPC near the reactions, and the applied load at failure was 243.9 kN for 99 affected nails (2.46 kN per nail) (Line et al. 2022a). The connection test of this investigation failed with a 15% lower average load of 2.09 kN per nail (Line et al. 2022b). It is worth noting that the nominal diaphragm shear capacity of 1.71 kN per nail for the splines resulted in 99 nails across the diaphragm length and width, resulting in a total nominal diaphragm shear capacity of 170 kN ($1.71 \text{ kN} \times 99$), and based on the result, the diaphragm failed at a load that was 44% greater than the calculated nominal capacity (Line et al. 2022a).

In the numerical model, plastic deformation in PPC was initiated at an in-plane deformation of 7 mm, where the applied load was approximately 70 kN (initiation of yielding in PPC). The simulation stopped at the applied shear load of 248 kN, where the PPC load was 2.21 kN and was considered to have failed. The numerical model predicted the post-peak behavior of the CLT diaphragm when the load is parallel to the panel joints. The comparison between the numerical and experimental curves shows that the developed numerical model can predict general load-displacement behavior. The estimated displacement at the midspan in the direction of loading was $U=64.5$ mm (less than a 10% difference from the experimental result). Figure 3.8 shows the applied load and deformations of a PPC and PBC for CLT_01. As can be seen, the load-displacement curves were well predicted, given that the experimental peak load values are 2.46 kN for PPC and 6.43 kN for PBC (Line et al. 2022a). It is worth noting that the displacement-controlled method was employed to run the FE models.



(a)



(b)

Figure 3.8: Load-displacement diagrams for: (a) panel-to-panel connection (PPC), (b) panel-to-beam connection (PBC)

In the experiment, the CLT_02 diaphragm was loaded three times to investigate the failure mode of the specimen. While the movement was observed close to PBC, no signs of failure were detected in any of the connections or wooden components (Line et al. 2022a). In the numerical model, when the load is applied perpendicular to the panel joints, the behaviour is well predicted up to the peak load, and the maximum displacement is equal to 34 mm. In the model, the loads in the PPC and PBC did not reach their respective capacities, similar to the corresponding experiment. The

deformation of the diaphragm was largely linear-elastic with limited plastic behavior due to the low load levels experienced by all the connections, given that mechanical connections in timber structures generally exhibit nonlinear load-deformation responses at high load levels. The limited plastic behavior of the system load-deformation response was thought to originate from the PBC, as reported in (Line et al. 2022a). As was discussed in Section 3.4.3, a steel strap was simulated following the experimental assumptions to act as part of the tension chord. The steel straps resisted the tensile force caused by the load applied in the direction perpendicular to the panel joints in both the experimental program (Line et al. 2022a) and the FE modeling undertaken in this study.

3.5 Parametric study

Following the verification of the FE models with experimental results, a parametric investigation was conducted to evaluate how the CLT diaphragm deformation and connection forces are affected by the three features discussed below:

1. PPC and PBC: The stiffness properties of the PPC (K_{p-p}) and PBC (K_{p-b}) were changed over a wide range of practical values.
2. Supporting beam conditions: This feature relates to the type of support the underlying beams provide to the CLT panels. The condition was varied by changing the location and the number of restrained support beams.
3. Panel joint staggering: Panel joint staggering was thought to improve the performance of diaphragms. Different joint staggering patterns were evaluated to identify the configuration that provided the most optimum mechanical performance.

Tables 2, 3, and 4 provide an overview of the above parameters and their variations. Each archetype represents an FE model that was simulated accordingly. It is noted that the analyses

discussed in Sections 3.5.3 were carried out in both loading directions, i.e., parallel and perpendicular to the panel joints; while the archetypes analyzed in Sections 3.5.1 and 3.5.2 were loaded perpendicular to the panel joints only. Archetypes in Sections 3.5.1 and 3.5.2 were loaded at four points, similar to the selected experiments (Line et al. 2022a). However, a uniform in-plane load was considered for archetypes in Section 3.5.3. Furthermore, the stiffness of the PPC and PBC was implemented as used in the selected experimental program (Line et al. 2022b), except in Section 3.5.1 where it was the main factor parametrically studied.

CLT panels in all three sections used the E1M5 proprietary grade (Structurlam 2021) of machine stress-rated spruce-pine-fir lumber for the outer layers and visually graded lumber for the center layer, as referenced in (Line et al. 2022a). Additionally, the 24F-V8 Douglas-fir glulam beams used in the structure were locally sourced (Structurlam 2021) and were the same as the experiment (Line et al. 2022a). It is essential to acknowledge that varying material properties could lead to differing results in the parametric study. The results of this parametric study can provide valuable insights into the behavior of CLT diaphragms, facilitating the optimal design and construction of these structural elements as a part of LLRS in buildings.

3.5.1 Stiffness of panel-to-panel (PPC) and panel-to-beam connections (PBC)

A previous study by D'Arenzo et al. (2019), performed analyses of the diaphragm loaded parallel to the panel joints; therefore, this section in the current study focused on the case of the load perpendicular to the panel joints. Table 3-2 summarizes the FE model inputs for different connection stiffnesses in the diaphragm with twelve CLT panels measuring $1.22 \text{ m} \times 3.66 \text{ m}$ and a thickness of 105 mm when the load is applied perpendicular to the panel joints. In this section, PPC and PBC were changed while all other parameters, such as diaphragm size and boundary conditions, were maintained constant.

Table 3-2: Summary of connection stiffness characteristics in archetype diaphragms loaded perpendicular to the panel joints

Archetype No.	PPC Stiffness (N/mm/mm)	PBC Stiffness (N/mm/mm)	Diaphragm Deformation at Midspan (mm)
1	100	1000	46
2	100	10 ⁴	36.9
3	100	10 ⁵	30.9
4	100	10 ⁶	29.1
5	100	Rigid (10 ⁷)	29
6	1000	100	104.9
7	1000	1000	37
8	1000	10 ⁴	28.7
9	1000	10 ⁵	25.6
10	1000	10 ⁶	23.9
11	1000	Rigid (10 ⁷)	23.8
12	10 ⁴	100	97.6
13	10 ⁴	1000	26.3
14	10 ⁴	10 ⁴	18.3
15	10 ⁴	10 ⁵	17
16	10 ⁴	10 ⁶	16.2
17	10 ⁴	Rigid (10 ⁷)	16.2
18	10 ⁵	100	92.9
19	10 ⁵	1000	21.8
20	10 ⁵	10 ⁴	13.3
21	10 ⁵	10 ⁵	11.9
22	10 ⁵	10 ⁶	11.4
23	10 ⁵	Rigid (10 ⁷)	11.3
24	10 ⁶	100	92.7
25	10 ⁶	1000	21.3
26	10 ⁶	10 ⁴	12.6
27	10 ⁶	10 ⁵	11.2
28	10 ⁶	10 ⁶	10.7
29	10 ⁶	Rigid (10 ⁷)	10.6
30	Rigid (10 ⁷)	100	92.5
31	Rigid (10 ⁷)	1000	21.3
32	Rigid (10 ⁷)	10 ⁴	12.6
33	Rigid (10 ⁷)	10 ⁵	11.1
34	Rigid (10 ⁷)	10 ⁶	10.6
35	Rigid (10 ⁷)	Rigid (10 ⁷)	10.5

As shown in Table 3-2, the range of connection stiffness is between 100 N/mm/mm (nominally connected) and 10,000,000 N/mm/mm (rigid connection, e.g., glued). The choice of 10^7 as the threshold for defining "rigid" results from a blend of practicality, and its alignment with the study's particular goals. This decision is underpinned by the observation that the distinction between 10^6 and 10^7 stiffness values does not significantly impact deflection, hence justifying the categorization as "rigid." In this study, the connection stiffness was normalized to the spacing of the fasteners. As expected, more rigid connections led to lower displacements. As shown in Figure 3.9, connection stiffness of more than 10^5 N/mm/mm did not significantly influence the diaphragm deflection. In the experimental study (Line et al. 2022a), the PPC in the diaphragm was established using common nails of 8d size, evenly spaced at 80 mm intervals. These connections possess an elastic stiffness of 3,500 N/mm/mm. On the other hand, the PBC employs STS fasteners with a spacing of 150 mm and a stiffness of 900 N/mm/mm. (Line et al. 2022a). The result of this parametric study can help designers and researchers understand the sensitive range for connection stiffness for diaphragm deflection.

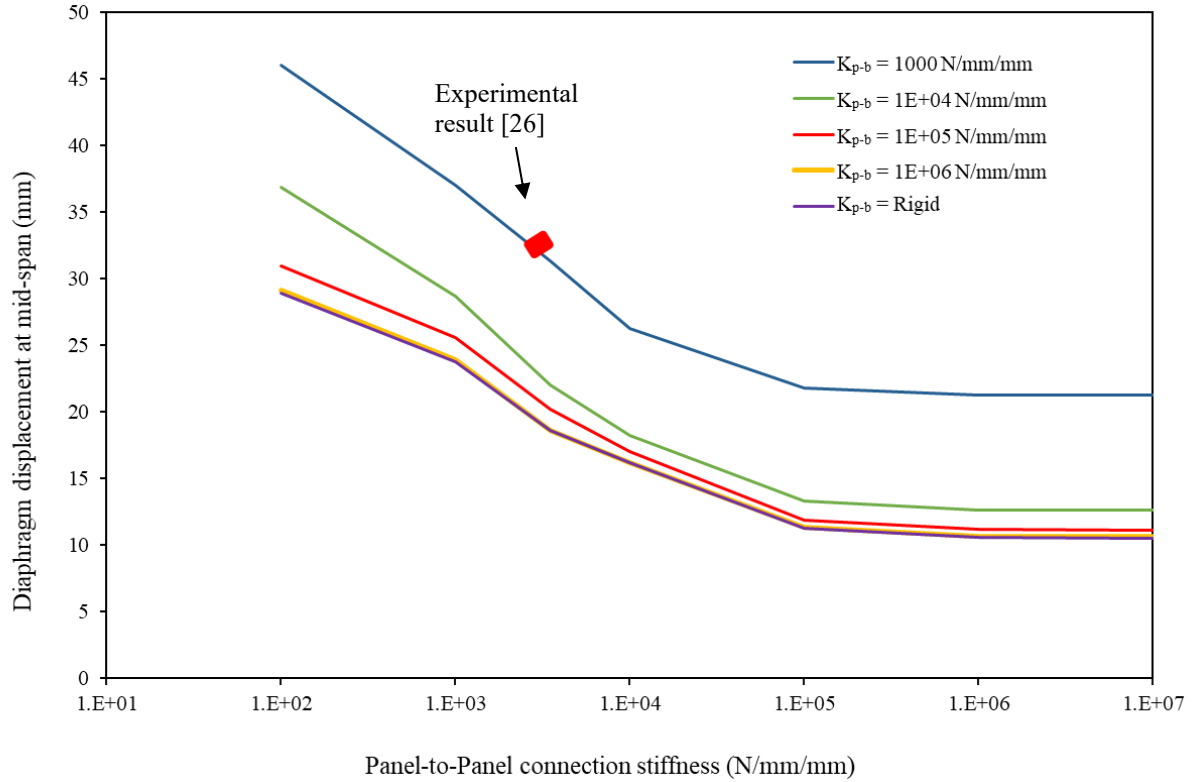


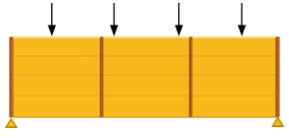
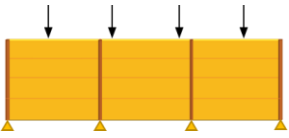
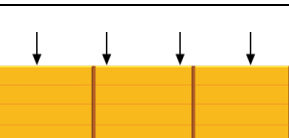
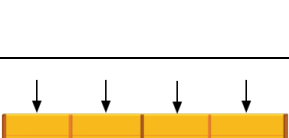
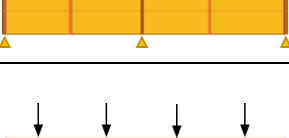
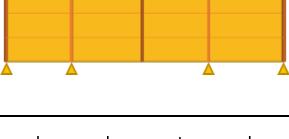
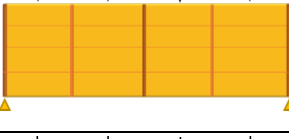
Figure 3.9: Variation of diaphragm displacement with the variation of PPC and PBC stiffnesses.

The response curves depicted in Figure 3.9 consistently exhibit a similar pattern for all PBC stiffness. This indicates that altering the PBC stiffness changes the deflection but does not affect the sensitive range for PPC stiffness. From Figure 3.9, the sensitive range for PPC stiffness appears to be $10^2 - 10^7$ N/mm/mm. It is important to note that diaphragm deformation does not undergo any significant changes when the stiffness of the PPC (K_{p-p}) exceeds 10^5 N/mm/mm or when the PBC (K_{p-b}) exceeds 10^4 N/mm/mm. This observation suggests that the effect of K_{p-b} on the overall behavior of the diaphragm may not be significant for a specific range of connection stiffness values when the load is applied perpendicular to the panel joints.

3.5.2 Effect of boundary conditions

The influence of the supporting beam locations and constraints on diaphragm deflections has also been studied under loading applied perpendicular to panel joints. Table 3-3 summarizes the FE archetypes for different boundary conditions in the diaphragm. Within each archetype, a deformation of the diaphragm is depicted in Figure 3.10 and Figure 3.11. The configurations involved 12 m-long CLT panels with a depth of 2.4 m. Diaphragms with a thickness of 315 mm were used and subjected to a four-point load distributed along the edges of the diaphragm. Furthermore, the glulam beams used in the structures have a depth of 250 mm and a width of 150 mm.

Table 3-3: Comparative analysis of diaphragm archetypes under varied boundary conditions in diaphragms loaded perpendicular to the panel joints

Archetype No.	Number of CLT panels	Boundary condition	Diaphragm mid-span deformation (U_{1m} , mm)	Configuration	Diaphragm size
1	12	Middle beams are not restrained in the load direction	67.2		36 m × 9.6 m
2	12	All beams are restrained in the load direction	10.4		36 m × 9.6 m
3	12	The left middle beam is restrained in the load direction (as shown)	23.7		36 m × 9.6 m
4	8	The middle beam is restrained	10.6		24 m × 9.6 m
5	8	Two side beams (light brown beams) are restrained in the load direction	13.5		24 m × 9.6 m
6	8	Middle beams are not restrained in the load direction	43.5		24 m × 9.6 m
7	8	All beams are Restrained in the load direction	5.3		24 m × 9.6 m

In archetype numbers 1-3, 12 panels formed the diaphragms within different constraints for the beams. As illustrated in Figure 3.10, the diaphragm exhibited significantly reduced deformation when both middle beams were restrained in the load direction. However, when only one middle beam was restrained, the diaphragm experienced approximately 50% larger deformation in an asymmetric pattern. U1 in Figure 3.10 denotes the diaphragm deformation in the direction of the applied load.

Archetype numbers 4-7 included two additional middle beams (indicated by the light brown) placed underneath the CLT panels rather than the edges. The middle beams do not interfere with the in-plane movements unless restrained in the load direction. The diaphragm comprised eight panels and five glulam beams: two beams under the CLT panels and three at the edges of the panels. Different constraints were considered for the beam ends, and the results for different deformation shapes are shown in Figure 3.11.

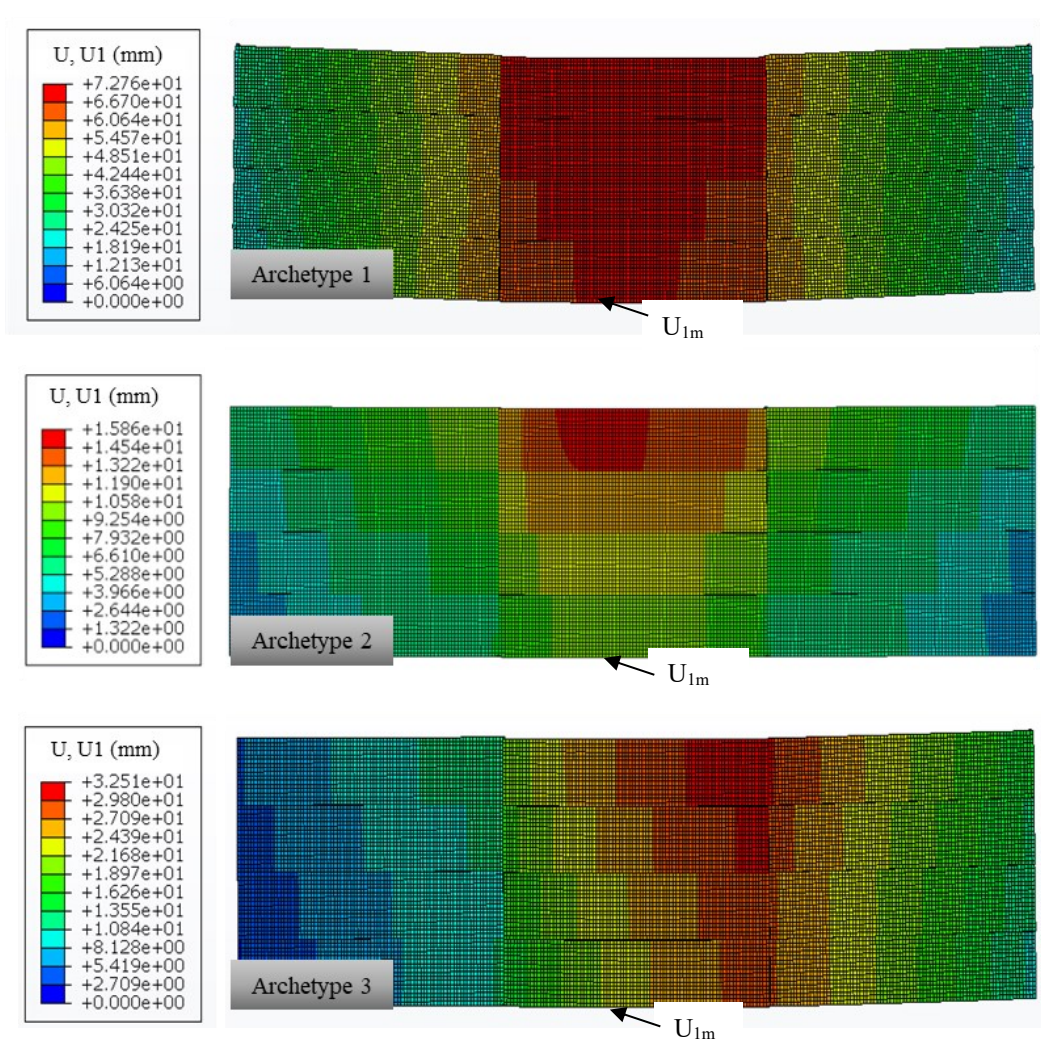


Figure 3.10: Deformation patterns of diaphragms with varied beam restraints (Archetypes 1-3)

The outcome for the diaphragm deformation was the same regardless of whether the beam beneath or the beam at the panel edge was restrained in the load direction (Archetypes 4 and 5). Moreover, the displacement approximately doubled in cases where no middle beams were restrained (Archetype 1) in the loading direction, as compared to scenarios where one beam was restrained (Archetype 3). Similarly, the displacement for Archetype 3 was approximately doubled when all beams were restrained (Archetype 2).

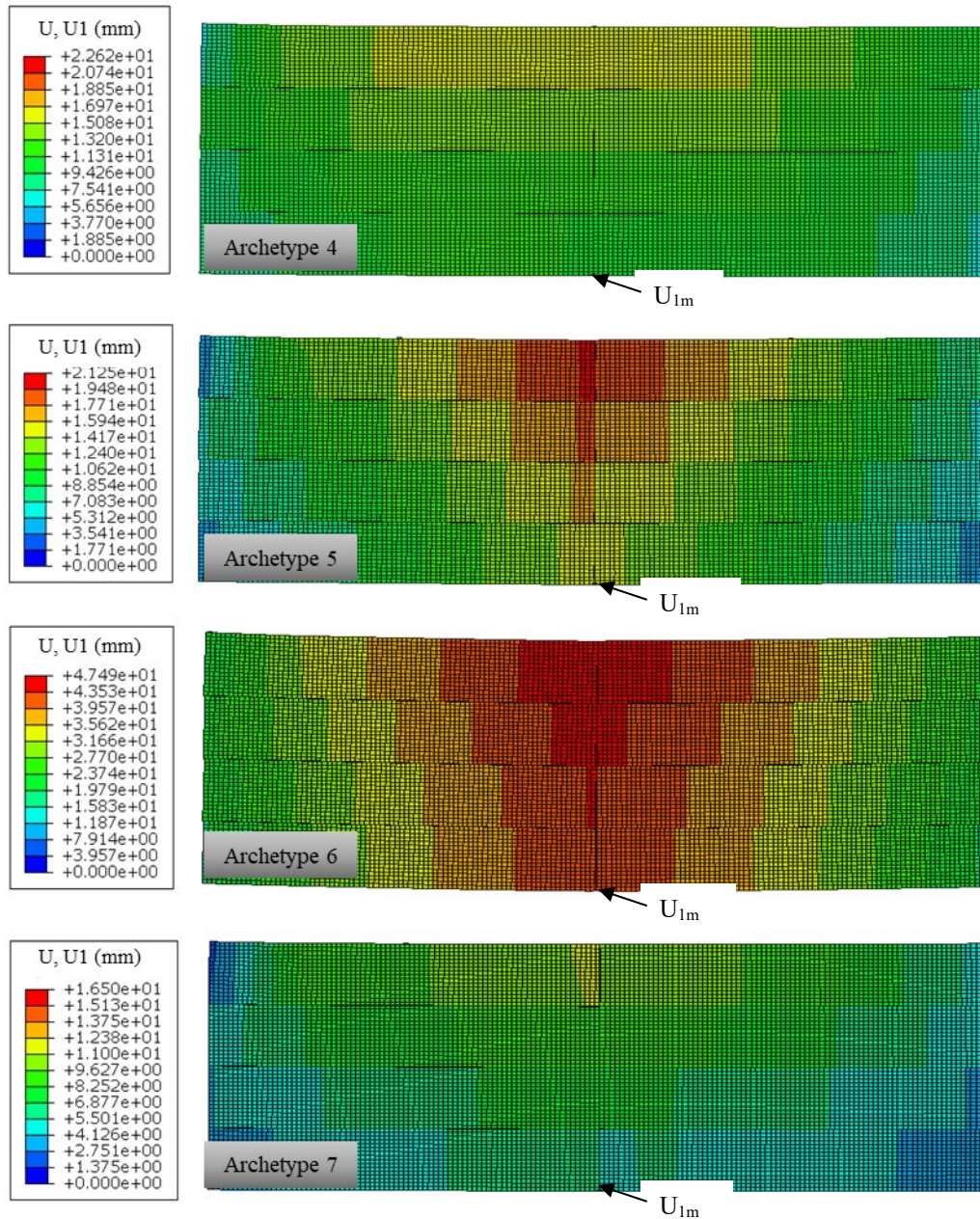


Figure 3.11: Deformation patterns of diaphragms with varied beam restraints (Archetypes 4-7)

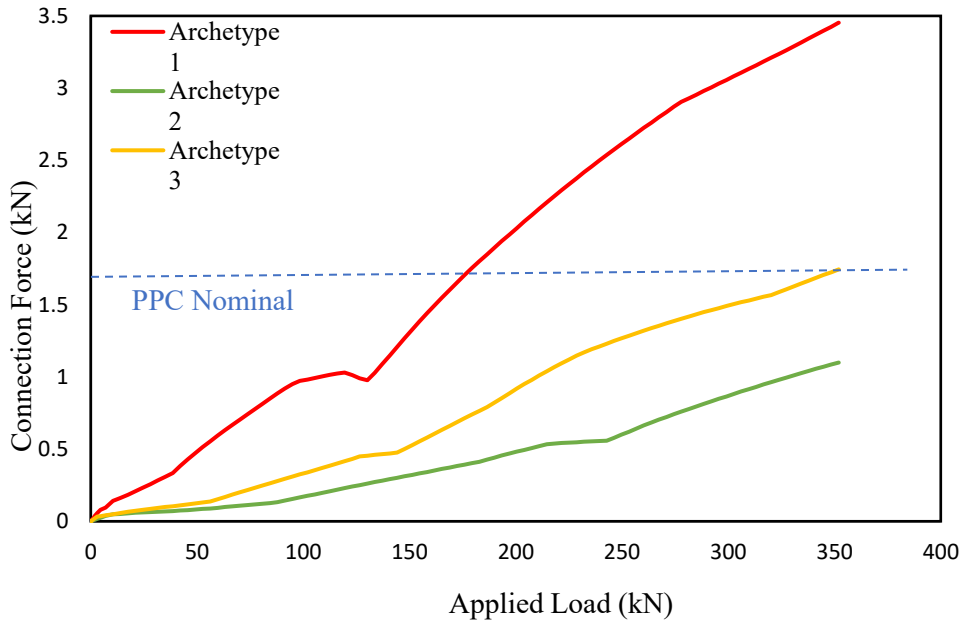
The deformed shapes shown in Figure 3.10 and Figure 3.11 demonstrate how the beam restrictions significantly affected diaphragm movement. Upon examination, it has been observed that there is a slight difference in the in-plane deformation when comparing archetypes that have a restraining middle beam at the panel joints versus those with restraining beams placed beneath the panels.

However, this difference is minimal and does not have a significant impact on the overall deformation of the archetypes under investigation.

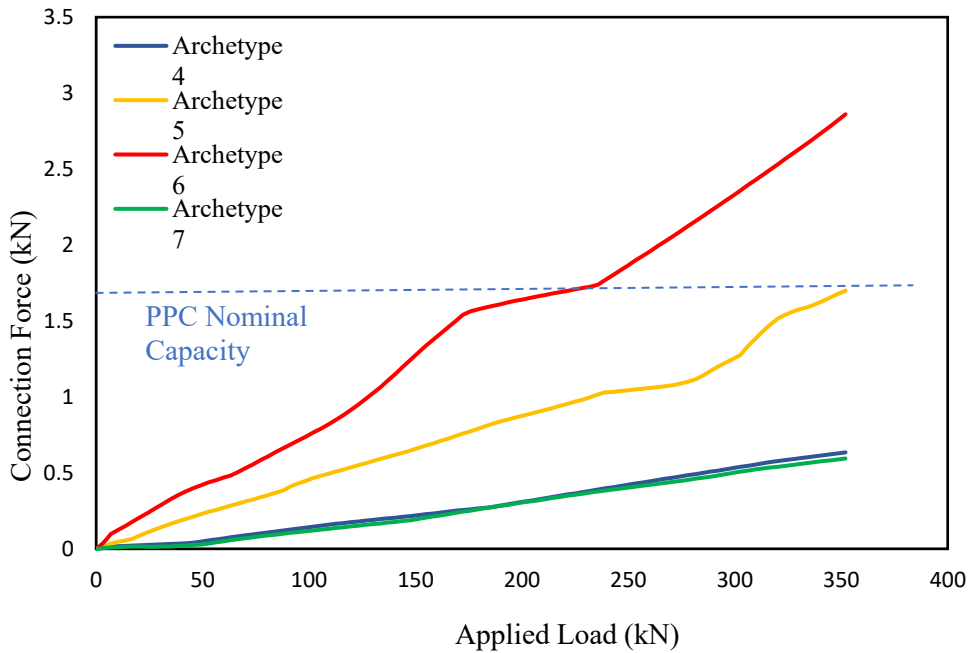
The load transfer in CLT diaphragms occurs mainly through the PPC, which is responsible for distributing the applied loads to the boundaries of the structure. The load on the PPC for each archetype is shown in Figure 3.12. The diaphragm was loaded up to the maximum load of 40 kN/m, the same load applied in the experimental program (Line et al. 2022a), and failures were only noticed within archetypes 1 and 6, as the PPC reached its intended lateral load capacities.

As shown in Figure 3.12(a), it can be observed that for Archetype 3, the PPC achieved its nominal lateral design capacity of 1.7 kN (Line et al. 2022a). In the case of Archetype 1, with the middle beams unrestrained, the PPC experienced a force that was twice the demand in the diaphragm with restrained beams (Archetype 3). Consequently, Archetype 1 led to a peak load of 3.5 kN, exceeding its intended nominal capacity by a factor of two, and was classified as a failure. Figure 3.12(b) compares the analysis results for Archetypes 4 and 7, revealing similar performance of the connections regardless of the restraining condition of the beam beneath. The PPC in Archetype 5, where the beams beneath are restrained, has a higher force demand compared to edge beams restrained (Archetype 4) and reached the nominal capacity at 1.7 kN. It is worth noting that the kinks in Figure 3.12 can reveal the yield point of the connection. The force demand for PPC in Archetype 6 is more than 80% higher than their nominal capacity and is considered to have failed. The study findings indicate that by restraining the middle beams at the panel joints, the in-plane deformation can be significantly reduced by up to 50%. Alternatively, if the beams beneath the panels are restrained, the designer can anticipate a 30% reduction in the in-plane deformation. Moreover, there is no discernible difference in in-plane deformation of the studied archetypes, irrespective of whether the middle beam at the edge of the CLT panels is restrained or if the beam

beneath is restrained, even though the force demands are higher in the latter scenario. This observation can guide designers to avoid unnecessary restraints and the associated cost, considering that both options yield comparable results in terms of in-plane deformation.



(a)



(b)

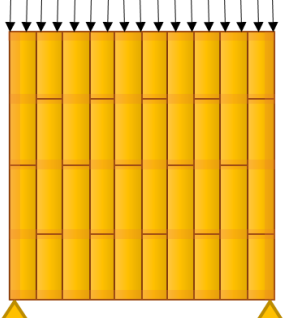
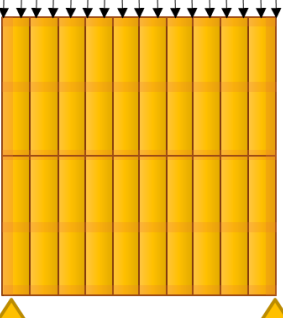
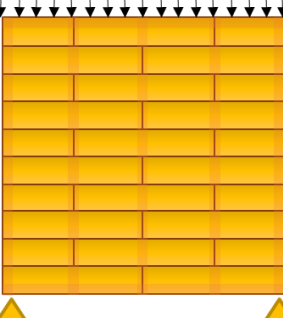
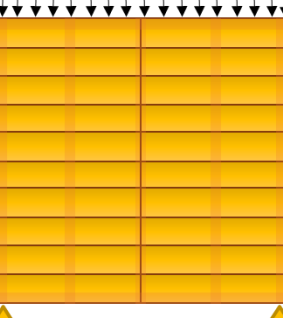
Figure 3.12: PPC force for diaphragm loading perpendicular to the panel joints

3.5.3 Panel installation pattern (joint staggering versus regular)

In this parametric study, the behavior of staggered and non-staggered CLT panels was examined under in-plane loading parallel and perpendicular to the panel joints. The study focused on 24 m by 24 m archetypes with CLT panels 12 m and 6 m long and a thickness of 175 mm. A uniformly distributed load of up to 15 kN/m is considered for the archetypes investigated in this study. The CLT grade and connection stiffness match those described in the experimental study (Line et al. 2022a). For the non-staggered diaphragm, the 12 m long CLT panels were arranged parallel to the panel joints.

In the staggered diaphragm, the 12 m and 6 m CLT panels were connected using interlocking joints and organized as shown in the drawings associated with Archetypes 1 and 3, to increase the structural redundancy. Such joints between panels offer structural redundancy, by providing alternate load paths for diaphragms subjected to lateral loads. Table 3-4 summarizes the results of the FE model analysis for different installation patterns in the CLT diaphragms when subjected to loads parallel and perpendicular to the panel joints. Designation in each archetype includes configurations for the CLT diaphragm that encompass variations in the layout of the CLT panels. Specifically, *Pa_S* depicts diaphragm loading parallel to the panel joints when the panels are staggered, while *Pa_NS* depicts loading for non-staggered panels. Similarly, *Per_S* and *Per_NS* represent perpendicular loading with staggered and non-staggered panels. Diaphragms loaded perpendicular to the panel joints are archetypes 3 and 4.

Table 3-4: Summary of diaphragm characteristics with different configurations (staggering pattern), loaded parallel and perpendicular to the panel joints in FE models.

Archetype No.	Panel length	Load direction	Panel joints	Configuration	Designation
1	12 m and 6 m	Parallel to the panel joints	Staggered		Pa_s
2	12 m	Parallel to the panel joints	Non-Staggered		Pa_NS
3	12 m and 6 m	Perpendicular to the panel joints	Staggered		Per_S
4	12 m	Perpendicular to the panel joints	Non-Staggered		Per_NS

3.5.3.1 Diaphragm loaded parallel to panel joints

For archetypes 1 and 2, as shown in Figure 3.13, the Pa_NS diaphragm is stiffer than Pa_S. However, the difference between the two archetypes in terms of stiffness is less than 15%. For the diaphragm loaded parallel to the panel joints, the primary source of deformation in the diaphragm is slip in the panel joint along the panel length (Abaqus 2020).

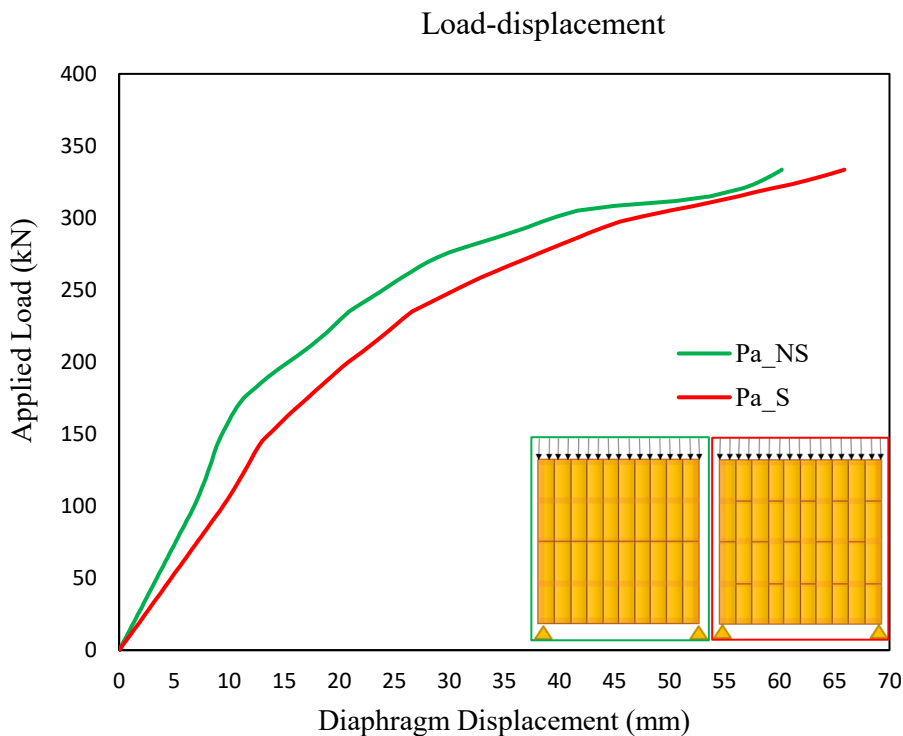


Figure 3.13: Mid-span Load-displacement curve for the diaphragm under in-plane loading when the load is parallel to the panel joints

In the numerical model, the wood components were assumed to perform linear-elastically, while the connections showed nonlinear behavior. Plastic deformation was initiated at around 150 kN load due to yielding in the connections. Figure 3.14 shows how the loads in the PPC and PBC change with load applied parallel to the panel joints. The nominal lateral design capacity is 4.3 kN for PBC and 1.7 kN for PPC, as reported in Line et al. (2022a). The load applied to PBC and PPC

is less than their nominal capacity. The maximum force demand in PPC for Pa_NS is 1 kN, while in the Pa_S diaphragm, PPC force demand is 1.2 kN per nail. It is important to note that none of the connections reached their specified nominal capacity, and the diaphragms were not deemed to have undergone failure.

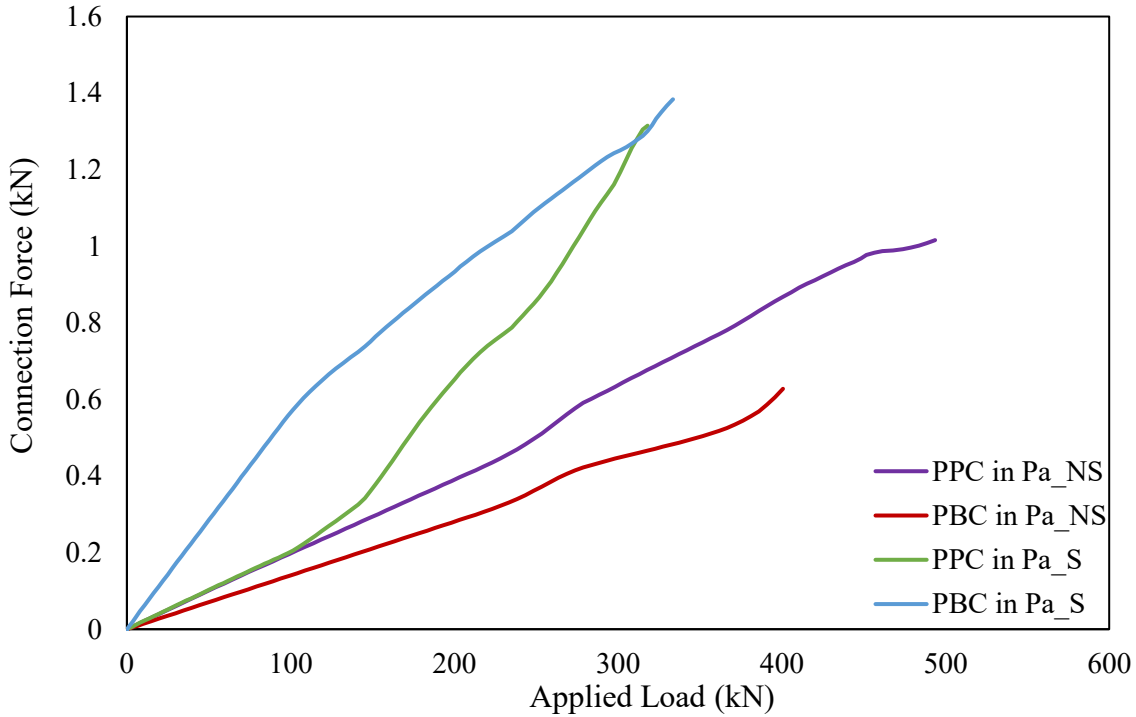


Figure 3.14: Connections force for diaphragm loading parallel to the panel joints

3.5.3.2 Diaphragm loaded perpendicular to panel joints

As shown in Figure 3.15, when the load is applied perpendicular to the panel joints, the staggered CLT diaphragm is stiffer than the non-staggered diaphragm. The maximum diaphragm deflection for Per_S is 36 mm for a 350 kN applied load, whereas for Per_NS, which has a greater capacity and a 700 kN applied load, the maximum deflection is 49 mm. According to the selected experimental study (Line et al. 2022a), a steel strap was simulated to function as a part of the

tension chord for loading perpendicular to the panel joints. In the Per_S diaphragm, the CLT panels at the diaphragm edges act as a chord and withstand the tensile force applied to the diaphragm.

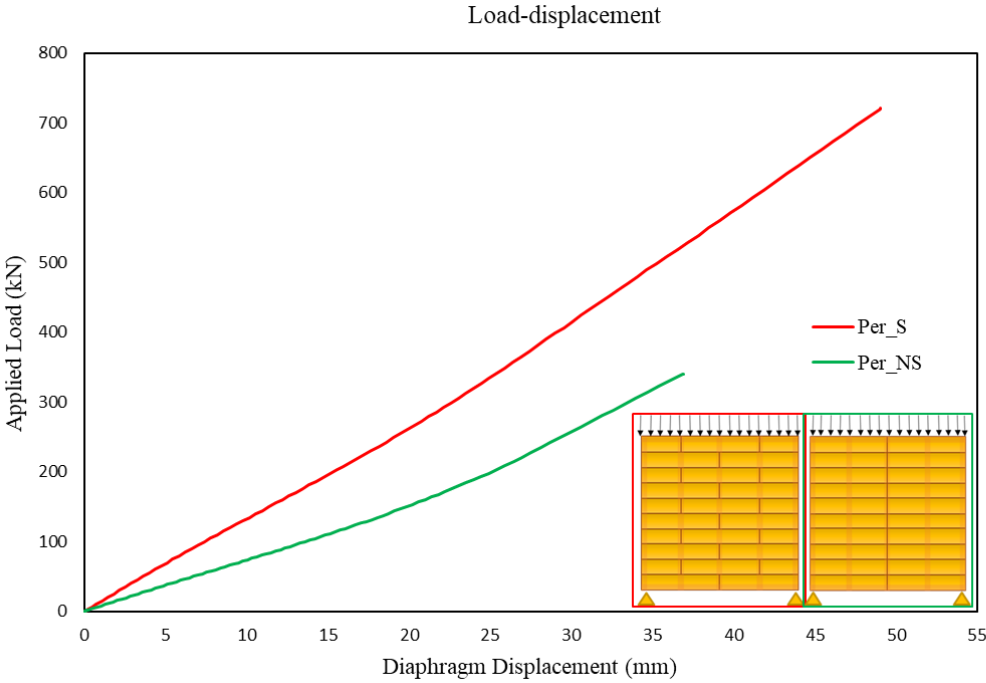


Figure 3.15: Mid-span Load-displacement curve for the diaphragm under in-plane loading when the load is perpendicular to the panel joints.

Due to the elastic behavior of the panels, the diaphragms deformed more linearly. The connection forces for each configuration were extracted to provide additional information on which connections caused the failure. Figure 3.16 shows the force of PPC and PBC versus the applied load of the diaphragms when the load is applied perpendicular to the panel joints. The nominal capacity for the PBC is 4.3 kN per screw and 1.71 kN for the PPC per nail (Line et al. 2022a).

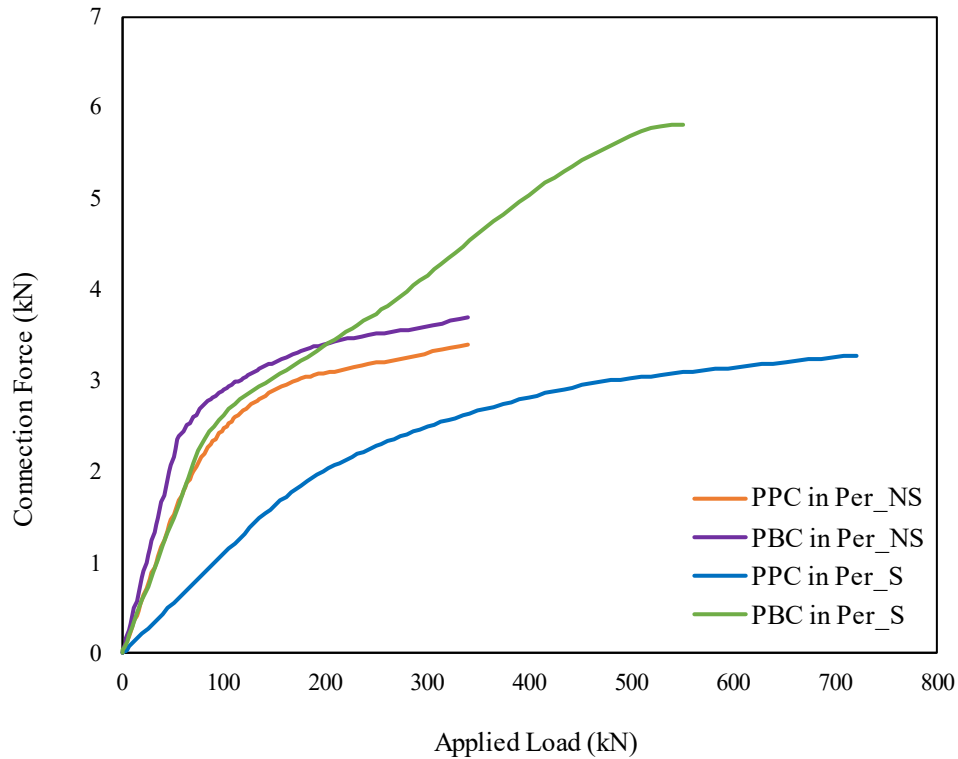


Figure 3.16: Connections force for diaphragm loading perpendicular to the panel joints

The result revealed that the Per_S exhibited greater stiffness and superior load-carrying capacity compared to the Per_NS. It appears that the breaking up of the panel joint alignment leads to a stiffer system. Figure 3.17 depicts the stress distribution (S11) in the load direction for both staggered and non-staggered panels in the diaphragm loading perpendicular to the panel joints. Staggered panels exhibit enhanced load-sharing capabilities due to their interconnected layout, which leads to a more efficient distribution of forces across the diaphragm. This uniform distribution of stress results in less localized deformation and strain concentration, ultimately contributing to higher structural stiffness.

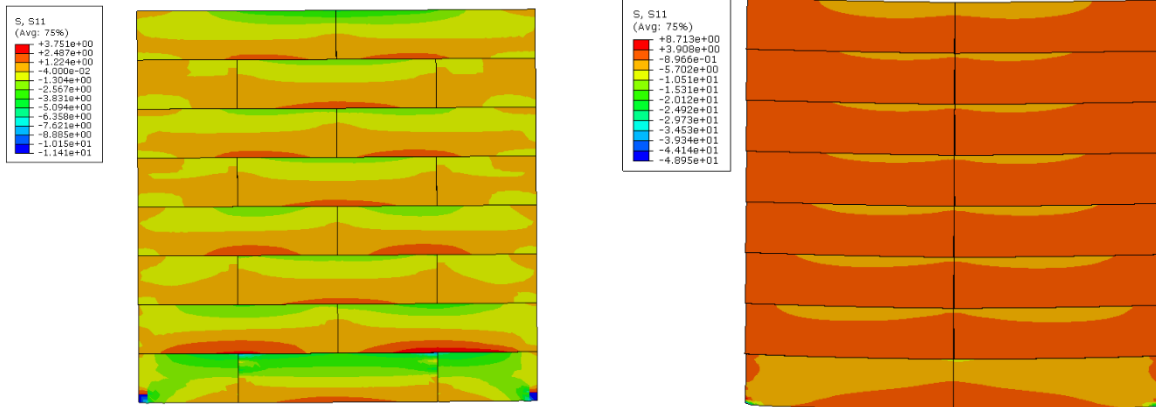


Figure 3.17: Stress distribution for the diaphragm under in-plane loading when the load is perpendicular to the panel joints

3.6 Conclusions

The present study developed FE models to represent the behavior of the CLT diaphragm under in-plane loading, both perpendicular and parallel to CLT joints. These models were validated using available test data. Various connection stiffnesses were investigated to identify the optimal stiffness for PPC and PBC. The manipulation of connection stiffness consistently impacts CLT diaphragm deformation, enabling reliable behavior prediction. It is noteworthy that, within the scope of archetypes studied, the impact of PBC stiffness appears less significant for particular connection stiffness ranges, compared to PPC, particularly under the perpendicular loading. The study also investigated various boundary conditions. The results demonstrate that the restriction of beams beneath the diaphragm significantly impacts in-plane movements and PPC forces, offering an avenue for tailored deformation control. Furthermore, the impact of staggered panels on CLT floor diaphragm loaded parallel and perpendicular to the panel joints was also explored. Staggered CLT diaphragms exhibit enhanced stiffness and capacity when loaded perpendicular, demonstrating their potential for efficient load-bearing performance. However, it's important to consider that the staggered panels may be more labor-intensive and susceptible to more material

waste. To conclude, this study provides valuable insights into CLT diaphragm behavior, optimal connection stiffness, boundary conditions, and the advantages of staggered panels. These findings offer a foundation for enhanced design strategies and utilization of CLT's potential in contemporary construction practices.

Chapter 4: Summary, conclusion, recommendations, and future work

4.1 Summary

The principal objective of this study was to address a gap in the behaviour of the CLT diaphragm when subjected to in-plane loads. This endeavour encompassed a series of analytical and numerical efforts, each undertaken to unravel the behaviour across varying scenarios. In the initial phase, an analytical model was constructed to calculate the deformation of the CLT diaphragm and the corresponding connection forces. The analytical model was carried out under the conditions of uniform in-plane loading perpendicular to the panel joints. The developed model underwent validation using a FE model. Additionally, a partial validation was performed by comparing the results from both the analytical and FE models with available experimental data.

In the subsequent phase, a parametric analysis was conducted utilizing the FE model. This study specifically investigated the influence of certain parameters on the deformation of the diaphragm. This thorough exploration encompassed a wide range of connection stiffness. Additionally, the research investigates different boundary conditions of the diaphragm, and thoroughly assessed the arrangement patterns of CLT panels within the diaphragm, considering both staggered and non-staggered panel joint configurations. The conclusions from this investigation are presented in this chapter, along with recommendations for future work.

4.2 Conclusions

The conclusions that can be drawn from this research are shown below:

- Utilizing the layered deep beam theory, an analytical framework was formulated to compute the mid-span deflection and the force in CLT-CLT panel connections of a simply supported diaphragm subjected to load applied perpendicular loading to the CLT panel joints. This model considers bending and shear deflections for each panel, as well as slip between panels. A comparison between the analytical model and FE model predictions shows good agreement between these predictions, thereby validating the analytical model. The analytical model has the potential to be adopted as a design tool.
- FE modelling approach adopted in this project provides a reasonable prediction of the in-plane behaviour of CLT diaphragm, as evidenced by comparing the predictions with full-scale experimental data, a clearer comprehension of CLT panel behaviour under both parallel and perpendicular loading directions was achieved.
- A parametric study was conducted using the validated FE model. The studied parameters were stiffness values for both panel-to-panel and panels-to-beam connections, boundary conditions, and the arrangement patterns of CLT panels within the diaphragm (staggered versus non-staggered). The key findings from the parametric study are summarized below:
 - While CLT panel connection stiffness significantly impacts diaphragm deflection when the load is applied parallel to the CLT panel joints, its influence is moderate when the load is applied perpendicular to the CLT panel joints.
 - Shear deflection within the CLT panels is the most significant contributor to total diaphragm deflection when the load is applied perpendicular to the CLT panel joints. Furthermore, as the span of the diaphragm increases, the impact of bending deflection becomes more pronounced. In addition, the effect of slip between CLT

panels diminishes with an increase in the depth of each CLT panel highlighting how the structural response changes with different sizes.

- The inquiry into boundary conditions showed the profound influence of beam restriction beneath the diaphragm. This key insight provides an avenue for deliberate deformation control, emphasizing the adaptability of CLT diaphragms in diverse scenarios.
- Diaphragm with staggered CLT panel joints performs better with reduced deflection and panel connection force when the load is applied perpendicular to the CLT panel joints. However, the increased labour and material waste associated with staggered CLT panel joints may underscore the structural benefit.

In summary, this study has provided insight into the in-plane behaviour of CLT diaphragms. The development of the analytical and FE modelling approaches and the findings extracted from the parametric study provides a basis for well-informed design strategies.

4.3 Recommendation for future research

This study, while providing an advancement in the knowledge related to CLT diaphragm behaviour, was limited in scope. Future research may focus on the following:

- Dynamic behaviour analysis: investigate the dynamic behaviour of CLT diaphragms under seismic and wind excitation and evaluate the difference in performance under monotonic (assumed in this study) and dynamic (real behaviour) loading. Dynamic loading introduces time-dependent effects that can lead to increasing deformations. These effects, such as creep and relaxation, may not be as pronounced in static loading scenarios.

- Connecting CLT diaphragm to LLRS: A key role of a diaphragm is to transfer the lateral loads arising from seismic and wind to vertical lateral load resisting system (LLRS). This transfer depends on the characteristics of the connection between diaphragm and LLRS. As was shown in this study, the connection stiffness can influence the force demand and deflection behaviour of the diaphragm. This topic should be investigated further.
- Concrete topping/slab: CLT diaphragms are often overlaid with a concrete topping or slab. Tendency of designers is to ignore the contribution of the concrete, which is a simple but not necessarily conservative approach. A focused investigation into such a hybrid system, that combines the inherent strength and rigidity of concrete and the flexible properties of CLT, is warranted.

Bibliography

- Abaqus, G. 2020. Abaqus 6.11. Dassault Systemes Simulia Corporation, Providence, RI, USA,.
- Afrin, H. 2019. Experimental investigations of shear connections with self-tapping-screws for cross-laminated-timber panels. University of British Columbia.
- ANSI, A. 2012. ANSI/APA PRG 320–2012 Standards for performance-rated cross-laminated timber. ANSI/APA, Tacoma, US Google Scholar,.
- ANSI, A.W.C., and NDS, A.W.C. 2014. National Design Specification (NDS) for Wood Construction—with Commentary. 2015 ed. Leesburg, VA: American Wood Council,.
- APA. 2019. Standard for Performance-Rated Cross Laminated Timber, ANSI/APA PRG 320. Tacoma, Washington, USA, **320**.
- Ashtari, S. 2012. In-plane stiffness of cross-laminated timber floors. University of British Columbia.
- AWC. 2018. National design specification for wood construction. ANSI/AWC Leesburg, VA.
- AWC. 2021. AWC (American Wood Council). 2021. Special design provisions for wind and seismic. ANSI/AWC SDPWS-2021. Leesburg, VA: AWC. ANSI/AWC Leesburg, VA.
- Barbosa, A.R., Rodrigues, L.G., Sinha, A., Higgins, C., Zimmerman, R.B., Breneman, S., Pei, S., van de Lindt, J.W., Berman, J., and McDonnell, E. 2021. Shake-table experimental testing and performance of topped and untopped cross-laminated timber diaphragms. *Journal of Structural Engineering*, **147**(4): 4021011. American Society of Civil Engineers.
- Barbosa, A.R., Rodrigues, L., Sinha, A., Higgins, C., Zimmerman, R.B., Breneman, S., Pei, S., Van De Lindt, J., Berman, J., and McDonnell, E. 2018. Numerical modeling of CLT diaphragms tested on a shake-table experiment. *World Conference on Timber Engineering (WCTE)*.

- Beairsto, C.J. 2020. Monotonic and Cyclic Testing of Cross-Laminated Timber Diaphragms.
- Blass, H.J., and Fellmoser, P. 2004. Design of solid wood panels with cross layers. *In* 8th world conference on timber engineering. Citeseer. p. 2004.
- Bogensperger, T., Moosbrugger, T., and Silly, G. 2010. Verification of CLT-plates under loads in plane. *In* Proceedings of 11th World Conference on Timber Engineering (WCTE2010). pp. 885–898.
- Brandner, R., Bogensperger, T., and Schickhofer, G. 2013. In plane shear strength of cross laminated timber (CLT): test configuration, quantification and influencing parameters. *In* Proceedings of 46th CIB-W18 Meeting, Vancouver.
- Brandner, R., Dietsch, P., Dröscher, J., Schulte-Wrede, M., Kreuzinger, H., and Sieder, M. 2017. Cross laminated timber (CLT) diaphragms under shear: Test configuration, properties and design. *Construction and Building Materials*, **147**: 312–327. Elsevier.
- Breneman, S., McDonnell, E., and Zimmerman, R.B. 2016. An approach to CLT diaphragm modeling for seismic design with application to a US high-rise project. *In* World Conference on Timber Engineering, WCTE. pp. 22–25.
- Brignola, A., Pampanin, S., and Podestà, S. 2009. Evaluation and control of the in-plane stiffness of timber floors for the performance-based retrofit of URM buildings. *Bulletin of the New Zealand Society for Earthquake Engineering*, **42**(3): 204–221.
- Ceccotti, A., Sandhaas, C., Okabe, M., Yasumura, M., Minowa, C., and Kawai, N. 2013. SOFIE project – 3D shaking table test on a seven-storey full-scale cross-laminated timber building. *Earthquake Engineering & Structural Dynamics*, **42**(13): 2003–2021. John Wiley & Sons, Ltd. doi:10.1002/EQE.2309.

- CEN, E.N. 2004. EN 1995-1-1: Eurocode 5: Design of Timber Structures–Part 1–1: General–Common Rules and Rules for Buildings. European Committee for Standardization CEN Bruxelles, Belgium.
- Chui, Y.H., and Barclay, D.W. 1998. Analysis of three-layer beams with non-identical layers and semi-rigid connections. *Canadian Journal of Civil Engineering*, **25**(2): 271–276. NRC Research Press Ottawa, Canada.
- Chui, Y.H., Spencer, J., Joyce, T., Daneshvar, H., Niederwestberg, J., and Spasojevic, M. 2019. Survey to Identify Mass Timber Research Needs and Priorities. : 1–44.
- CSA O86. 2019. CSA O86-19. Engineering design in wood. Toronto, Ontario, Canada: CSA Group,.
- Daneshvar, H., Niederwestberg, J., Dickof, C., and Chui, Y.H. 2021. Structural behaviour of deep CLT lintels subjected to concentric and eccentric loading. *Journal of Building Engineering*, **43**: 103101. Elsevier.
- D’Arenzo, G., Casagrande, D., Reynolds, T., and Fossetti, M. 2019. In-plane elastic flexibility of cross laminated timber floor diaphragms. *Construction and Building Materials*, **209**: 709–724. Elsevier.
- Dujic, B., Aicher, S., and Zarnic, R. 2006. Racking behaviour of light prefabricated cross-laminated massive timber wall diaphragms subjected to horizontal actions. *Otto Graf Journal*, **17**: 125–142.
- Dujic, B., Pucelj, J., and Zarnic, R. 2004. Testing of racking behavior of massive wooden wall panels. 37th CIB-W18 Meeting, Edinburgh, Scotland. Paper 37-15-2.

- Fakhrzare, M., Daneshvar, H., and Chui, Y.H. 2023. Analytical Model Development for CLT Diaphragms Loaded Perpendicular to the Length of Panels. *Journal of Structural Engineering*, **149**(6): 04023059. American Society of Civil Engineers.
- Fakhrzare M., Daneshvar H., & Chui YH. 2023b. Numerical Parametric Study of Cross-laminated Timber Diaphragms under In-plane Loading. *Construction and Building Materials*, (Under review).
- Flaig, M., and Blaß, H.J. 2013. Shear strength and shear stiffness of CLT-beams loaded in plane. *In Proceedings of 46th CIB-W18 Meeting, Vancouver*.
- Gagnon, S., Bilek, E.M.T., Podesto, L., and Crespell, P. 2013. CLT Introduction to cross-laminated timber. In: *CLT handbook: cross-laminated timber*/edited by Erol Karacabeyli, Brad Douglas.--US ed. 2013; pp. 1-45.,: 1–57.
- Gagnon, S., Mohammad, M., Toro, W.M., and Popovski, M. 2014. Evaluation of in-plane shear strength of CLT. *In World Conference on Timber Engineering*. pp. 1–7.
- Gavric, I., Fragiaco, M., and Ceccotti, A. 2015. Cyclic behaviour of typical metal connectors for cross-laminated (CLT) structures. *Materials and structures*, **48**(6): 1841–1857. Springer.
- Goodman, J.R., and Popov, E.P. 1968. Layered beam systems with interlayer slip. *Journal of the Structural Division*, **94**(11): 2535–2548. American Society of Civil Engineers.
- Gsell, D., Feltrin, G., Schubert, S., Steiger, R., and Motavalli, M. 2007. Cross-laminated timber plates: Evaluation and verification of homogenized elastic properties. *Journal of structural engineering*, **133**(1): 132–138. American Society of Civil Engineers.
- Hossain, A., Popovski, M., and Tannert, T. 2019. Group effects for shear connections with self-tapping screws in CLT. *Journal of Structural Engineering*, **145**(8): 4019068. American Society of Civil Engineers.

- Joyce, T.P.R.D. 2014. Connections for CLT diaphragms in Steel-Frame Buildings. University of New Brunswick.
- Karacabeyli, E., Gagnon, S., and Pîrvu, C. 2019. Canadian CLT handbook: cross-laminated timber. FPInnovations: Pointe-Claire, QC, USA,.
- Kode, A. 2018. Testing of a full-scale mass timber diaphragm. Colorado State University.
- Kode, A., Amini, M.O., van de Lindt, J.W., and Line, P. 2021. Lateral Load Testing of a Full-Scale Cross-Laminated Timber Diaphragm. Practice Periodical on Structural Design and Construction, **26**(2): 4021001. American Society of Civil Engineers.
- Lau, W. 2016. The University of British Columbia's Brock Commons takes the title for tallest wood tower. Architect Magazine.
- Lenon, C. 2015. Design and behavior of a mid-rise cross-laminated timber building. Colorado School of Mines.
- Line, P., Nyseth, S., and Waltz, N. 2022a. Full-Scale Cross-Laminated Timber Diaphragm Evaluation. I: Design and Full-Scale Diaphragm Testing. Journal of Structural Engineering, **148**(5): 4022037. American Society of Civil Engineers.
- Line, P., Nyseth, S., and Waltz, N. 2022b. Full-scale cross-laminated timber diaphragm evaluation. II: CLT diaphragm connection tests. Journal of Structural Engineering, **148**(5): 4022038. American Society of Civil Engineers.
- Loss, C., Piazza, M., and Zandonini, R. 2016. Connections for steel–timber hybrid prefabricated buildings. Part I: Experimental tests. Construction and Building Materials, **122**: 781–795. Elsevier.

- Moosbrugger, T., Guggenberger, W., and Bogensperger, T. 2006. Cross-laminated timber wall segments under homogeneous shear - With and without openings. *In* 9th World Conference on Timber Engineering 2006, WCTE 2006. pp. 219–228.
- Moroder, D. 2016. Floor diaphragms in multi-storey timber buildings. University of Canterbury.
- NBCC. 2015. National Building Code of Canada 2015. Institute for Research in Construction, National Research Council of Canada
- NDS, A.W.C. 2014. National Design Specification (NDS) for Wood Construction—with Commentary. 2015 ed. Leesburg, VA: American Wood Council,.
- Nordic 2022. Nordic Structure mass timber technical guide for Cross Laminate timber, clt Canadian Version. Nordic mass timber construction, Intelligence in Wood.
- Pei, S., Van de Lindt, J., Barbosa, A.R., Berman, J., Blomgren, H.-E., Dolan, J., McDonnell, E., Zimmerman, R., Fragiaco, M., and Rammer, D. 2018. Full-scale shake table test of a two story mass-timber building with resilient rocking walls. *In* In: Proceedings, 16th European conference on earthquake engineering. Thessaloniki, Greece: 1-10. pp. 1–10.
- Popovski, M., and Karacabeyli, E. 2012. Seismic behaviour of cross-laminated timber structures. *In* Proceedings of the World Conference on Timber Engineering.
- Richardson BL. Examination of the Lateral Resistance of Cross-Laminated Timber in Panel-Panel Connections . 2015. scholar (1). Master’s Thesis., Virginia Polytechnic Institute and State University, Blacksburg, Virginia, USA; 2015.
- Sadeghi, M., and Smith, I. 2014. Edge connections for CLT plates: In-plane shear tests on half-lapped and single-spline joints. *In* Proceedings of 13th World Conference on Timber Engineering, August. pp. 10–14.

- SAP2000. 2005. CSI Analysis Reference Manual for SAP2000. Computers and Structures Inc. Berkeley, USA.
- Shahnewaz, M., Alam, S., and Tannert, T. 2018. In-plane strength and stiffness of cross-laminated timber shear walls. *Buildings*, **8**(8): 100. Multidisciplinary Digital Publishing Institute.
- Smith, I., Asiz, A., Snow, M., and Chui, Y.H. 2006. Proposed Canadian/ISO Approach for Deriving Design Values from Test Data. International Council for Research and Innovation in Building and Construction Working Commission W-18 (Timber Structures), Florence, Italy, Aug. 28–31.
- Spickler, K., Closen, M., Line, P., and Pohll, M. 2015. Cross laminated timber: Horizontal diaphragm design example. White paper reference,.
- Structurlam. 2021. Structurlam mass timber technical guide for Cross Laminate timber, clt and Glulam, Canadian Version. Structurlam mass timber corporation, intelligence in wood.
- Sullivan, K. 2017. Behavior of Cross-laminated Timber Diaphragm Panel-to-panel Connections with Self-tapping Screws.
- Sullivan, K., Miller, T.H., and Gupta, R. 2018. Behavior of cross-laminated timber diaphragm connections with self-tapping screws. *Engineering Structures*, 168: 505–524. Elsevier.
- Timoshenko, S. 1983. History of strength of materials: with a brief account of the history of theory of elasticity and theory of structures. Courier Corporation.
- Tupenaite, L., Zilenaite, V., Kanapeckiene, L., Gecys, T., and Geipele, I. 2021. Sustainability assessment of modern high-rise timber buildings. *Sustainability*, 13(16): 8719. MDPI.
- Wallner-Novak, M., Augustin, M., Koppelhuber, J., and Pock, K. 2018. Cross-Laminated Timber Structural Design Volume 2: Applications. ProHolz Austria.

Yawalata, D., and Lam, F. 2011. Development of technology for cross laminated timber building systems. Vancouver, BC: University of British Columbia.

Appendix A: CLT diaphragm design example subjected to lateral load

A.1. Introduction

This appendix serves as a practical illustration of CLT diaphragm design, employing the formula established in Chapter 2 of the present study. The objective is to demonstrate a design methodology that aligns with the stipulated regulations for CLT diaphragms, as outlined in Clause 11.9 of the CSA O86:19, Engineering Design in Wood, along with the commentary.

The purpose of this example is to provide engineers and designers with a clear and tangible application of the prescribed design approach.

A.2. Design example

The aim here is to design a CLT diaphragm with a focus on the force determination for the panel-to-panel connections and the diaphragm deflection when the load is perpendicular to the panel joints, as shown in Figure A. . Unless otherwise noted, all code references presented are from CSA O86-19.

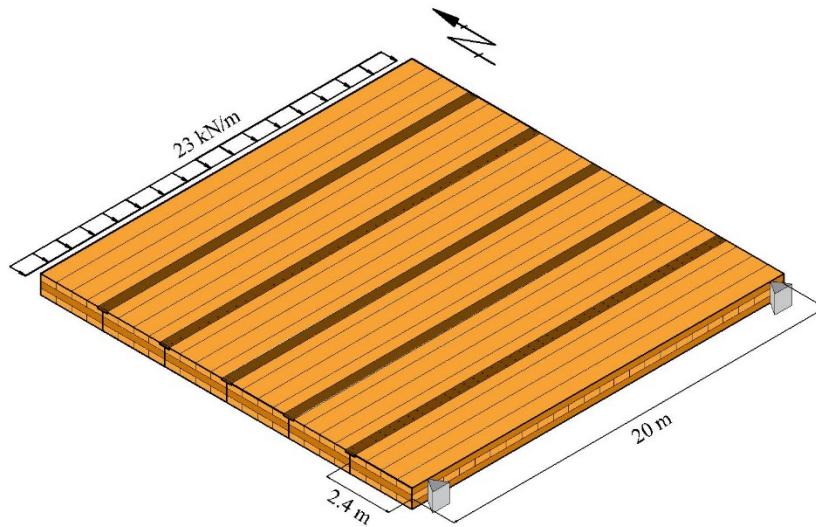


Figure A. 1: A CLT diaphragm loaded perpendicular to panel joints.

A.2.1. Geometry

Diaphragm span	$L = 20 \text{ m}$
CLT panel thickness	$t = 105 \text{ mm}$
CLT panel width	$w = 2.4 \text{ m}$
Number of CLT panels	$n = 6$
Diaphragm depth (width)	$h = n \times w = 14.4 \text{ m}$

A.2.2. Material properties

CLT manufacturer	Nordic Structure	<i>Nordic 2022</i>
CLT grade	3-ply Grade E1	
CLT effective shear modulus	$G_{\text{eff}} = 600 \text{ MPa}$	<i>Nordic 2022,</i>
CLT Modulus of Elasticity in the major strength axis	$E = 11700 \text{ MPa}$	<i>Nordic 2022,</i>

CLT panel relative density	$G_2 = 0.42$	<i>Table A.11</i>
Panel-to-panel joint side member Douglas fir plywood	$G_1 = 0.49$	<i>Nordic 2022</i>

A.2.3. Fastener properties

Nail diameter	$d_F = 2.8 \text{ mm}$	
Nail yield strength	$f_y = 50 (16 - d_F) = 657 \text{ MPa}$	<i>§12.9.3.2</i>
Nail length	$l_{\text{nail}} = 50.8 \text{ mm}$	
Number of nails per m	$n_f = 4$	
Number of shear planes	$n_s = 1$	
Spacing of nails	$s = 250 \text{ mm}$	
Service-creep factor	$k_m = 1.0$	<i>Table A.23</i>
Penetration into side member	$t_1 = 14 \text{ mm}$	
Penetration into main member	$t_2 = 36.8 \text{ mm}$	

A.2.4. Loading

Specified load due to wind	$q_w = 23 \text{ kN/m}$
Factored load due to wind	$q_{w,f} = 1.4 \times q_w = 33 \text{ kN/m}$
Diaphragm maximum factored shear force	$V_f = \frac{q_{w,f} L}{2} = 330 \text{ kN}$

A.2.5. Design factors

Load duration factor	$K_D = 1.15$	<i>§5.3.2, Short for seismic and wind</i>
System factor	$K_H = 1.0$	<i>§7.4.4</i>
Service condition factor	$K_{Sv} = 1.0$	<i>Table 7.3</i>

Treatment factor	$K_T = 1.0$	§7.4.3, §12.2.1, <i>Untreated</i>
Connections service-condition factor	$K_{SF} = 1.0$	Table 12.1
Toe-nailing factor	$J_A = 1.0$	§12.9.3
End grain factor	$J_E = 1.0$	§12.9.3
Diaphragm factor	$J_D = 1.3$	§12.9.3, <i>Nail in diaphragm</i>
Nail clinching factor	$J_B = 1$	§12.9.3
Connection factors	$J_F = J_E J_A J_B J_D = 1.3$	§12.9.3
Resistance factor for wood in connection with nail	$\phi_w = 0.8$	§12.9.3.2

A.2.6. CLT panel shear capacity

Gross cross-sectional area	$A_g = h \times t = 1.5 \times 10^6 \text{ mm}^2$	
Resistance factor for shear	$\phi_v = 0.9$	§7.5.7.3
Specified strength in shear	$f_v = 2.0 \text{ MPa}$	<i>Nordic 2022</i>
Specified strength in shear	$F_v = f_v (K_D K_H K_{SV} K_T) = 2.3 \text{ MPa}$	§7.5.7.3
Shear resistance	$V_r = \frac{2}{3} \phi_v F_v A_g$	§7.5.7.3b
Shear force utilization check	$V_r = 2070 \text{ kN} > V_f = 330 \text{ kN}$	

A.2.7. Lateral resistance of panel-to-panel nail connections

		§12.9.3.2
Embedment strength of side member	$f_1 = 104 G_1 (1 - 0.1 d_f) = 36.3 \text{ MPa}$	
Embedment strength of the point-side member	$f_2 = 50 G_1 (1 - 0.01 d_f) J_x = 18.36 \text{ MPa}$	$J_x = 0.9$ for CLT
Embedment strength of point-side member	$f_3 = 110 G_2^{1.8} (1 - 0.01 d_f) J_x = 20.18 \text{ MPa}$	
Case a)	$n_a = f_1 d_f t_1 = 1460 \text{ N/nail}$	
Case b)	$n_b = f_2 d_f t_2 = 1939 \text{ N/nail}$	

Case c) $n_c = \frac{1}{2} f_2 d_f t_2 = 969 \text{ N/nail}$

Case d) $n_d = f_1 d_f^2 \left(\sqrt{\frac{1}{6} \frac{f_3}{(f_1+f_3)} \frac{f_y}{f_1} + \frac{1}{5} \frac{t_1}{d_f}} \right) = 602 \text{ N/nail}$

Case e) $n_e = f_1 d_f^2 \left(\sqrt{\frac{1}{6} \frac{f_3}{(f_1+f_3)} \frac{f_y}{f_1} + \frac{1}{5} \frac{t_2}{d_f}} \right) = 1078 \text{ N/nail}$

Case f) $n_f = f_1 d_f^2 \frac{1}{5} \left(\frac{f_2 t_2}{f_1 d_f} + \frac{t_1}{d_f} \right) = 680 \text{ N/nail}$

Case g) $n_g = f_1 d_f^2 \left(\sqrt{\frac{2}{3} \frac{f_2}{(f_1+f_2)} \frac{f_y}{f_1}} \right) = 621 \text{ N/nail}$

Lateral resistance per shear plane $n_u = \min (n_a, \dots, n_g) = 602 \text{ N/nail}$

Lateral deformation of wood-to-wood connection with nail $\Delta = 0.5 d_f k_m \left(\frac{P}{n_u} \right)^{1.7}$ §A.12.9.3.3

Nail Stiffness from P-Δ curve $\rightarrow K_s = 2500 \text{ N/mm}$

A.2.8. Factored lateral resistance of connection

$N_u = n_u K_D K_{SF} K_T = 0.692 \text{ kN/nail}$ §12.9.3.2

$N_r = \phi_w N_u n_f n_s J_F = 0.8 \times 0.692 \times 4 \times 1 \times 1.3 = 2.51 \frac{\text{kN}}{\text{m}}$ §12.9.3.2

A.2.9. Force in panel-to-panel connection

Equations are from current thesis

$N(x) = \left(-m \frac{q_{w,f}}{\lambda^2} \left(\tanh \left(\tanh \left(\frac{\lambda x}{2} \right) \right) (\lambda x) - (\lambda x) + 1 \right) + m q \left(\frac{L}{2} x - \frac{x^2}{2} \right) \right)$ Eq. (2-51)

$K_1 = \frac{1}{\frac{S}{n_f K_s} + \left(\frac{5t}{6 G_{eff}} \right)} = 0.3$ Eq. (2-45)

$$\lambda^2 = K_1 b \left(\frac{n^2 t}{4 n E I} + \frac{1}{E t} \right) \quad \text{Eq. (2-66)}$$

$$= 0.30 \times 105 \left(\frac{6^2 (2400^2)}{4 \times 6 \times 11700 \times 1.21 \times 10^{11}} + \frac{1}{1.21 \times 10^{11} \times 2400} \right) = 1.1 \times 10^{-6}$$

$$m = \frac{t}{\lambda^2} \left(\frac{K_1}{n E I} \right) = \frac{2400}{1.4 \text{E-}06} \times \left(\frac{0.3}{6 \times 11700 \times 105 \times 2400^3 / 12} \right) = 7.2 \times 10^{-8}$$

Eq. (2-64)

Maximum force in panel-to-panel connections occurs where shear stress is maximum at $x = 0$ and $x = L$.

$$N(x=0) = m \frac{q}{\lambda^2} = 1.4 \frac{\text{kN}}{\text{m}}$$

$$N_r = 2.5 \frac{\text{kN}}{\text{m}} > N_f = 1.4 \frac{\text{kN}}{\text{m}} \rightarrow$$

2.8mm diameter x 50.8mm nails @ 250 mm spacing are used.

A.2.10. Diaphragm deflection

$$\delta_{\text{dia}} = \frac{5qL^4}{B384EI} + \frac{qL^2}{8kAG_{\text{eq}}} + \frac{Cm'qL^2}{8tK_1} \quad \text{Eq. (2-63)}$$

1- Deflection due to bending

$$B = 3n^2 + n = 198 \quad \text{Eq. (2-68)}$$

$$\delta_b = \frac{5qL^4}{B384EI} = \frac{5 \times 23 \times 20000^3}{114 \times 384 \times 11700 \times (105 \times 2400^3 / 12)} = 0.3 \text{ mm}$$

2- Deflection due to shear

$$\delta_v = \frac{qL^2}{8AkG_{\text{eq}}} = \frac{23 \times 20000^2}{8 \times 105 \times 14400 \times \frac{5}{6} \times 600} = 1.5 \text{ mm}$$

3- Deflection due to slip between panels

$$C = \frac{3n^2}{B} = 3 \times \frac{6^2}{114} = 0.94 \quad \text{Eq. (2-68)}$$

$$\delta_c = \frac{Cm'qL^2}{8tK_1} = \frac{0.94 \times 7.2E-08 \times 23 \times 20000^2}{8 \times 2400 \times 0.3} = 0.2 \text{ mm}$$

4- Total Diaphragm deflection

$$\delta_{\text{dia}} = \delta_b + \delta_v + \delta_c = 0.5 + 1.5 + 0.12 = 2.12 \text{ mm}$$

A.3. Design summary

CLT panels → Grade E1 (Nordic 2022), 3-ply, 20m × 2.4m

Nail panel-to-panel connections → Surface spline:

2.8mm x 50.8mm nails @ 250 mm spacing

14 mm Douglas fir Plywood